ROLE OF CARRIER SIZE, HEMODYNAMICS AND HEMORHEOLOGY IN THE EFFICACY OF VASCULAR-TARGETED SPHERICAL DRUG CARRIERS

by

Phapanin Charoenphol

A dissertation submitted in partial fulfillment
of the requirements for the degree of
Doctor of Philosophy
(Chemical Engineering)
in The University of Michigan
2012

Doctoral Committee:

      Assistant Professor Omolola Eniola-Adefeso, Chair
      Professor Mark A. Burns
      Professor Erdogan Gulari
      Associate Professor Joseph L. Bull

To Dad and Mom

For your love, support and encouragement

ACKNOWLEDGEMENTS

It is my pleasure to thank those who have made this thesis possible: my advisor, my thesis committee members, my colleagues, my friends and my family. I sincerely appreciate the support that I received from all directions.

First, I would like to express my deepest gratitude to my advisor, Professor Omolola Eniola-Adefeso, for giving me an opportunity to work in this lab, in the past five years. I am deeply grateful with her guidance on my research, her patience on revising my manuscripts and oral presentations and her caring on everything toward my degree. Her enthusiasm in research has inspired me along the way.

I would like to sincerely thank Professor Mark Burns, Professor Erdogan Gulari and Professor Joseph Bull for serving on my committees and their thoughtful suggestions, valuable discussion, time and attention along my studies.

I would like to thank Dr. David Pinsky for an opportunity in collaborating with his lab and use of his laboratory equipment. I am also extremely grateful to Dr. Diane Bouis, who was patiently trained me with animal handling.

I would like to thank all of my colleagues in Lola lab: Ryan Huang, Katawut Namdee, Supriya Mocherla, Michael Heslinga, Peter Onyskiw, Alex Thompson and Sean (Ming-Hsin) Li, for providing me a great environment in doing research and sharing their comments on my works. I also enjoyed our conversations in the lab. It would be a lonely and boring lab without them. I especially thank Ryan Huang for his help and guidance in experimental techniques since the beginning of my research work.

I also wish to thank all of my blood donors for their time and kindness providing me many litres of blood over the years enabling me to conduct the experimental work within this thesis.

I would like to thank all of my Thai friends at University of Michigan and friends in Chemical Engineering Department for their precious friendships and supports. It would be impossible to thank all of them, but I would like to extend thanks particular to Tanawan Pinnarat, Thitiporn Sukaew, Radaphat Chongthammakun, Panchika Prangkio, Nitayanan Chaiwatanayon, Tul Suriyalak, Niravun Pavenayotin, Nirand Pisutha-arnond, Ida (Xue) Chen and Marjan Varedi. Special thanks go to Bruce (Li-Jung) Tai, my dearest friend, who always cheer me up and stand by me through good and bad times.

Lastly, I would like to thank my family, Dad (Nirat Charoenphol), Mom (Nattiya Charoenphol), my two older brothers, Kom (Panawat Charoenphol) and Shane (Sarute Charoenphol), my aunt (Sairoong Theeraratsatit) and my uncle (Sam Thongrong) for supporting, encouraging me with their best wishes and especially for always giving me their care and love. I love you.

TABLE OF CONTENTS

LIST OF FIGURES

LIST OF TABLES

LIST OF ABBREVIATIONS

EC	Endothelial Cell
LDB	Leukocyte-depleted Blood
PCL	Poly caprolactone
PDB	Platelet-depleted Blood
PLGA	Poly (lactic-co-glycolic) acid
PPFC	Parallel Plate Flow Chamber
PRB	Plasma-removed blood
PS	Polystyrene
RBC	Red Blood Cell
RB	Reconstituted Blood
TDD	Targeted Drug Delivery
VSFC	Vertical-Step Flow Channel
VTC	Vascular-Targeted Carrier
VTDC	Vascular-Targeted Drug Carrier
WB	Whole Blood
WBC	White Blood Cell
WSR	Wall Shear Rate

ABSTRACT

Role of Carrier Size, Hemodynamics and Hemorheology
in the Efficacy of Vascular-Targeted Spherical Drug Carriers

by

Phapanin Charoenphol

Chair: Omolola Eniola-Adefeso

Spherical polymeric particles in the submicron down to tens nanometers size range are extensively proposed for use as vascular-targeted drug carriers (VTDCs); however, very limited studies have explored their capacity to efficiently localize and adhere to the vascular wall. The studies presented in this dissertation are focused on characterizing the role of particle size, blood flow dynamics (hemodynamics) and blood cells (hemorheology) on dictating the targeting (localization and binding) efficiency of VTDCs at the vascular wall in physiological human bulk blood flow via *in vitro* parallel plate flow assays.

The presented results show that the binding efficiency of VTDCs is a function of particle size in all flow types (i.e. laminar, pulsatile and recirculating flow) and is strongly modulated by the presence of red blood cells (RBCs). Specifically, the migration of RBCs away from the wall under shear flow creating the RBC-free layer (CFL) at the wall vicinity where leukocytes and microspheres are disproportionally concentrated whereas nanospheres tend to get trapped within the RBC core. The binding of localized particle is either enhanced or hindered depending on the ratio of particle size to the CFL width that can vary with the volume fraction of RBCs (% Hct), blood vessel size and wall shear rate. White blood cells (WBCs) tend to hinder microsphere binding due to their collision with bound particles associated with their tethering on the vascular wall, which increases the drag force on particles leading to particle removal. Overall, the presented results suggest that intermediate-size microspheres, 2–5 μm, not nanospheres or large microspheres, are the optimal particle sizes for targeting the wall from human blood flow in medium to large-sized blood vessels relevant in several cardiovascular diseases. The relevance of the presented *in vitro* results were valid with *ex vivo* model of mouse blood where it is found that the subtle differences in RBC sizes and hemorheology among various animal models utilized in drug delivery research can differently manipulate the particle dynamics and their eventual adhesion in blood flow; thus, raising the awareness of possible result deviation from animal models to human.

CHAPTER 1

INTRODUCTION

1.1 Background and Significance

Targeted drug delivery is a non-invasive process by which drug carriers are guided to deliver encapsulated/attached therapeutic agents at a targeted location, commonly via intravenous route. This approach has gained interest over conventional drug treatment, i.e. oral administration in which medications are distributed throughout the systemic blood circulation, by providing

(1) An increased drug efficacy at the targeted sites associated with the ability of drug carriers to sustain drug release over time, which can increase patient's compliance and

(2) A minimized deleterious side effect to other healthy tissues often associated with the systemic delivery of highly potent drugs.

Targeted drug delivery is often achieved via two different mechanisms: passive and active targeting. Passive targeting is achieved via the localization and entrapment of nanocarriers into target sites having a unique physical morphology, e.g. the enhanced permeability and retention effect (EPR) associated with vascular wall in cancer. In this phenomenon, the fast production of blood vessels in response to tumor growth results in

the abnormal structure of the vasculature with leaky tight junctions existing between endothelial cells. This vasculature architecture coupled with an ineffective lymphatic drainage allows the accumulation of nano-size particle to be trapped and retained inside the tissue without being filtered out due to lacking of lymphatic system [1, 2]. On the other hand, active targeting requires the specific interactions between receptors at the targeted sites and their recognitive ligands. Due to its specificity, this latter mechanism offers controllable and precise targeting and is widely applicable for treating several human diseases [2-4].

The vascular (blood vessel) wall has become a promising focus for targeted drug delivery since the endothelium (a cell monolayer lining the luminal surface of blood vessels) is readily accessible for intravenously administered targeting agents and due to the better understanding in the active role of endothelium plays in the physiological and pathological processes such as angiogenesis and inflammation [5, 6]. Recently, vascular targeting has been explored for localized delivery of therapeutics in several diseases including cancer as well as in pulmonary and cardiovascular diseases [7, 8]. This dissertation, however, is focused on vascular-targeted drug delivery via inflammation for treating chronic inflammatory diseases, particularly coronary artery disease (CAD) that results from atherosclerosis.

Due to the increasing incidence of high fat diet, sedentary lifestyles and smoking habits, recently, cardiovascular diseases including atherosclerosis remain the major cause of morbidity and mortality in the world [9, 10]. Current therapies for atherosclerosis include routine oral static drug and invasive bypass surgery. Major coronary events can still occur for patients who have underdone intense statin treatment [11] and surgical

2

interventions cannot prevent reoccurrence. Due to such limitations, development of an alternative therapy that can eliminate the surgical need and improve the drug efficacy relative to statin treatment is necessary. Targeted drug delivery via inflamed vascular wall is one of the promising treatments for atherosclerosis since inflammation is involved in all stages of atherosclerotic plaque development and progression [12].

1.1.1 Inflammation

Inflammation is a natural process by which living tissue responds to harmful stimuli resulting from physical injury or destructive microorganism. The presence of foreign antigens in the body triggers the recruitment of white blood cells (WBCS) or leukocytes from blood flow to the injured site, leading to acute inflammation – an initial positive response from the body. However, the failure to shut down inflammatory response can lead to the continuous recruitment of leukocytes, resulting in chronic inflammation, involved in the progression of several human diseases.

Neutrophils are the most abundant leukocytes in blood and the most active in inflammation. During the inflammation process, in attempting to remove harmful stimuli and initiate the healing process, neutrophils are recruited from the blood stream to accumulate at the injured site within minutes of inflammatory signal [13]. Initially, neutrophils are tethered and then transient to rolling adhesion along the inflamed vascular wall via their surface-expressed carbohydrate ligand, PSGL-1 (P-selectin Glycoprotein Ligand 1), interacting with selectins, i.e. P- and E-selectin, upregulated by endothelium of the vascular wall in response to inflammatory stimuli. Subsequently, in close proximity to the vessel wall, integrins membrane proteins, i.e. macrophage-1 antigen (Mac-1) and lymphocyte function-associated antigen-1 (LFA-1), present on rolling

3

neutrophil, are activated by chemoattractant released from the inflamed endothelium. Upon activation, integrins interact with intracellular adhesion molecule-1 (ICAM-1) and/or vascular adhesion molecule-1 (VCAM-1) upregulated on the endothelial wall leading to leukocyte firm adhesion. Afterwards, neutrophils creep and transmigrate via junction adhesion molecules (JAMs) or platelet endothelial cell adhesion molecule (PECAM-1) into the underlying injured tissue to remove the harmful stimuli. The schematic of leukocyte adhesion cascade is shown in Fig. 1.1 [14].

Due to this specific and well-ordered leukocyte adhesion cascade occurred at the injured vascular wall during inflammation, it provides an avenue for vascular-targeted drug delivery, particularly for treating chronic inflammatory diseases, by imitating the leukocytes to a vascular-targeted drug carrier (VTDC).
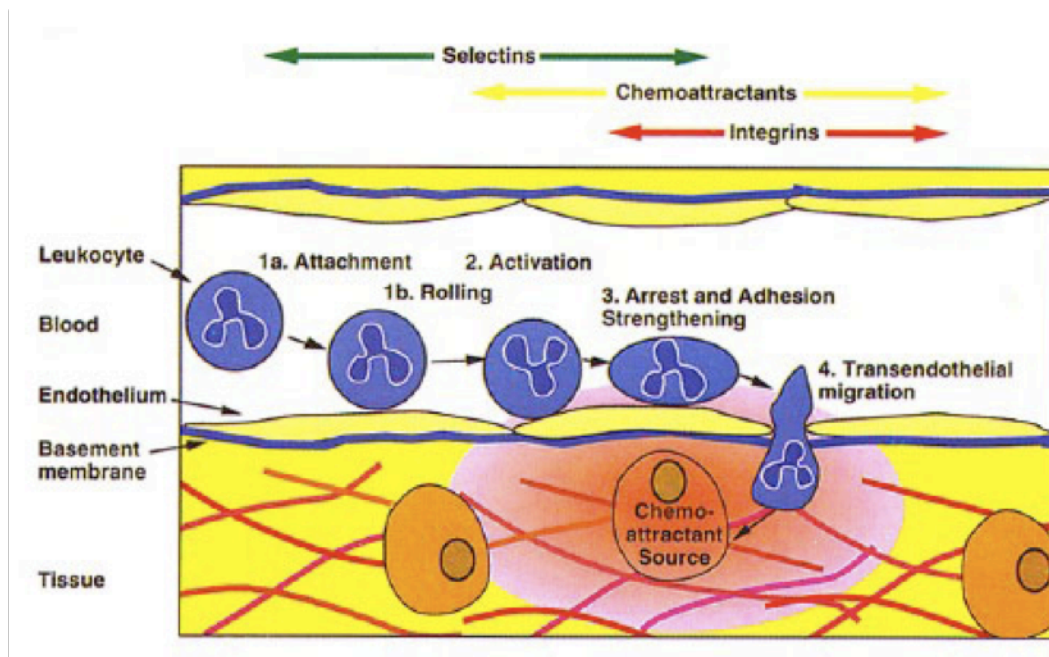
Figure 1.1 White blood cell (or leukocyte) adhesion cascade during inflammation [14]

1.1.2 Vascular-Targeted Drug Carrier (VTDC)

To design an effective vascular-targeted drug carrier (VTDC), several criteria need to be considered including targeting, hemodynamics and carrier physical properties.

1.1.2.1 Targeting Property

The ability of drug carrier to localize therapeutic agents selectively to a diseased location is achieved by decorating the drug carrier surface with counteract ligands of receptors expressed at the targeted sites. For instances, selectins, ICAM-1 and VCAM-1 are attractive receptors to target on inflamed endothelium [15, 16]. The common counter-ligands for selectins include PSGL-1, sialyl-lewis x (sLe^x), sialyl-lewis A (sLe^A, a sialylated fucosylated tetrasaccharide naturally found on neutrophil surface) and HuEP, a humanized murine selectin blocking antibody [17, 18]. Due to the high association rate of these ligands associated with selectins, the ligand-bearing carrier can be easily captured to the wall via selectins under high shear flow; meanwhile, the carrier also tends to roll along endothelium or readily be detached if shear force interacting on the particle is larger than their adhesive force [19]. Monoclonal antibodies are common ligands proposed against ICAM-1 and VCAM-1. Due to the low association rate of these ligand-receptors, antibody-coated particle can only interact with these receptors under low shear force, though these particles can withstand the higher drag force once adherence due to their low dissociation rate [19].

Targeting ligands are generally employed on VTDC via avidin-biotin chemistry [17] or other linkages, e.g. polyethylene glycol (PEG), commonly used for prolong particle circulation time *in vivo* [20]. Ligands can be used alone or in conjunction with other ligands, i.e. multiple receptors targeting. In general, targeting inflammation via

selectins is preferable than ICAM-1 since a basal level of ICAM-1 is present on endothelium in healthy tissues [19]. Thus, targeting via ICAM-1 alone may not differentiate between normal and diseased tissues. Overall, several works have shown that these leukocyte-mimetic drug carriers can recognize and vividly target the inflamed tissue both *in vitro* and *in vivo* [17, 18, 21].

1.1.2.2 Hemodynamics Property

Prior to their interaction with the target sites, the drug carriers must be able to circulate in blood flow and localize through the dense population of blood cells to the vascular wall vicinity. Hemodynamics describes the movement of blood cells in the circulatory system, which is imposed by different flow dynamics that can vary with the size, location and structure of blood vessels [22, 23]. Previous works have shown that red blood cells (RBCs), the most abundant blood cells, play important roles on initiating and promoting the binding of white blood cells and platelets during inflammation and hemostasis processes, respectively [24, 25]. Thus, it is likely that RBCs would also significantly manipulate the behavior of drug carriers in blood flow. Additionally, shear force associated with blood flow also governs all stages of drug carrier margination, i.e. manipulate the interaction with RBCs and the diffusion and convection of particles to the wall proximity, control the ligand-receptor binding rate on endothelium and dictate the particle adherence fate at the vascular wall [26]. Overall, hemodynamics is an important factor that prescribes the localization and the binding of drug carriers at the target site.

1.1.2.3 Physical Property

Several particle types, such as micelles, dendrimers, immunoliposome and polymeric particles, have been commonly proposed for use as VTDCs and their

application in various diseases has been extensively reviewed elsewhere [27, 28]. Due to their simple fabrication process, high drug loading capacity, tunable carrier degradation rate and hence controllable drug release profile, polymeric spheres are typical and prefer for use as VTDCs [29]. The particle can be fabricated via various simple procedures such as oil-in-water emulsion (O/W) method where therapeutic agents are encapsulated inside the polymer matrix during the process [30]. Altering the material or composition of this polymer can generally control the rate of drug release and carrier degradation [29]. Biodegradable and biocompatible polymers such as poly (lactic–co-glycolic acid) (PLGA) and poly (caprolactone) (PCL) are desirable for *in vivo* use since these polymers can break down in physiological environment into disintegrated polymers that evoke little or no immune response [30, 31].

In addition to the type of drug carriers, particle shape and size are parameters that also play an important role in drug carrier fate. Though, many particle shapes, including rod, disc and worm-like shapes, has recently gained interest for use as VTDCs due to their ability to avoid immune clearance, which enhance their circulation time *in vivo* [32, 33], spherical particles are still widely used for targeting therapeutics to the vascular wall. This is likely due to their ease in fabrication and well-defined model for hydrodynamic interactions. Spherical particles sized in the submicron down to tens of nanometer range have been extensively proposed as VTDCs due to their ability to navigate through the microvasculature without treat of occlusion in capillaries, the smallest blood vessels (5-7 μm in diameter in humans) and are less vulnerable to immune clearance [34, 35]. However, in addition to their circulation ability, the ideal drug carriers must also

(1) Be able to navigate through the dense blood cells to reach the blood vessel wall, and

(2) Remain in the adhesive state on the endothelium long enough to release their drug cargo or be internalized (get engulfed by the cells).

These two constraints constitute the *binding efficiency* of vascular-targeted carriers.

Particles	Target Sites	Experimental Set Up
6 μm PLGA [36]	Inflammatory molecules coated substrate	*In vitro* flow adhesion assay in saline
3.4 μm Microbubbles [37]	Inflamed endothelial cells	*In vitro* flow adhesion assay in saline
270 nm PLGA [38]	Inflamed endothelial cells	*In vitro* static adhesion assay in saline
4.5 μm Iron Oxide [39]	Aortic root of ApoE$^{-/-}$ mice	*In vivo* via local left ventricular injection
2 μm PS [40]	Aorta of ApoE$^{-/-}$ mice	*In vivo* via local jugular injection
17 nm Micelles [41]	Plaques lesion (stage V) of ApoE$^{-/-}$ mice	*In vivo* via tail vein injection
60 nm PLA [42]	Mouse injured vasculature	*In vivo* via tail vein injection

Table 1.1 Vascular-targeted carrier used in imaging and therapeutic delivery, particularly targeting to inflamed endothelial cells *in vitro* flow assay and to atherosclerotic plaque *in vivo*.

In existing works, a wide size range of spherical particles from nano- up to micron scale have been employed for VTDC, as summarized in Table 1.1. Nevertheless, these works mainly described the ability of VTDCs to successfully localize to the targeted site in simple buffer flow *in vitro* or *in vivo* while neglecting to determine their overall binding efficiency, i.e. the total numbers of VTDCs reaches the targeted area

relative to the total feed. Though nanoparticles may be preferable to use *in vivo*, due to their ease in circulation, it is not clear how the binding efficiency of these particles relate to other particle size. To date, very limited work has evaluated the role of size on prescribing the binding efficiency of spherical drug carriers to the vascular wall (Table 1.2).

Particle Size	Media	WSR	Particle Adhesion Trend
5-20 μm [26]	Saline	75-600 s^{-1}	(1) At low WSR: size independent (2) At high WSR: small particle favors adhesion
0.1-20 μm [43]	Viscous Saline (μ=10 cP)	1 s^{-1}	(1) Particle size smaller or larger than a critical particle size (~ 300 nm) would have a propensity to the wall. (2) A critical particle size varies with particle density.
0.05-10 μm [44]	Saline	7.75 s^{-1}	Large particles have higher adhesion.
0.96-5.2 μm [45]	Washed blood (15% Hct RBCs in Saline)	430-1630 s^{-1}	Only particle larger than 2 μm display near-wall excess (no adhesion).

Table 1.2 Summary of works investigating the role of size on spherical particle adhesion under shear flow.

As summarized in Table 1.2, the role of size on the particle binding at the wall are still inconclusive and many of the existing work have not been done in physiological manner. Though the computational work from Decuzzi et al and the experimental work from Gentile et al claimed that large microspheres had higher propensity for adhesion [43], Patil et al suggested that small particles demonstrated higher binding, particularly at high WSR relevant in physiological conditions [26]. Nevertheless, these works were

conducted in saline while neglecting red blood cells (RBCs) that play a significant influence on particle margination as indicated by their important role on the binding of white blood cells and platelets [24, 25]. Eckstein and his colleagues studied particle localization (no adhesion) in the presence of RBCs (15% Hct, the volume fraction of RBCs in blood) and suggested that particle larger than 2 μm (up to 5 μm) tend to accumulate in the wall proximity [45]. However, the particle localization may not absolutely translate to their binding trend *in vivo*, since the average percent of hematocrit in whole blood is about 40-45% Hct and the level of hematocrits have been shown to effect the binding density of blood cells [24]. Therefore, this study aims to elucidate the potential role of hemodynamics and particle size in prescribing the binding efficiency of vascular-targeted drug delivery in physiological blood flow.

Initially, the particle binding experiments will be observed in simple reconstituted blood flow consisting of plasma and RBCs (i.e. blood devoid of WBCs and platelets). The physiological range of shear rate and size of blood vessels and different flow types, i.e. laminar (commonly exists in vein and microcirculation), pulsatile and recirculating flow (generally occurs in medium to large-sized arteries and bifurcation area) encountered *in vivo* will be incorporated in this study.

Moreover, this work would further investigate the potential influence of WBCs and platelets on the adhesion of VTDC by conducting the flow adhesion experiments in whole blood flow. To date, no work, to my knowledge, has been presented to elucidate the interplay between these blood cells and particles especially on dictating the particle margination. Instead, most of previous works have been focused on the interaction of

particle to blood cells that may affect cells functionality, i.e. study the particle biocompatibility [27, 46].

In another aspect, due to the potential significant role of RBCs, the subtle differences of RBC size varied with different animal models [47] may possibly have influences on particle adhesion. To date, only few investigators have realized differences between animal and human blood rheology that could provide the great variation on the margination of blood cells and particle. Indeed, in one work, the significant differences of platelet adhesion in several mammalian whole bloods were observed [48] and these differences could be explained by the variation of animal RBC size, as suggested by Aarts et al [49]. However, it is still not clear how different RBC size along with other blood cell components would affect the binding efficiency of vascular-targeted drug carrier (VTDC) with different sizes. Thus, this dissertation would attempt to seek for the clarification.

1.2 Organization of the dissertation

This dissertation thesis consists of seven chapters.

Chapter 1 briefly introduces background and significance, literature review and the scope of my experimental works.

Chapter 2 indicates the source of materials and describes the experimental procedures employed in Chapters 3 to 6.

Chapter 3 discusses the role of particle size in dictating the binding efficiency of vascular-targeted drug carrier (VTDC) in *in vitro* laminar flow assay. Specifically, sLe^A- or aICAM- conjugated polymeric spherical particles with size ranging from 200 nm to 10 μm in diameter were used as VTDC. Polystyrene particles were preferable to biodegradable particles due to their uniform size distribution, which enables repeatable and consistent experiments. The adhesion of these particles in saline and reconstituted laminar blood flow (plasma and red blood cell) was examined via a parallel plate flow chamber (PPFC) with flow over a monolayer of activated human umbilical vein endothelial cells (HUVECs). This experimental setup is commonly used for an *in vitro* model of inflamed endothelial lining of blood vessels and is employed throughout the dissertation. Particle binding in typical ranges of shear rate and blood vessel size found *in vivo* were incorporated in this experimental study.

Chapter 4 investigates the role of particle size on the efficiency of VTDC in targeting the particular disease, i.e. atherosclerosis. Specifically, particle binding was observed in disturbed reconstituted blood flow (i.e. pulsatile and recirculating flow), which is a typical blood flow existed in medium to large sized arteries and at bifurcation area where the deposition of atherosclerotic plaque usually occurred.

Chapter 5 elucidates the significance of blood cells, including red blood cells, white blood cells (leukocytes) and platelets, on the behavior of particle with different sizes in blood flow. The binding of particles was investigated in various blood compositions, i.e. reconstituted blood with distinct volume fraction of red blood cell (% hematocrit), whole blood (WB), platelet-depleted blood (PDB) and leukocyte-depleted blood (PDB), allowing us to understand the role of blood cells on particle localization and adhesion in blood flow.

Chapter 6 examines the potential effect of red blood cell size and hemorheology, which vary with different animal models, on the particle binding efficiency. In particular, particle binding was studied in washed blood flow (RBCs suspended in saline) with various sizes of RBCs, obtained from human and several animals including mouse, pig, cow and goat. In addition, the experiments were further conducted in human and mouse whole blood to study the possible contribution of plasma and other blood components. The results from this chapter would raise awareness of the possible difference in results obtained from animal models to represent human.

Chapter 7 draws the conclusion and summarizes the significant findings from this dissertation to the field of study. Several topics are also proposed for future research.

References

1. Gao X, Cui Y, Levenson RM, Chung LWK, Nie S. In vivo cancer targeting and imaging with semiconductor quantum dots. Nature biotechnology. 2004;22:969-976.

2. Peer D, Karp JM, Hong S, Farokhzad OC, Margalit R, Langer R. Nanocarriers as an emerging platform for cancer therapy. Nature Nanotechnology. 2007;2:751-760.

3. Pison U, Welte T, Giersig M, Groneberg DA. Nanomedicine for respiratory diseases. European journal of pharmacology. 2006;533:341-350.

4. Wickline SA, Neubauer AM, Winter PM, Caruthers SD, Lanza GM. Molecular imaging and therapy of atherosclerosis with targeted nanoparticles. Journal of Magnetic Resonance Imaging. 2007;25:667-680.

5. Carmeliet P. Angiogenesis in health and disease. Nature medicine. 2003;9:653-660.

6. Szmitko PE, Wang CH, Weisel RD, de Almeida JR, Anderson TJ, Verma S. New markers of inflammation and endothelial cell activation. Circulation. 2003;108:1917-1923.

7. Neri D, Bicknell R. Tumour vascular targeting. Nature Reviews Cancer. 2005;5:436-446.

8. Spragg DD, Alford DR, Greferath R et al. Immunotargeting of liposomes to activated vascular endothelial cells: a strategy for site-selective delivery in the cardiovascular system. Proceedings of the National Academy of Sciences. 1997;94:8795.

9. Roger VL, Go AS, Lloyd-Jones DM et al. Heart Disease and Stroke Statistics—2011 Update1. Circulation. 2011;123:e18-e209.

10. Yusuf S, Reddy S, Ôunpuu S, Anand S. Global burden of cardiovascular diseases. Circulation. 2001;104:2855-2864.

11. Libby P, Aikawa M. Stabilization of atherosclerotic plaques: new mechanisms and clinical targets. Nature medicine. 2002;8:1257-1262.

12. Libby P, Ridker PM, Maseri A. Inflammation and atherosclerosis. Circulation. 2002;105:1135-1143.

13. Kaneider NC, Leger AJ, Kuliopulos A. Therapeutic targeting of molecules involved in leukocyte–endothelial cell interactions. FEBS Journal. 2006;273:4416-4424.

14. Springer TA. Traffic signals for lymphocyte recirculation and leukocyte emigration: the multistep paradigm. Cell. 1994;76:301.

15. Barthel SR, Gavino JD, Descheny L, Dimitroff CJ. Targeting selectins and selectin ligands in inflammation and cancer. Expert opinion on therapeutic targets. 2007;11:1473-1491.

16. Mollà M, Gironella M, Miquel R et al. Relative roles of ICAM-1 and VCAM-1 in the pathogenesis of experimental radiation-induced intestinal inflammation. International Journal of Radiation Oncology* Biology* Physics. 2003;57:264-273.

17. Eniola AO, Willcox PJ, Hammer DA. Interplay between rolling and firm adhesion elucidated with a cell-free system engineered with two distinct receptor-ligand pairs. Biophysical journal. 2003;85:2720-2731.

18. Ham ASW, Goetz DJ, Klibanov AL, Lawrence MB. Microparticle adhesive dynamics and rolling mediated by selectin-specific antibodies under flow. Biotechnology and bioengineering. 2007;96:596-607.

19. Lawrence MB, Springer TA. Leukocytes roll on a selectin at physiologic flow rates: distinction from and prerequisite for adhesion through integrins. Cell. 1991;65:859-873.

20. Radermacher KA, Beghein N, Boutry S et al. In vivo detection of inflammation using pegylated iron oxide particles targeted at E-selectin: a multimodal approach using MR imaging and EPR spectroscopy. Investigative radiology. 2009;44:398.

21. Muro S, Dziubla T, Qiu W et al. Endothelial targeting of high-affinity multivalent polymer nanocarriers directed to intercellular adhesion molecule 1. Journal of Pharmacology and Experimental Therapeutics. 2006;317:1161.

22. Ku DN. Blood flow in arteries. Annual Review of Fluid Mechanics. 1997;29:399-434.

23. Pries AR, Secomb TW, Gaehtgens P, Gross JF. Blood flow in microvascular networks. Experiments and simulation. Circulation research. 1990;67:826-834.

24. Munn LL, Melder RJ, Jain RK. Role of erythrocytes in leukocyte-endothelial interactions: mathematical model and experimental validation. Biophysical journal. 1996;71:466-478.

25. Turitto VT, Baumgartner HR. Platelet interaction with subendothelium in a perfusion system: physical role of red blood cells. Microvascular research. 1975;9:335-344.

26. Patil VRS, Campbell CJ, Yun YH, Slack SM, Goetz DJ. Particle diameter influences adhesion under flow. Biophysical journal. 2001;80:1733-1743.

27. Huang RB, Mocherla S, Heslinga MJ, Charoenphol P, Eniola-Adefeso O. Dynamic and cellular interactions of nanoparticles in vascular-targeted drug delivery (review). Molecular membrane biology. 2010;27:190-205.

28. Koo OM, Rubinstein I, Onyuksel H. Role of nanotechnology in targeted drug delivery and imaging: a concise review. Nanomedicine: Nanotechnology, Biology and Medicine. 2005;1:193-212.

29. Freiberg S, Zhu XX. Polymer microspheres for controlled drug release. International journal of pharmaceutics. 2004;282:1-18.

30. Jain RA. The manufacturing techniques of various drug loaded biodegradable poly (lactide-co-glycolide)(PLGA) devices. Biomaterials. 2000;21:2475-2490.

31. Kumari A, Yadav SK, Yadav SC. Biodegradable polymeric nanoparticles based drug delivery systems. Colloids and Surfaces B: Biointerfaces. 2010;75:1-18.

32. Champion JA, Katare YK, Mitragotri S. Particle shape: a new design parameter for micro-and nanoscale drug delivery carriers. Journal of Controlled Release. 2007;121:3-9.

33. Geng Y, Dalhaimer P, Cai S et al. Shape effects of filaments versus spherical particles in flow and drug delivery. Nature nanotechnology. 2007;2:249-255.

34. Abra RM, Hunt CA. Liposome disposition in vivo:: III. Dose and vesicle-size effects. Biochimica et Biophysica Acta (BBA)-Lipids and Lipid Metabolism. 1981;666:493-503.

35. Moghimi SM, Porter CJH, Muir IS, Illum L, Davis SS. Non-phagocytic uptake of intravenously injected microspheres in rat spleen: influence of particle size and hydrophilic coating. Biochemical and biophysical research communications. 1991;177:861-866.

36. Omolola Eniola A, Hammer DA. In vitro characterization of leukocyte mimetic for targeting therapeutics to the endothelium using two receptors. Biomaterials. 2005;26:7136-7144.

37. Weller GER, Villanueva FS, Tom EM, Wagner WR. Targeted ultrasound contrast agents: In vitro assessment of endothelial dysfunction and multi-targeting to ICAM-1 and sialyl Lewisx. Biotechnology and bioengineering. 2005;92:780-788.

38. Zhang N, Chittasupho C, Duangrat C, Siahaan TJ, Berkland C. PLGA Nanoparticle− Peptide Conjugate Effectively Targets Intercellular Cell-Adhesion Molecule-1. Bioconjugate chemistry. 2007;19:145-152.

39. McAteer MA, Schneider JE, Ali ZA et al. Magnetic resonance imaging of endothelial adhesion molecules in mouse atherosclerosis using dual-targeted microparticles of iron oxide. Arteriosclerosis, thrombosis, and vascular biology. 2008;28:77-83.

40. Deosarkar SP, Malgor R, Fu J, Kohn LD, Hanes J, Goetz DJ. Polymeric particles conjugated with a ligand to VCAM-1 exhibit selective, avid, and focal adhesion to sites of atherosclerosis. Biotechnology and bioengineering. 2008;101:400-407.

41. Peters D, Kastantin M, Kotamraju VR et al. Targeting atherosclerosis by using modular, multifunctional micelles. Proceedings of the National Academy of Sciences. 2009;106:9815.

42. Chan JM, Zhang L, Tong R et al. Spatiotemporal controlled delivery of nanoparticles to injured vasculature. Proceedings of the National Academy of Sciences. 2010;107:2213.

43. Decuzzi P, Lee S, Bhushan B, Ferrari M. A theoretical model for the margination of particles within blood vessels. Annals of biomedical engineering. 2005;33:179-190.

44. Gentile F, Curcio A, Indolfi C, Ferrari M, Decuzzi P. The margination propensity of spherical particles for vascular targeting in the microcirculation. Journal of Nanobiotechnology. 2008;6:9.

45. Eckstein EC, Tilles AW, Millero FJ. Conditions for the occurrence of large near-wall excesses of small particles during blood flow. Microvascular research. 1988;36:31-39.

46. Dobrovolskaia MA, Aggarwal P, Hall JB, McNeil SE. Preclinical studies to understand nanoparticle interaction with the immune system and its potential effects on nanoparticle biodistribution. Molecular pharmaceutics. 2008;5:487-495.

47. Gregory TR. Nucleotypic effects without nuclei: genome size and erythrocyte size in mammals. Genome. 2000;43:895-901.

48. Grabowski EF, Didisheim P, Lewis JC, Franta JT, Stropp JQ. Platelet adhesion to foreign surfaces under controlled conditions of whole blood flow: human vs rabbit, dog, calf, sheep, pig, macaque, and baboon. ASAIO Journal. 1977;23:141.

49. Aarts PA, Bolhuis PA, Sakariassen KS, Heethaar RM, Sixma JJ. Red blood cell size is important for adherence of blood platelets to artery subendothelium. Blood. 1983;62:214-217.

CHAPTER 2

MATERIALS AND METHODS

This chapter describes the procedures used for all experimental studies in this dissertation. In general, particle (vascular-targeted drug carrier) adhesion experiments were conducted in a parallel plate flow chamber with controlled wall shear rate and flow types at body temperature. The binding of particle on activated endothelial cells in blood flow was observed and analyzed via the inverted light microscope equipped with a digital camera.

2.1   Materials

Interleukin 1-β (IL1-β) was purchased from Fitzgerald Industries International (Concord, MA). Medium 199, penicillin, streptomycin, fungizone and HEPES buffer were purchased from Invitrogen (Carlsbad, CA). Fetal and bovine calf serums (FCS and BCS) were purchased from Hyclone (Logan, UT). Endothelial cell growth supplement (ECGS) was purchased from BD Biosciences (San Jose, CA). NeutrAvidin was purchased from Pierce Biotechnology, Inc. (Rockford, IL). Biotinylated, multivalent sialyl Lewis A (sLe^A) carbohydrate was purchased from GlycoTech (Gaithersburg, MD).

Biotinylated human ICAM-1 antibody (aICAM) Clone HA58 and Clone BBIG-I1 were purchased from eBioscience (San Diego, CA) and R&D Systems (Minneapolis, MN), respectively. Biotinylated human VCAM-1 antibody (aVCAM) Clone 1G11B1 was purchased from Abcam (Cambridge, MA). Carboxylated-functionalized, avidin-functionalized polystyrene spheres, Quantum PE and FITC MESF calibration beads were purchased from Bangs Laboratories Inc. (Fishers, IN). Biotin-4-fluorescein was purchased from Molecular Probe (Carlsbad, CA). PE-labeled anti-human CLA was purchased from Miltenyi Biotech (Auburn, CA). PE conjugated Rat IgG isotype control and PE conjugated anti-Mouse IgG were purchased from BD Pharmingen (San Diego, CA). Fluorescein conjugated goat anti-mouse IgG was purchased from Jackson ImmunoResearch Laboratories Inc. (West Grove, PA). Fluorescein conjugated anti-hE-selectin/CD62E, anti-hVCAM/CD106 and anti-hICAM/CD54 were purchased from R&D Systems (Minneapolis, MN). Isolated animal red blood cells (pig, cow and goat) were purchased from Lampire Biological Laboratories (Pipersville, PA). Dextran (MW 250,000) was purchased from MP Biomedicals (Solon, OH). Glutaraldehyde was purchased from Polysciences (Warrington, PA). Ethylenediaminetetraacetic acid (EDTA) was purchased from Boston Bioproducts Inc. (Worcester, MA). Dulbecco's phosphate buffered saline (DPBS), Bovine Serum Albumin (BSA) and all other chemical/cell reagents were purchased from Sigma Aldrich (Saint Louis, MO).

2.2   Particle Avidin Attachment

NeutrAvidin protein was covalently coupled to carboxylate-modified polystyrene spheres via carbodiimide (EDAC) chemistry as described in [1]. Briefly, 800 μL of 5

mg/mL NeutrAvidin in 50 mM MES buffer (pH 3.8) was added to sphere pellets (5.6×10^8 beads for 5.75 μm) and incubated on an end-to-end rotor for 15 mins at room temperature. Subsequently, 800 μL of 75 mg/mL EDAC in 50 mM MES buffer was added to the avidin-particle mixture and pH was adjusted to 8.5 via 1M NaOH. After an overnight incubation (~20 hrs), the reaction was quenched via 30 mins incubation with glycine at 100 mM (final concentration in the particle mixture). NeutrAvidin conjugated spheres were washed twice and resuspended in 50 mM PBS (50 mM sodium dihydrogen phosphate and 50 mM sodium phosphate dibasic, pH 7.4). Spheres were kept at 4°C until use.

2.3   Preparation of Vascular-Targeted Spheres

Avidin-coated spheres, 0.20, 0.51, 2.07, 5.72, 9.77 and 15.14 μm in size, obtained commercially or derived in the lab were conjugated with biotinylated Sialyl Lewis A (sLe^{A}, a carbohydrate ligand that binds to selectins) or human ICAM-1 antibody (aICAM) (Clone HA58 for Chapter 3 or Clone BBIG-I1 for Chapter 4) or human VCAM-1 antibody (aVCAM) (Clone 1G11B1), as previously described [2]. Briefly, avidin-coated spheres were incubated with the targeting ligands in 50 mM PBS with 1% BSA on an end-to-end rotor for 45 mins at room temperature. Concentration of ligands in solution used for each particle size was varied to ensure the same ligand surface density for all spheres. After conjugation, spheres were washed twice in DPBS+ (DPBS, 1% BSA, Ca2+, Mg2+ pH=7.4) and resuspended in the desired flow buffer.

2.4 Ligand Site Density Determination

Ligand-conjugated microspheres were incubated with 10 µg/mL of PE conjugated anti-human CLA (HECA-452), Fluorescein conjugated goat anti-Mouse IgG and PE conjugated anti-Mouse IgG for labeling sLe^A, aICAM and aVCAM-coated spheres, respectively, in DPBS+ for 20 mins on an end-to-end rotor at room temperature. Spheres were then washed twice in DPBS+, and fluorescence intensities were measured via BD FACSCalibur. Site density determination was as described in [3]. Briefly, the intensities were converted to ligand surface density via a calibration curve relating the fluorescence peaks of Quantum Standard Beads to their molecules of equivalent soluble fluorochrome (MESF); fluorophor to protein (F/P) ratio between the primary antibody (PE) to protein was assumed to be 1:1. A site density of approximate 1000, 4700 and 4500 sites/µm^2 were used for *in vitro* experiments with sLe^A, anti-ICAM-1 and anti-VCAM-1-coated spheres, respectively.

2.5 Preparation of Endothelial Cell (EC) Monolayer

Human umbilical vein endothelial cells (HUVECs) were harvested from fresh umbilical cords obtained from Mott children's hospital (Ann Arbor, MI), as previously described [4]. Briefly, HUVEC were harvested from human umbilical veins via the well-known collagenase perfusion method [5], pooled and cultured in tissue culture flasks pretreated with gelatin (0.2% w/v). The growth medium comprised of M199 supplemented with 10% FBS, 10% BCS, 1% penicillin-streptomycin, 1% fungizone, 1% HEPES buffer, 1 µg/ml heparin, and 50 µg/ml endothelial cell (EC) growth supplement. For flow experiments, pooled HUVEC were subcultured onto 30 mm glass cover slips

pretreated with 1% w/v gelatin cross-linked with 0.5% glutaraldehyde [6]. HUVEC on coverslips were kept at 37°C in a humidified 5% CO_2 incubator until confluent. Confluent HUVEC monolayers were activated with IL-1β at 1 ng/mL for 4, 8 or 24 hrs before use for experiments with sLe^A-, aVCAM- or aICAM-spheres, respectively. To confirm E-selectin, ICAM-1 and VCAM-1 expression, activated HUVECs were detached from glass coverslip with 0.25% trypsin and resuspended in DPBS at 4°C. Detached cells were then incubated with 10 μg/mL of fluorescein (FITC)-conjugated anti-hE-selectin antibody, anti-hICAM antibody and anti-hVCAM antibody for 30 mins at 4°C. Cell fluorescence intensity was measured via flow cytometry. Each cell monolayers was used only once.

2.6 Preparation of Whole Blood (WB), Reconstituted Blood (RB), Washed Blood, Platelet-Depleted Blood (PDB) and Leukocyte-Depleted Blood (LDB)

Fresh human blood was obtained via venipuncture according to a protocol approved by the University of Michigan Internal Review Board and in line with the standards set by the Helsinki Declaration. Venous blood was collected from healthy adult donors into a 60 ml syringe containing acetate-citrate-dextrose, ACD, as anticoagulant. This anticoagulated whole blood (WB) was either used in flow experiments as is or with 6%wt dextran solution (250 MW at 1.4 mL/10 mL of blood) added in for some control experiments (WB+D, used in Chapter 5).

To prepare reconstituted blood (cell-free plasma and RBCs, used in Chapter 3 and 4) and human washed blood (saline and RBCs, used in Chapter 6), a 6 % wt dextran-250 solution (1.4 mL/10 mL of blood) was added into anticoagulated whole blood. This

mixture was sit upright at room temperature for ~ 2 hrs allowing RBCs to sediment to the bottom layer from the leukocyte-platelet rich plasma at the top layer. Cell-free plasma was obtained by centrifugation of the top layer at 2500 g for 10 mins to remove platelets and leukocytes. RBCs collected from the bottom layer was washed with DPBS and centrifuge at 500 g for 10 mins prior to resuspending in the cell-free plasma or DPBS+ at desired percent of hematocrit (% Hct), i.e. volume fraction of RBCs, to obtain the reconstituted blood (RB) or washed blood, respectively. For instances, 40% Hct reconstituted blood was prepared from the mixture of 40 % v/v of RBCs with 60% v/v of the cell-free plasma.

To obtain platelet-depleted blood (PDB, used in Chapter 5), the anticoagulated whole blood was centrifuged with zero break at 300 g for 10 mins twice to obtain the separation of platelet-rich plasma (PRP) at the top layer and blood cells at the bottom layer. Subsequently, platelets were removed from PRP by centrifugation at 2500 g for 10 mins and the supernatant, i.e. platelet-poor plasma, was recombined with blood cells to obtain PDB.

To prepare leukocyte-depleted blood (LDB, used in Chapter 5), a 6% wt dextran-250 solution (1.4 mL/10 mL of blood) was added into the anticoagulated whole blood and red blood cells (RBCs) were allowed to sedimentation to the bottom layer for 2 hrs at room temperature. The top layer containing platelets and WBC in plasma was then centrifuged at 300 g for 8 mins to remove WBCs. LDB was obtained from the recombination of WBC-removed supernatant with RBCs.

For experiments studying the physical effect of WBC (Chapter 5), poly (lactic-co-glycolic) acid (PLGA) polymeric spheres fabricated via oil-in-water method with size

ranging from 6 – 13 μm (average size = 8 μm) were used as non-functional WBCs (with no adhesive function). After fabrication, the PLGA spheres were incubated with DPBS+ and 1% BSA for 2 hrs to block non-specific binding of spheres to the endothelial cells. The spheres with concentrations of $4x10^6$ particles/mL of blood (the normal concentration of WBC in whole blood) were then added into LDB to represent the non-functional WBCs in whole blood.

To prepare pig, cow and goat washed blood (used in Chapter 6), isolated pig, cow and goat RBCs were obtained commercially (Lampire Biological Lab, Pipersville, PA) and washed in DPBS once to remove the excess anticoagulant (at 1000 g 30 mins) prior to suspension in DPBS+ with 1% BSA to 40% Hct. Mouse whole blood was collected from surplus mice, generously provided by the breeding colony of Unit of Laboratory Animal Medicine (ULAM). All animal procedures were approved by ULAM and University Committee on Use and Care of Animals (UCUCA) at the University of Michigan. Briefly, blood was drawn from anaesthetized mice by a cardiac puncture into a syringe containing heparin as an anticoagulant. Pooled mouse whole bloods were centrifuged at 1000 g for 30 mins to collect mouse RBCs. However, it is difficult to isolate pure mouse RBCs from mouse whole blood by centrifugation. Thus, the pellets from this spin contained all mouse blood cells including RBCs, WBCs and platelets. Isolated mouse blood cells were then washed in DPBS once to minimize the excess anticoagulant and/or plasma constituents and were spun down at 1000 g for 30 mins. These RBCs were then resuspended in DPBS+ with 1% BSA at 40% Hct to yield mouse washed blood.

For human and animal whole blood experiments (used in Chapter 6), mouse whole blood containing heparin and human whole blood containing ACD were stored at 4°C overnight before used. To prepare plasma-removed blood (PRB), human and mouse whole blood were centrifuged down at 600 g for 30 mins to remove plasma. All blood cells were then resuspended in DPBS+, at the same % hematocrit as originally in whole blood.

All blood components were kept at 37°C until used.

2.7   Flow Adhesion Experimental Set Up

A circular parallel plate flow chamber (PPFC) equipped with a straight (for laminar and pulsatile flow) or vertical step channels (for recirculating flow) (GlycoTech, Gaithersburg, MD) were used for *in vitro* flow adhesion assays. Specifically, a silicon rubber gasket with rectangular cutout was attached to a flow chamber deck. An activated HUVEC monolayer cultured on a glass coverslip was placed over the gasket and vacuum-sealed to the flow deck such that the HUVEC monolayer formed the bottom substrate of the flow chamber assay. The rectangular cutout in the gasket defined the flow channel and the gasket thickness dictated the channel height. Flow experiment setup was as described in [7] with minor modifications. Briefly, the flow channel was rinsed with DPBS+ prior to the start of flow adhesion experiments to clear cell surface debris and air bubbles in the channel. Ligand-coated spheres of a given size suspended in buffer/blood at fixed concentration 5 x 10^5 spheres/mL (unless otherwise noted) were introduced into the flow channel from an inlet reservoir via a programmable syringe pump (KD Scientific, model no. 780212, Holliston, MA). Flow adhesion assays were observed on a

Nikon TE 2000-S inverted microscope fitted with a digital camera (Photometrics CoolSNAP EZ with a Sony CCD sensor). Digital recording of experiments was via Metamorph analysis software.

For experiments exploring particle adhesion to the cell monolayer against gravity, the flow chamber was inverted such that the HUVEC monolayer made up the top plate of PPFC and the particle adhesion occurred at the upper surface. Particles interacting with the cell monolayer were observed at a given instance (with continued flow) by careful flipping of the chamber back to the upright position. For vertical flow adhesion assays, the flow chamber was oriented vertically with flow and particles were allowed to adhere to the lateral surface. All adhesion experiments were conducted at 37°C and each cell monolayer was used once (i.e. only one experimental run per monolayer). Unless otherwise noted, particles in flow were exposed to the monolayer surface for 5 mins. Since HUVEC used were pooled over multiple donors, variation in adhesion molecule expression between batches is expected to be minimum.

2.7.1 Laminar Flow Assays

For all flow experiments, wall shear rate (γ_w (s^{-1}); WSR) within the flow channel was controlled via the adjustment of volumetric flow rate (Q) according to

$$\gamma_w = \frac{6Q}{h^2 w}; s^{-1} \quad (1)$$

where Q is the volumetric flow rate (mL/min), h is the channel height (254 μm, unless otherwise noted) and w is the channel width (1 cm unless otherwise noted). The wall shear stress (τ_w - dynes/cm^2) can be calculated by multiplying the WSR by blood viscosity (μ), which is a function of temperature, Q, and blood hematocrit.

2.7.2 Pulsatile Flow Assays

A programmable syringe pump was used to induce pulsatile flow in the horizontal PPFC. Pulsatile flow assays utilized two flow profiles (Fig. 2.1). In profile I, blood was pulsed about 0 s^{-1} with a net flow in the forward direction. Specifically, the syringe pump was set to run continuous loops of 14 s forward flow followed by 7 s backward flow for 15 mins with maximum Q set at 1.29 mL/min (200 s^{-1}), 3.225 mL/min (500 s^{-1}) and 6.45 mL/min (1000 s^{-1}) for experiments with aVCAM-, aICAM- and sLe^A-spheres, respectively. HUVEC monolayers were exposed to particles in pulsatile flow for 15 min. This flow time was chosen to ensure the same volume of particles pass through the chamber as in laminar experiments (5 mins of flow) since net forward flow with the pulsatile setting above occurs in one-third of the total cycle time (7 out of 21 s). In pulsatile profile II, flow was pulsed solely in the forward direction at ~3.1 mL/min (480 s^{-1}) for a total of 5 mins with the minimum and maximum forward flow rates set at 0.774 mL/min (120 s^{-1}) for 4 s and 7.74 mL/min (1200 s^{-1}) for 2 s with no period of pause. Pulsatility in the flow channel was confirmed via visual analysis of video record of experiments and tracking of instantaneous volumetric flow rate Q(t), as shown in Fig. 2.1.
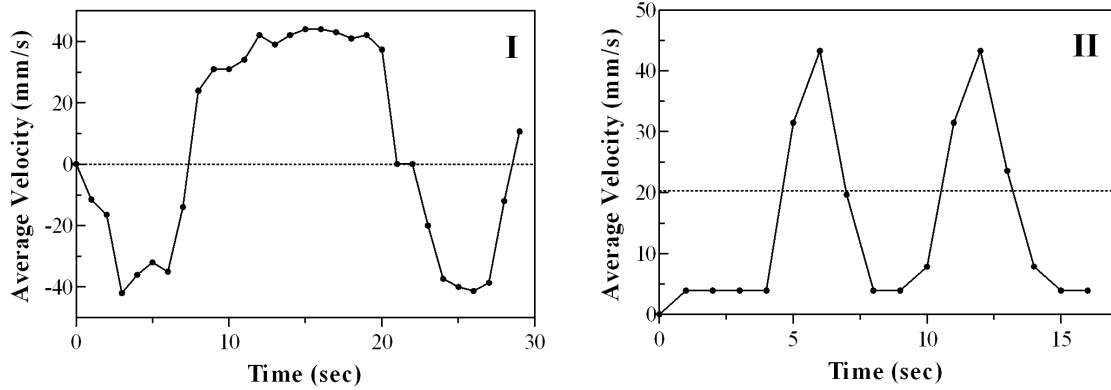
Figure 2.1 Velocity profiles of pulsatile flow

Flow profile (I) pulsing between 1000 s^{-1} and -1000 s^{-1} of WSR with a net forward flow and flow profile (II) pulsing about 480 s^{-1} of WSR (maximum and minimum WSR = 1200 s^{-1} and 120 s^{-1}).

2.7.3   Recirculating Flow Assays

Recirculating flow assays employed a vertical-step flow channel (VSFC) [8] (Fig. 2.2) with entrance and main channel heights of 127 μm and 508 μm (0.5 cm width), respectively. The step height was defined via layering of two gaskets – a half-length channel (custom cut) placed directly on ECs and a full-length channel placed on top of the first gasket. The sudden expansion at the step creates a recirculating flow (region 1 – Fig. 2.2) where a two-dimensional flow with a parallel (V_x) and a normal flow velocity (V_z) with respect to the channel bottom wall is established. The recirculation vortex extends from the step to a reattachment point (region 2) where flow parallel to the wall is stagnant (i.e. $V_x = 0$) and only V_z is present.   Beyond the reattachment, flow moves forward, and a laminar profile is reestablished at far downstream (region 3). Laminar flow adhesion in the VSFC was analyzed at 200 and 500 s^{-1} of WSR in the main

chamber, while pulsatile flow experiments were conducted with profile II, for a total of 5 mins.
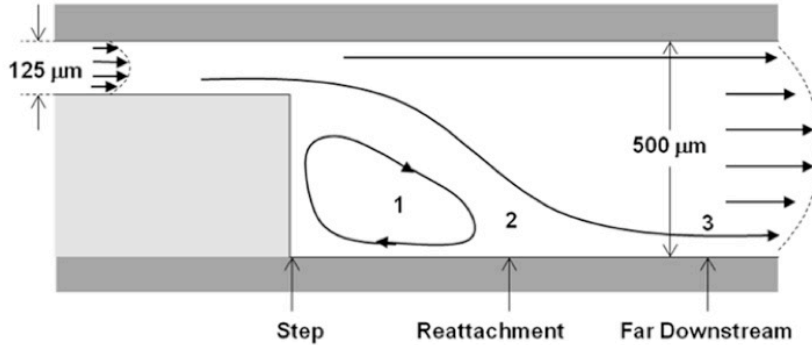
Figure 2.2 A schematic of a vertical step flow channel

2.8 Data Analysis

Particle binding density (#/mm^2) is obtained by manually counting the number of particles bound on the cell monolayer every minute (for rate of attachment data) or after 5 or 15 mins of flow (for particle binding data) and dividing this number by the area of the field of view (20x magnification, A = 0.152 mm^2, unless otherwise stated). To account for potential variation in fluxes along the chamber length, data was collected at a constant position along the length of the chamber for all experiments. Particles were considered firmly adherent if they remained stationary for > 10 s. Each data point shown in graphs represents an average over at least three experiments and includes at least ten fields of view per experiment. Standard error bars were plotted. In some analysis, particle adhesion was normalized, i.e. the number of particles bound at 5 mins per area was divided by the total number of particles that entered the chamber based on particle concentration in blood, volumetric flow rate through the channel and flow time. For

31

recirculating flow experiments, the number of particles bound downstream of the step channel was counted in 100 μm intervals (area of strip = 0.034 mm^2) – e.g. data reported for 200 μm represents particles bound between the 100 and 200 μm distant from the expansion step. For adhesion at far downstream where laminar flow is re-established, the adherent particles were counted at the 5000 μm distance from step [9]. Each data point represents an average over at least three experiments and includes at least five fields of view per experiment. Differences in adhesion levels were analyzed using a student t test, one-way ANOVA with Tukey post-test and two-way ANOVA with Bonferroni post-test. A value of $p < 0.05$ or $p < 0.01$ (in Chapter 5) was considered statistically significant, otherwise stated.

References

1. Hermanson GT, Mallia AK, Smith PK. Immobilized affinity ligand techniques. Academic Press San Diego; 1992

2. Eniola AO, Rodgers SD, Hammer DA. Characterization of biodegradable drug delivery vehicles with the adhesive properties of leukocytes. Biomaterials. 2002;23:2167-2177.

3. Brunk DK, Hammer DA. Quantifying rolling adhesion with a cell-free assay: E-selectin and its carbohydrate ligands. Biophysical journal. 1997;72:2820-2833.

4. Burns AR, Bowden RA, MacDonell SD et al. Analysis of tight junctions during neutrophil transendothelial migration. Journal of cell science. 2000;113:45.

5. Huang AJ, Furie MB, Nicholson SC, Fischbarg J, Liebovitch LS, Silverstein SC. Effects of human neutrophil chemotaxis across human endothelial cell monolayers on the permeability of these monolayers to ions and macromolecules. Journal of cellular physiology. 1988;135:355-366.

6. Burns AR, Walker DC, Brown ES et al. Neutrophil transendothelial migration is independent of tight junctions and occurs preferentially at tricellular corners. The Journal of Immunology. 1997;159:2893.

7. Eniola-Adefeso O, Huang RB, Smith CW. Kinetics of LFA-1 Mediated Adhesion of Human Neutrophils to ICAM-1—Role of E-Selectin Signaling Post-Activation. Annals of biomedical engineering. 2009;37:737-748.

8. Chiu JJ, Wang DL, Chien S, Skalak R, Usami S. Effects of disturbed flow on endothelial cells. Journal of biomechanical engineering. 1998;120:2.

9. Skilbeck C, Westwood SM, Walker PG, David T, Nash GB. Dependence of adhesive behavior of neutrophils on local fluid dynamics in a region with recirculating flow. Biorheology. 2001;38:213-228.

CHAPTER 3

POTENTIAL ROLE OF SIZE AND HEMODYNAMICS IN THE EFFICACY OF VASCULAR-TARGETED SPHERICAL DRUG CARRIER

ABSTRACT

Targeting drug carriers to the vascular wall is of interest for localized delivery of therapeutics in many human diseases. Nanometer-sized spherical particles are widely proposed for use as carriers for vascular targeting, yet very little evidence has been presented as to their ability to interact with the vascular wall. Thus, this work focuses on elucidating the effect of particle size along with hemodynamics, blood rheology, and vessel size on the adhesion efficiency of targeted polymeric spheres to inflamed endothelium from laminar blood flow *in vitro* via parallel plate flow chamber assay (PPFC). My results shows that the binding efficiency of spheres to the endothelium from blood flow generally increased with increasing particle size, wall shear rate and channel height for particle sizes from 100 nm up to 10 μm. Nano-sized particles showed minimal adhesion to the endothelium from blood flow in horizontal (gravity and anti-gravity direction) and vertical channels on the order of small to medium-sized venules and arteries when compared to micron-sized spheres. Overall, the presented data suggest that

spheres 2 μm to 5 μm are optimal for targeting the wall in medium to large vessels

relevant in several cardiovascular diseases.

3.1 Introduction

In recent years, vascular targeting has been explored for localized delivery of therapeutics in cancer [1, 2] as well as in pulmonary and cardiovascular diseases [3-5]. However, existing literature have focused on identifying suitable endothelial cell targets (surface-expressed proteins), targeting molecules (e.g. antibodies/peptides) or characterizing the drug release properties of delivery vehicles. While biological cues and cellular processes are important in the endothelial response in human diseases, the characteristic forces ascribed to blood flow dynamics (hemodynamics) are a crucial part of understanding this process and its involvement in the pathogenesis of these diseases. Similarly, hemodynamics is important in the adhesive interactions of leukocytes (white blood cells) with the endothelium – a hallmark of the natural immune response. As such, hemodynamics must be an important consideration in the design of vascular-targeted drug carriers (VTDC) – yet has been absent in existing literature. To date, little emphasis has been placed on how physical characteristics, such as shape and size, along with hemodynamics will prescribe the ability of VTDC to marginate (localize and adhere) to the vessel wall.

Due to their ease of fabrication and well-defined model for hydrodynamic interactions, spherical particles have been widely studied for targeting therapeutics to the vascular wall [6-8]. Particles size in the submicron down to tens of nanometer range are particularly attractive for intravenous delivery since they can pass through the microcirculation with ease [8] and are less vulnerable to immune clearance [6, 9]. However, in addition to their ability to navigate the circulatory network, VTDC must (1) possess the ability to find and bind the vessel wall from blood stream and (2) remain

bound long enough to release drug cargo or be internalized by the endothelial cells – these two constraints constitute *the binding efficiency* of targeted carriers. To date, very limited work exists in the literature evaluating the role of size on the eventual binding efficiency of spherical carriers to the vascular wall. In one work, Decuzzi and co-workers using a theoretical model for particle margination from the blood stream suggested that there is a critical radius ($R_{critical} \sim 50 - 250$ nm, depending on particle density) for spheres at which their localization time to the wall from blood flow is maximum, and that VTDC with size larger (or smaller) than $R_{critical}$ would have a higher propensity for the vessel wall [10]. Their model accounted for a higher concentration of nano-sized spheres near the wall than micron-sized spheres based on the assumption that nanospheres can be injected into the blood stream at a higher concentration than microspheres. In addition, this model only focused on particle margination from close proximity to the wall and thus did not fully address the ability of targeted particles to navigate through the dense population of blood cells to reach the wall. To date, no evidence has been put forth in the literature to suggest that nanospheres will navigate through blood similar to or better than microspheres; thus, a higher injection concentration for nanospheres may not necessarily translate to a higher concentration at the vessel wall. Existing experimental works evaluating the effect of size/volume on the margination of spherical particles from mid-stream to the wall for potential vascular-targeting applications via parallel plate flow chamber (PPFC) assays only studied these interactions in buffer [11, 12]. Thus, it is not clear if predictions made from such works would hold in blood flow.

Blood rheology is a known important factor in the interaction of leukocytes with the endothelium *in vivo*. Specifically, the physical properties of erythrocytes or red blood cells (shape, size and deformability) allow them to be preferentially positioned in the centerline of blood flow forcing other blood cells (leukocytes and platelets) into a red blood cell (RBC)-free plasma layer (CFL) located towards the vessel wall thereby increasing the probability of leukocyte-endothelium interaction [13, 14]. While particle size and hemodynamics may be irrelevant in the microcirculation, these parameters will likely prescribe the binding efficiency of spherical carriers in medium to large blood vessels that are often associated with several chronic inflammatory and cardiovascular diseases (e.g. atherosclerosis) [15, 16]. Indeed, investigators have shown increased binding of vascular-targeted 10 μm spherical particles to cultured endothelium (~170%) when a physiological amount of RBCs is added to the flow medium similar to the previously described RBC-effect on neutrophils [17]. It is not clear, however, if these observed RBC-effect (enhanced margination) would also exist for the adhesion of smaller size spheres. Though a few studies of the localization (only – no adhesive interactions) of small spheres to the wall from blood flow existed have suggested that particles larger than 2 μm (up to 5 μm) can disproportionately accumulate (near wall excess) to the wall, it is not clear how accumulation will translate to particle adhesion to the wall in blood flow [18, 19]. Thus, the work presented herein aims to elucidate the potential role of hemodynamics and size in prescribing the binding efficiency of VTDC in flow mimicking physiological conditions *in vivo* via PPFC. Specifically, spherical particles conjugated with sialyl-Lewis A (sLe^A), a ligand specific to the endothelial-expressed selectins, and with diameters ranging from 100 nm up to 10 μm were evaluated in a

PPFC for their ability to effectively bind to activated endothelial cells (aECs) from blood flow.

3.2   Results

The experimental set up used in this chapter is described in detail in Chapter 2.

3.2.1   Sialyl Lewis A-coated spheres specifically adhere to activated HUVEC monolayer from flow in a PPFC

Spheres with 10 μm diameter were used to confirm the specificity of sLe^A to activated ECs (aECs). Overall, these spheres coated with sLe^A were easily captured to the surface of IL1-β-activated endothelial cells from flow in the presence or absence of RBCs in a PPFC as shown in Fig. 3.1. As reported by others, the presence of RBCs enhanced the adhesion of particles to the EC surface [8] over particles in buffer (DPBS+) and plasma flow with no RBCs. The level of particle adhesion in plasma without RBCs was significantly lower than adhesion in buffer with no RBCs due to the viscosity of plasma being 1.5-fold higher than that of buffer (i.e. a higher viscosity translates to a higher wall shear stress that negatively affects particle adhesion in flow). However, there was no significant difference in the adhesion of particles with RBCs in plasma compared ones with RBCs in buffer (not shown) at this WSR. Control experiments with sLe^A spheres flowing over non-activated ECs, avidin-coated spheres over aECs, or sLe^A spheres over aECs in the presence of EDTA (i.e. removal of divalent ions necessary for sLe^A-selectin interactions) all showed no particle adhesion, thus confirming the specificity of the interaction between spheres and aECs.
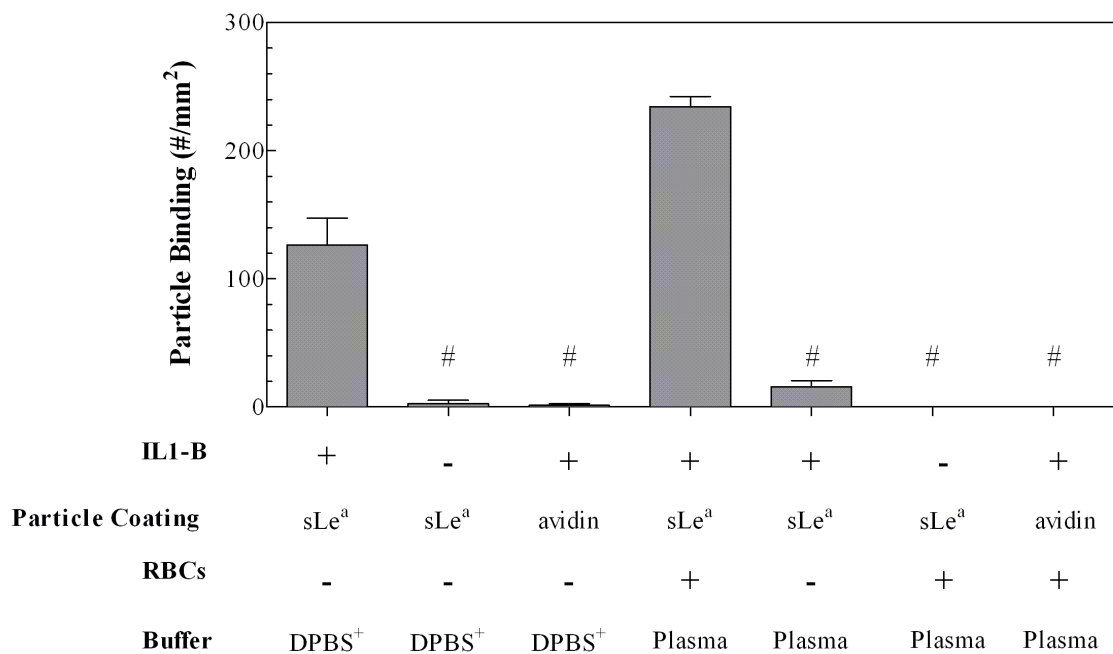
Figure 3.1 Adhesion of sLe^A- or avidin-coated 10 μm spheres from flow to EC monolayer in a parallel plate flow chamber and in the presence or absence of red blood cells (RBCs). WSR in the chamber = 200 s^{-1}.

n ≥ 3 and # = p < 0.01 compare to sLe^A particles on IL1-β-activated endothelial cells.

3.2.2 Effect of size on particle adhesion to HUVEC from flow

sLe^A -coated spheres sized from 100 nm to 10 μm were allowed to interact with aECs in a reconstituted blood flow (RBCs in homologous plasma with no leukocytes or platelets) at 30% hematocrit and with the WSR and channel height set at intermediate values of 200 s^{-1} and 254 μm. The 200 s^{-1} WSR is a representative of flow in post capillary venules and the 254 μm height is in line with diameters of arterioles and venules in humans [20, 21]. The sLe^A site density on spheres was adjusted to ~800 sites/μm^2 via flow cytometry. For flow experiments, the particle concentration was held constant at 5x10^5 particles per mL of blood for all particle sizes. It was found that the level of particle adhesion (per unit area at 5-min) on aECs at the above conditions decreased when the particle diameter (size) decreased from 10 μm to 0.1 μm as shown in Fig. 3.2A. Minimal amount of binding occurred for particles smaller than 2 μm in size. For all experiments (the range of WSR studied), spheres at ≥ 800 sLe^A sites/μm^2 displayed only firm adhesion to the cell monolayer. When the particle concentration was increased to 1 and 5 x 10^6 particles/mL of blood at fixed %Hct, the level of particle binding increased proportionally without affecting the adhesion trend seen with particle size (data not shown). Since for many drug delivery applications, carrier payload (i.e. volume) is of the utmost important [22], I conducted some experiments at a fixed volume concentration of 2.44 x10^7 μm^3 per mL of blood for all particle sizes (i.e. 5x10^4 particles/mL for 10 μm versus 3.5x10^8 particles/mL for 0.5 μm). Similar to experiments at fixed number concentration, particle volume adhesion increased with an increase in particle size up to 10 μm as shown in Fig. 3.2B.
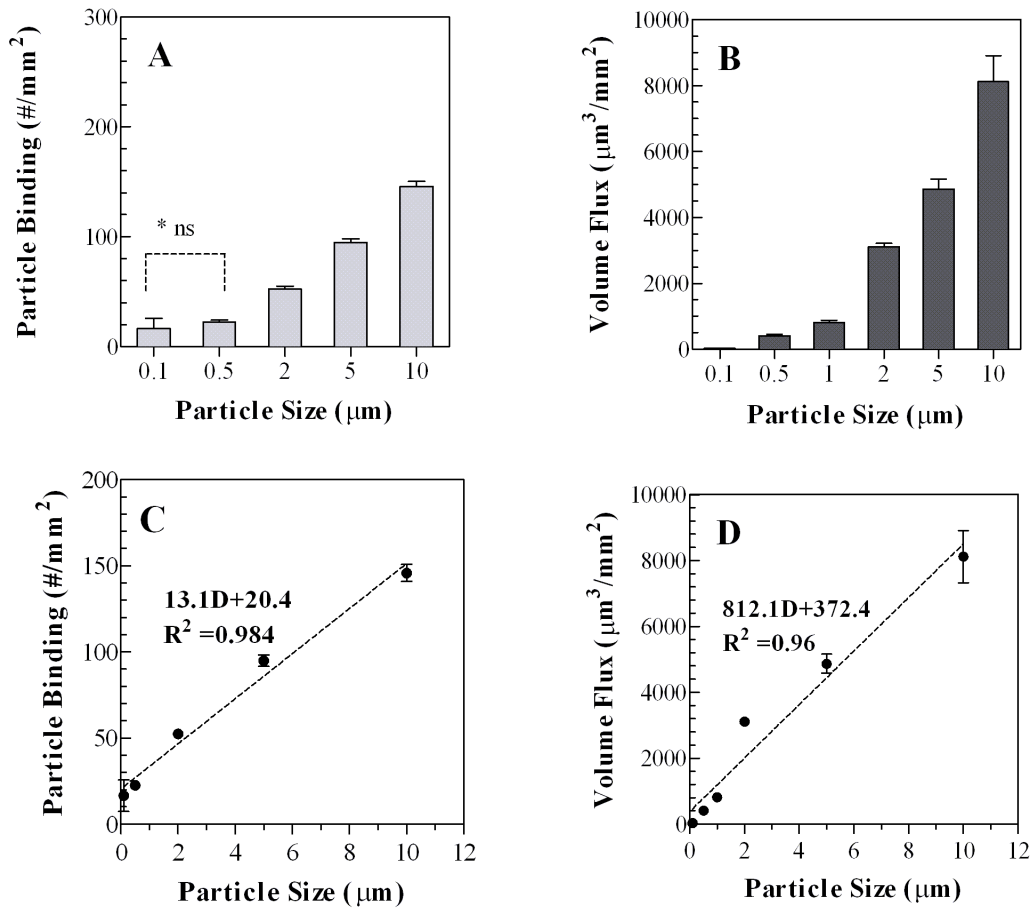
Figure 3.2 Adhesion of sLe^A-coated spheres from blood flow to aEC monolayer in a PPFC at (A, C) a fixed number concentration of 5×10^5 particle/mL blood and (B, D) a fixed volume concentration of 2.44×10^7 μm^3/mL blood for all particle sizes (n ≥ 3).

Channel height = 254 μm. Wall shear rate = 200 s^{-1}. D is particle diameter (μm) and *ns = not significantly difference.

The particle binding (Fig. 3.2A) and volume flux (Fig. 3.2B) replotted with particle size on a linear scale at the x-axis showed that the adhesion of spheres at both fixed particle concentration and volume linearly increased with particle diameter (Fig. 3.2 C and 3.2 D). Since the adhesion trend with fixed volume was the same as with fixed particle concentration, the rest of the studies reported herein were conducted with particle concentration fixed at 5 x 10^5/mL and 30% Hct to conserve material.

3.2.3 Effect of wall shear rate (WSR) on particle adhesion is a function of particle size and the presence of RBCs in flow

Previous studies of particles/cells in flow have shown that their adhesive behavior depends on the magnitude of WSR [23, 24]. Thus, I investigated the role of WSR on particle adhesion to aEC monolayer from blood flow in the horizontal flow chamber at WSRs ranging from 200 to 1500 s^{-1} – typical values of *in vivo* human blood flow [20, 21]. These experiments were conducted at a fixed channel height of 254 μm. At 200 s^{-1}, the level of particle adhesion increased with increasing particle size for most particles tested as shown in Fig. 3.3A. The adhesion of 0.1 μm particles was not significantly different from that of 0.5 μm at this WSR (data not shown). When the WSR was increased to 500 s^{-1}, adhesion increased only when the particle size increased from 0.5 μm up to 5 μm. The adhesion of 10 μm spheres at this shear rate was significantly lower than those measured for 2 and 5 μm particles. A further increase in WSR to 1000 and 1500 s^{-1} resulted in adhesion, which only increasing with an increase in particle size from 0.5 μm up to 2 μm. Further increases in size beyond 2 μm at these WSRs resulted in the same or significantly lower binding than displayed by 2 μm particles. Furthermore, 2 and

43

5 μm showed increase in adhesion levels with each step increases in WSR from 200 s^{-1} up to a critical value (WSR$_{crit}$). Beyond this WSR$_{crit}$, adhesion levels decreased with an increase in WSR. While 10 μm spheres appear to not have a critical WSR for adhesion between 200 and 1500 s^{-1}, a reduction in WSR to 100 s^{-1} resulted in the appearance of a WSR$_{crit}$ for these particles at 200 s^{-1} (Fig 3.3A-insert). On the contrary, the apparent WSR$_{crit}$ displayed by 0.5 μm was found to not be significant via two-way ANOVA. Again, 0.1 μm spheres displayed minimal adhesion at all WSRs (not shown). Overall, the magnitude of the WSR$_{crit}$ for a given particle was a function of its size.

To determine if the significant drop in particle binding beyond WSR$_{crit}$ is due to a deficiency in particle delivery to the surface (i.e. ability of particle to localize through RBCs to the wall) or higher hemodynamic forces disrupting receptor-ligand interactions/increasing particle detachment, experiments were conducted at 500 s^{-1} with 10 μm particles having a significantly higher surface sLe^{A} density than the 800 sites/μm2 used for the data displayed in Fig. 3.3A. At a WSR of 500 s^{-1} and 254 μm channel height, a 2.5-fold increase in sLe^{A} site density for 10 μm particles (from 800 to 2000 sites/μm^{2}) resulted in equivalent increase in particle binding as shown in Fig. 3.3B. A similar or higher (up to 5000 site/μm^{2}) fold increase in sLe^{A} site did not yield a significant change in the level of binding for 2 (not shown) or 5 μm particles at 500 s^{-1} – a WSR which is less than the WSR$_{crit}$ for these particles. Thus, it can be concluded that the significant drop in adhesion beyond WSR$_{crit}$ is due to higher disruptive hemodynamic forces interfering with particle adhesion rather than ineffective particle localization to the wall.
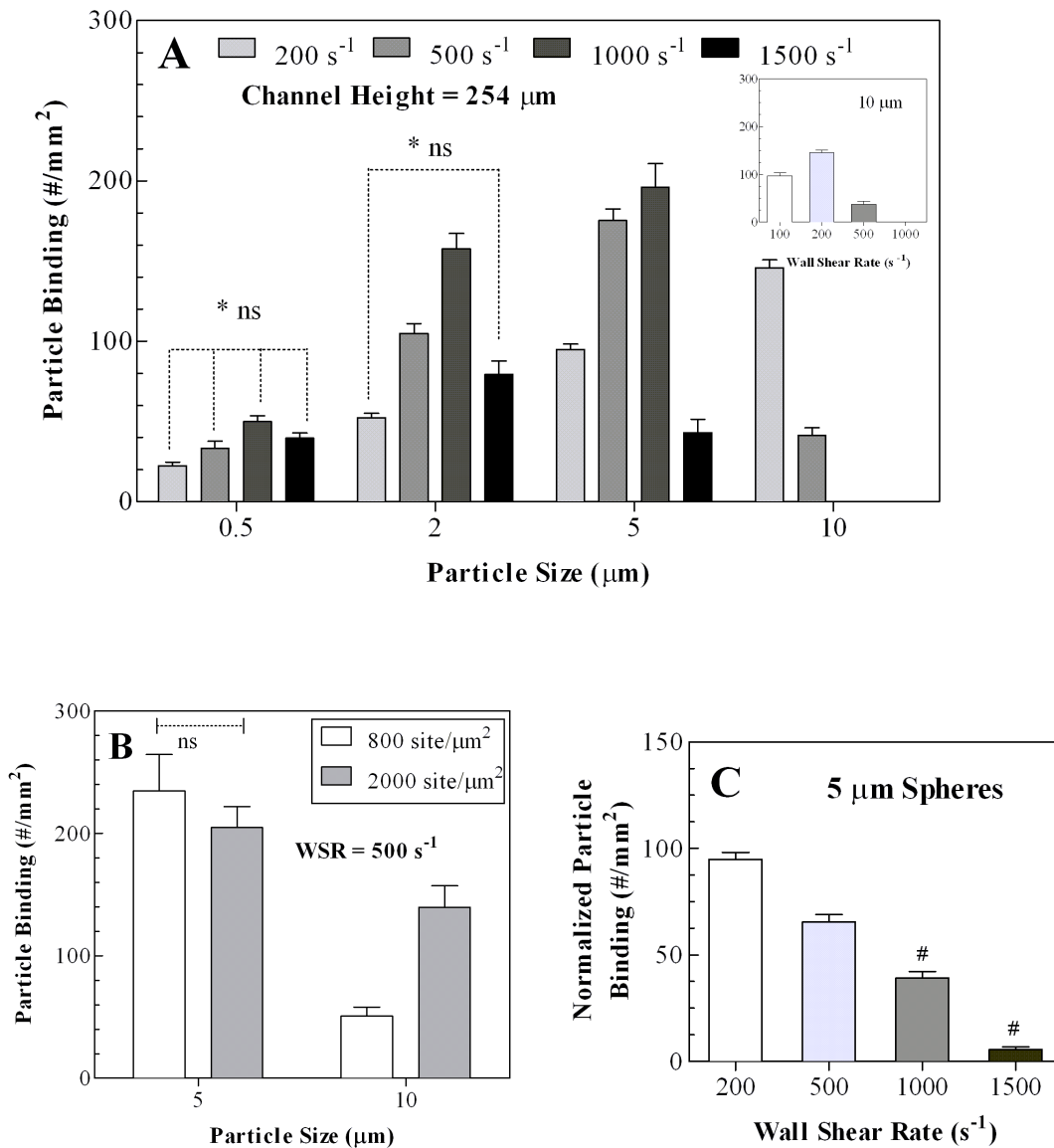
Figure 3.3 (A) Adhesion of sLe^A spheres (~800 sites/µm^2) as a function of wall shear rate in the chamber. (B) Adhesion of 5 and 10 µm spheres as a function of sLe^A site density at 500 s^{-1}. (C) Binding flux of 5 µm spheres at different shear rates normalized to the total number of particles introduced into the chamber at each shear rate.

Particle concentration fixed at 5x10^5 particles/mL blood. Channel height = 254 µm. n ≥ 3 and # = p < 0.01 compare to binding at 200 s^{-1}. *ns = not significant.

To better understand the increase in particle adhesion with increase in WSR in the range that is less than the WSR_{crit}, the data in Fig. 3.3A was normalized to the total number of particles introduced into the flow chamber at each WSR. Normalized particle adhesion remain the same or decreased as the shear rate increased from 200 to 1500 s^{-1} as shown in Fig. 3.3C. A similar trend was seen when a constant flux of particles (6.45x10^5 particles/mL) was introduced over aEC at all WSR, i.e. particle concentration was 5x10^5/mL at 200 s^{-1} versus 1x10^5/mL at 1000 s^{-1} (data not shown). When particle adhesion occurred in saline buffer, i.e. no RBCs, an opposite adhesion trend was observed. Particle adhesion decreased (or remained the same for particle smaller than or equal to 2 μm, displaying minimal adhesion) as the WSR increased from 100 s^{-1} to 640 s^{-1} as shown in Fig. 3.4.

3.2.4 Effect of channel height on particle adhesion

To determine whether the trends observed with WSR and particle size are generally applicable, I varied the channel height between 127, 254, 508 and 762 μm – a range representative of arterioles and venules. Adhesion at all channel heights was observed at 200 s^{-1} by adjustment of the channel flow rate according to equation 1 (in Chapter 2) (e.g. $Q_{254μm} = 4Q_{127μm}$). For 127 and 254 μm channel heights, adhesion increased with an increase in particle size up to 10 μm as shown in Fig. 3.5A. At 508 and 762 μm heights, adhesion only significantly increased as size increased from 0.5 to 5 μm. However, the magnitude of adhesion at a fixed particle size significantly increased as the channel height increased from 127 to 762 μm for all particle size larger than 0.5 μm.
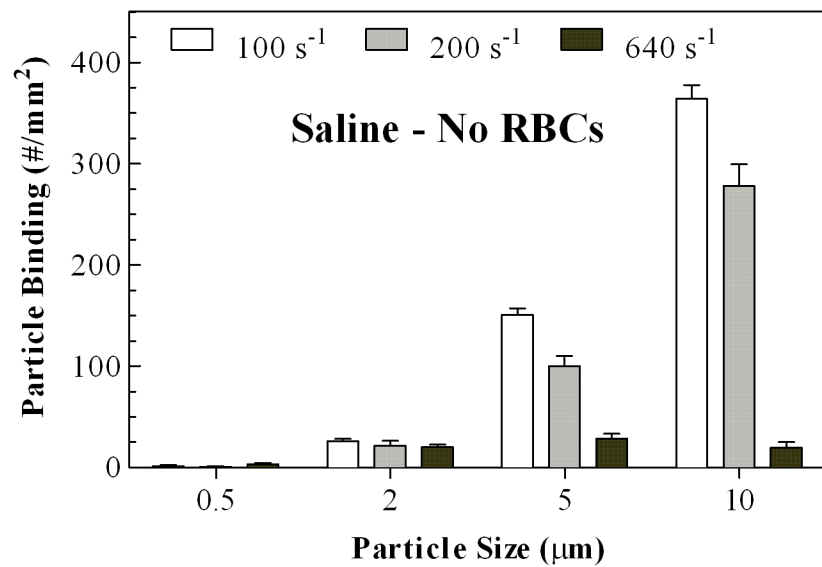
Figure 3.4 Adhesion of sLe^A spheres in saline (DPBS+) buffer (no RBCs) to aEC
monolayer as a function of wall shear rate in a horizontal PPFC.
Particle concentration fixed at 1×10^6/mL of buffer. Channel height = 254 μm.
$n \geq 3$.
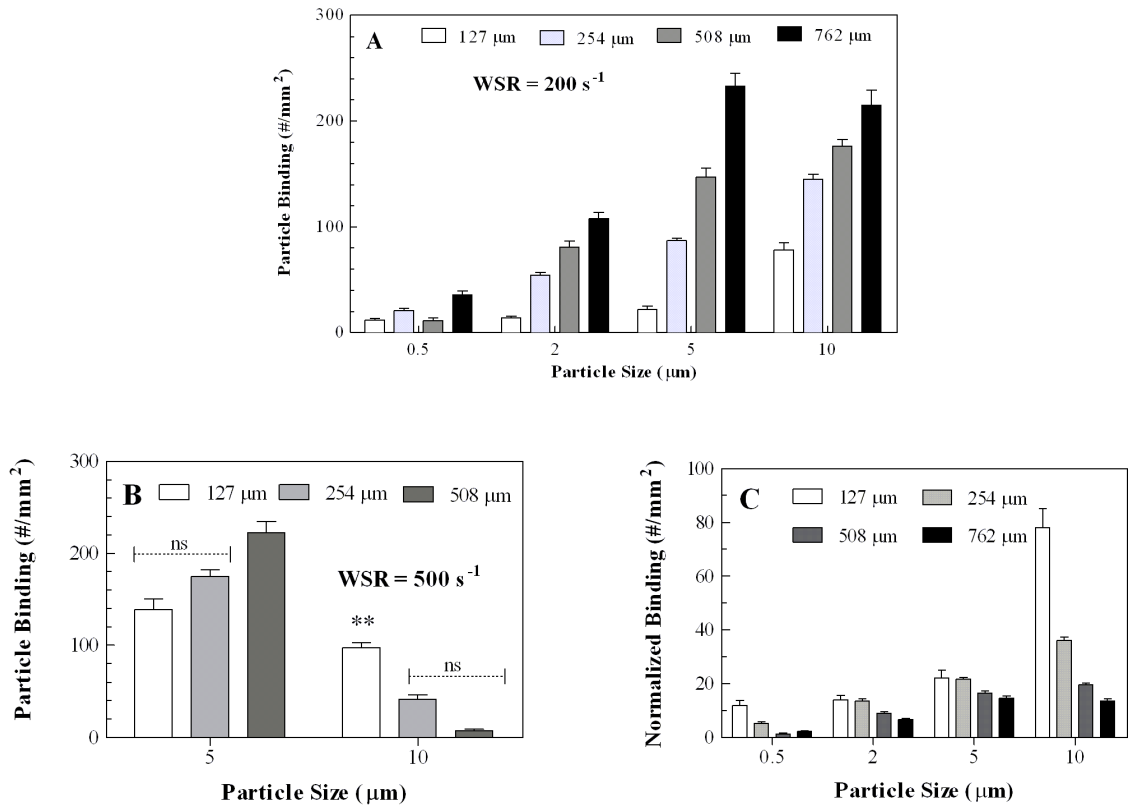
Figure 3.5 Adhesion of sLe^A spheres as a function of channel height. (A) Wall shear rate = 200 s^{-1}, (B) Wall shear rate = 500 s^{-1}. (C) Binding of spheres at different channel heights normalized to the total number of particles introduced into the chamber at each channel height.

Particle concentration fixed at 5x10^5 particles/mL blood. n $\geq$ 3. *ns = not significant and ** = not significant compared to immediate smaller particle size at fixed channel height.

Overall, 0.1 (not shown) and 0.5 μm spheres showed minimal levels of adhesion at most channel heights: there was no significant difference in adhesion levels seen at the different heights tested. Data reported in the previous section suggested that particle adhesion in blood flow was strongly dependent on the magnitude of WSR in the chamber. Thus, it is likely that the trend in adhesion with changing channel height is coupled to the magnitude of the fixed WSR. To verify this, adhesion of 5 and 10 μm particles (sizes most vulnerable to WSR) at various channel height was observed at 500 s^{-1}. The data presented in Fig 3.5B, showed a reversal in adhesion trend seen for 10 μm particles as the channel height increased. While adhesion trend remained the same for 5 μm particles at 500 s^{-1}, the magnitude of increase in adhesion with an increase in channel height at this WSR was smaller than seen at 200 s^{-1}. To better understand the increase in particle adhesion with increase in channel height, the data in Fig. 3.5A was normalized to the total number of particles introduced into the flow chamber at each channel height. Normalized particle adhesion remain the same or decreased as the channel height increased from 127 to 762 μm as shown in Fig. 3.5C Again, when adhesion assays were conducted with particles in saline buffer, adhesion was either the same or lower for all particles as the channel height increased similar to the data in Fig. 3.4 (data not shown).

3.2.5   Effect of gravity on particle adhesion

Since adhesion in the horizontal chamber occurs in the direction of gravity, it is possible that the higher adhesion with larger particles is due to their larger weight (i.e. gravity). Thus, experiments were conducted in inverted and vertical channels to assess the potential contribution of gravity to particle adhesion from blood flow. Fig. 3.6A

shows adhesion levels as a function of particle size and channel height in an inverted chamber where particle interaction with aECs monolayer occurred against gravity. For this setup, minimal particle adhesion was seen at the 127 μm height for all particle sizes tested in blood. A channel height increase to 254 μm resulted in a significant increase in binding for particles 2 μm or larger. A further increase in channel height to 508 μm similarly resulted in a significant increase in adhesion for these particles. Overall, the adhesion at heights larger than 127 μm increased with increasing particle diameter (0.5 to 10 μm). When WSR in the inverted chamber was varied from 200 to 500 s^{-1} at a fixed channel height, particle binding to the aEC monolayer followed the same trend as seen in the upright chamber (i.e. adhesion in the direction of gravity), where higher adhesion levels were recorded at 500 s^{-1} when compared to that at 200 s^{-1} only for particles 5 μ m or smaller (Fig. 3.6B). Control experiments with particles in saline or plasma with no RBCs (Fig. 3.6A - insert) yielded no particle adhesion to the wall in the inverted chamber for all particle sizes and channel heights studied. Particle adhesion in the vertical chamber was also similar to that in upright and inverted chambers with adhesion increasing with an increase particle diameter at 254 μm channel height and 200 s^{-1} (Fig. 3.7). Again, increasing the WSR within the chamber to 500 s^{-1} showed particle adhesion increasing with an increase in particle size up to 5 μm. There was also no significant difference in adhesion levels seen between adhesion in upward and downward flow for all particles tested in the vertical chamber (data not shown). Overall, the magnitude of particle binding in the inverted or vertical chamber was mostly the same as that seen in the horizontal channel (Figs. 3.3 and 3.5). A significant difference in binding was only seen with 5 and 10 μ m particles at low channel heights/WSRs in the inverted chamber.
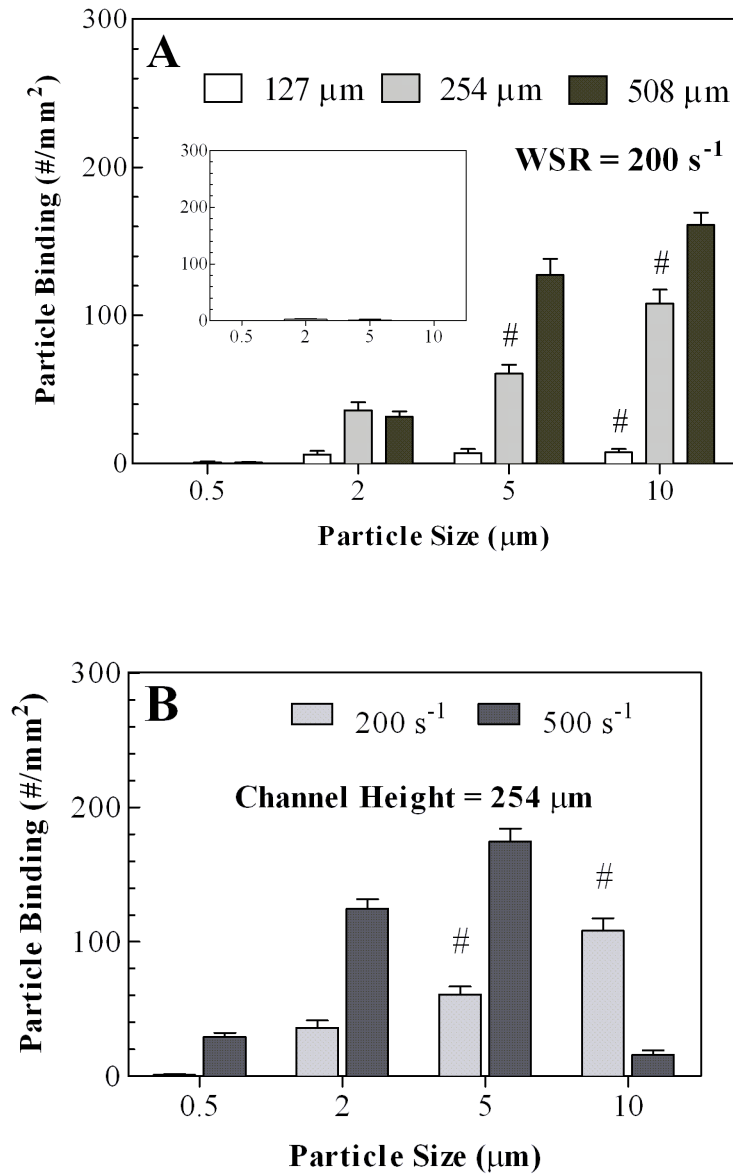
Figure 3.6 Adhesion of sLe[A]-spheres from blood flow to aEC monolayer in an inverted PPFC (adhesion in the anti-gravity direction) as a function of (A) channel heights at 200 s^{-1} (B) shear rate at 254 μm channel height. Insert A = Adhesion of sLe[A]-spheres in plasma with no red blood cells in an inverted PPFC at 254 μm channel height (control experiment).

Particle concentration fixed at 5×10^5 particles/mL blood. $n \geq 3$ and # = $p < 0.05$ compare to adhesion in horizontal flow channel.
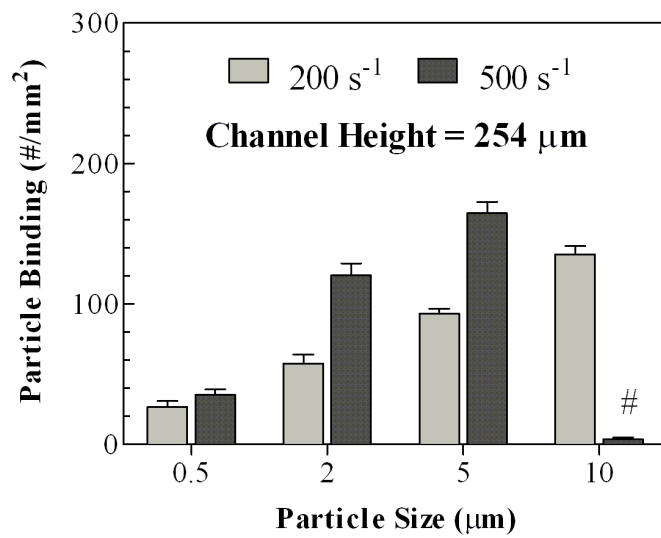
Figure 3.7 Adhesion of sLe^A-spheres from blood flow to aEC monolayer as a function of
wall shear rate in a vertically oriented PPFC with upward flow (adhesion in
the lateral direction).

Channel height = 254 μm. Particle concentration fixed at 5x10^5 particles/mL
blood. n ≥ 3 and # = p < 0.05 compare to adhesion in horizontal flow channel.

3.3 Discussion

Of the many physiological processes regulated by the endothelium, inflammation - a normal host response to tissue injury - is of particular interest for vascular targeting due to its known involvement in the pathogenesis of several human diseases, including atherosclerosis [25]. Selectins, ICAM-1 and VCAM-1 are the biological molecules primarily expressed by endothelial cells during inflammation to help recruit leukocytes to the vascular wall – a hallmark of inflammation response. Many researchers have explored targeting therapeutics to the vascular wall in human diseases via inflammation and its endothelial-expressed leukocyte adhesion markers (LAMs); where polymeric microspheres conjugated with selectin counter-receptor or antibodies against LAMs show specific interaction with inflamed endothelium from flow both *in vitro* and *in vivo* [26-28]. Most of these works, however, have focused on carrier characteristics or the specificity of targeting ligand. Here, I explore the role of particle size and hemodynamics in the ability of targeted polymeric spheres to adhere to inflamed endothelium from physiological flow *in vitro*. Specifically, polystyrene spheres of different sizes conjugated with sLe[A], a carbohydrate ligand specific to the selectins, were allowed to interact with activated monolayer of human umbilical vein endothelial cells (HUVECs) from blood flow in a PPFC. Similar PPFC adhesion assays have been successfully used to elucidate the biophysics of leukocyte-endothelium interactions [29, 30], and sLe[A] was the molecule of choice for mediating particle adhesion due to its superior capacity for adhesive interaction with the selectins from high shear (fast on-rate) over most antibodies specific to LAMs [31, 32]. Overall, my results show that the efficiency of targeted

particles binding to HUVEC from flow in the presence of blood cells is a function of particle size, channel height and wall shear stress within the flow channel.

Specifically, I found that the adhesion of sLe^A-coated spheres increased as their diameter increased from 0.5 to 10 μm at 200 s^{-1}. Experiments conducted at fixed particle volume concentration in this WSR range resulted in particle volume adhesion levels increasing with an increase in particle diameter (Fig. 3.2B). A conversion of volume adhesion data back to number binding followed by a normalization to the total number of particle fed suggested that particle margination efficiency also increased when particle size increased from 0.5 to 10 μm in this shear range. While it is plausible that margination could be affected by particle concentration in itself (e.g. particle margination efficiency is higher at higher particle concentration), my experiments with particle concentrations between 1 x 10^5 and 5 x 10^6/mL showed that binding increased proportionally with particle concentration (data not shown). This adhesion trend seen at this intermediate WSR agrees with a previous report by Decuzzi et al., where the adhesion (volume and number) of spheres to the wall in low shear (~7.75 s^{-1}) buffer flow increased as the particle diameter increased from 500 nm to 10 μm [12].

As the WSR in my assays increased to high levels (500 – 1500 s^{-1}), the increase in adhesion with an increase in particle size progressively excluded larger particles (Fig. 3.3A). This coupling effect of size and WSR on the adhesion of spherical particles has been previously reported by Goetz et al. [11] and can be explained by the interplay between three processes governing particle margination (delivery from midstream and

binding) to the wall: 1) transport of particle to the wall that is typically regulated by convection and diffusion, 2) reaction between particle ligands and cell surface-expressed receptor at the wall (or forward reaction rate) that is controlled in part by receptor/ligand density and particle slip velocity (i.e. particle translational velocity due to Q and adjusted for wall effect) [33], and 3) detachment of particles that is regulated by WSR and the reverse reaction rate [34]. At constant and adequate receptor and ligand densities, a higher slip velocity and/or a larger particle diameter negatively affects particle binding. Thus, when low WSRs (resulting from low Q) exist in the chamber, localization of particle to the wall dominates (i.e. transport-limited regime – TLR) and appears to favor larger particles (i.e. the slip velocity and disruptive forces that regulate adhesion and detachment are relatively low). Indeed, experiments with a 3- to 6-fold increase in sLe^A site density on particles did not increase adhesion when in the transport-limited WSR range (e.g. binding of 5 μm particles with 800 and 2000 sLe^A sites/μm^2 at 500 s^{-1} – Fig. 3.3B). At higher WSRs, particle adhesion occurs in a "reaction-limited" regime (RLR) where high slip velocities and disruptive forces exist and disproportionately affect larger-sized particles [11] (i.e. larger particles display lower binding relative to smaller ones). Hence, increasing the sLe^A site density on particle size equal to or larger than 2 μm translated to a significant increase in particle binding when in the RLR (e.g. Fig. 3.3B).

This sort of "shear threshold" effect on particle binding is even more evident when exploring the effect of WSR on adhesion for a given particle size. The presented data in Fig. 3.3A shows that particles size equal to or larger than 2 μm displayed increases in their binding with an increase in WSR up to a critical point. Beyond this critical point,

adhesion decreased with further increases in WSR. Overall, the magnitude of the critical WSR decreased as the particle size increased from 2 to 10 μm. A statistical analysis of the adhesion data for nanospheres (two-way ANOVA) suggested that these particles did not display a critical WSR, i.e. particles smaller than 2 μm displayed minimal adhesion for all WSR. While Goetz and co-workers previously defined a transport and reaction-limited adhesion regimes for particles adhesion from buffer flow to reactive surfaces in a PPFC [11], they did not show an increase in particle adhesion with an increase in WSR for particles of similar sizes and WSR range (75 - 600 s^{-1}) as studied here (i.e. no occurrence of critical WSR). The most notable differences between my study and one by Goetz and co-workers are in the type (and possibly density) of adhesion ligand used (PSGL-1 versus sLe^A) and the absence of RBCs in their adhesion assays. Though differences in ligand type and/or density are plausible reasons for the differences in the observed trend for particle adhesion, I find that the existence of a critical shear for particle binding disappeared when adhesion occurred in saline buffer (absence of RBCs) at the same WSR range studied by Goetz and co-workers (Fig. 3.4). Thus, it could be concluded that the shear threshold effect at a fixed particle diameter and the overall adhesion trend reported herein result from the presence of RBCs in flow.   Indeed, several investigators have reported that RBCs interaction with particles or cells in blood flow affect the adhesion of the latter to reactive surfaces both *in vitro* and *in vivo*, where enhanced particle/cell margination is seen in the presence of RBCs [14, 35, 36]. However, many of these reports have focused on the effect of blood hematocrit levels and RBC aggregation on particle/cell binding. Very limited works have evaluated the effect of shear on the magnitude of particle/cell margination to the vessel wall from blood flow.

56

In one work, Eckstein and co-workers reported that the localization of non-targeted spheres to the wall or "near wall excess (NWE)" in the presence of RBCs increased with an increase in WSR up to 400 s^{-1} in a 100 μm diameter channel and found that particles smaller than 2 μm did not show NWE at all conditions studied [19]. Their study, however, was done at a 15% Hct – hemorheology and the level of leukocyte margination changes with variation in blood hematocrit up to 30% Hct [35]. Jain and co-workers, however, reported that the efficiency of lymphocyte adhesion to the wall from blood flow (~30% Hct) decreased with an increase in WSR with no obvious evidence of lymphocyte NWE [37]. Similarly, adhesive dynamics simulation by Chang and Hammer showed a decrease in cell adhesion with increasing WSR; however, their study focused on a WSR range (1 - 12 s^{-1}) much lower than studied herein [33].

Thus, the question remains: what is responsible for the shear threshold effect on particle binding? While it is likely that the shear threshold at fixed particle sizes seen herein is due to the biphasic response of reaction rate to WSR (i.e. force loading on receptor-ligand bond), shear threshold effect relating to receptor-ligand reaction rates for particle/cell adhesion in the presence or absence of RBCs have only been repeatedly shown for interactions involving L- and P-selectins [23, 24, 38, 39]. Particle adhesion to aEC as reported herein is via E-selectin, i.e. minimal expression of P-selectin occurs with IL-1β activation for 4-hr [40], and L-selectin is only found on leukocytes. Also, the fact that particle adhesion did not respond to increases in sLe^A site density (improved reaction rate) in the TLR suggests that RBC-induced particle localization to the wall is not enhanced at higher WSR. Lipowsky and Pearson previously reported a similar

57

observation with leukocytes where little change in the *in vivo* margination of these cells was seen with increasing shear [36]. Instead, I suggest that the effect of particle binding with WSR at fixed particle sizes reported here is likely due to physical interactions between RBCs and targeted particles as previously suggested by Jain and co-workers [37]. Specifically, separate from the initial RBC-mediated localization of particles to the wall, RBC collision with particles in the plasma layer (RBC-free layer) produces a normal acting adhesive force that enhances particle collision with the wall and their subsequent adhesion. Thus, when in the transport-limited adhesion regime, the excess RBC-generated force aids particles in overcoming the increasing slip velocity and disruptive forces resulting from increases in flow velocity and WSR, respectively. This, in turn, helps particles maintain the same binding efficiency with increasing WSR in this regime (e.g. adhesion efficiency of 5 μm spheres from 200 – 500 s^{-1}; Fig. 3.3C). The maintained adhesion efficiency then results in higher binding with higher WSR since a higher number of particles enter the flow chamber per time at higher WSRs. In addition to their lack of NWE as previously suggested [19], it is likely that particles smaller than 2 μm did not respond to increases in WSR due to their minimal physical interaction with RBCs since they are significantly smaller than the height of the plasma layer (~2 - 12 μm in height [14, 41]).

Adhesion assays in horizontal chambers with varying channel height at a fixed WSR of 200 s^{-1} also showed particle fluxes increasing with increases in channel height from 127–762 μm for all particles greater than 2 μm. However, the normalization of particle binding to the number of particles passing over a fixed area showed that the

efficiency of particle binding decreased with most channel height increase for all particle sizes studied herein. This decrease in binding efficiency with an increase in channel height may in part be due to a higher particle slip velocity at fixed WSR as the channel increases.

Adhesion assays in inverted and vertical chambers showed similar adhesion trends as seen with assays in horizontal channel for all particle sizes. This observation suggests minimal contribution of gravity to particle localization to the wall. The lack of significance in the magnitude of particle adhesion to the wall observed in vertical and horizontal chambers reported herein agrees with a previous report by Abbitt and Nash [42]. While this observed similarity in particle (and cells) adhesion between these two chamber orientations may suggest gravity does not play a role in adhesion in horizontal channels, the significant decrease in adhesion observed for large particles (5 and 10 μm) in the inverted versus horizontal chamber may suggest otherwise. However, it is likely that the significant decrease in adhesion seen in inverted chambers is related to potential differences in the characteristics of the RBCs-free plasma layer between the top and bottom of the PPFC. Reports in the literature have shown that the average plasma layer thickness can differ significantly between the top and bottom wall in a horizontally aligned channel or vessel *in vivo* [43, 44].

References

1. Bicknell R. Vascular targeting and the inhibition of angiogenesis. Annals of Oncology. 1994;5:45-50.

2. Schnitzer JE. Vascular targeting as a strategy for cancer therapy. New England Journal of Medicine. 1998;339(7):472-474.

3. Bendas G, Krause A, Schmidt R, Vogel J, Rothe U. Selectins as new targets for immunoliposome-mediated drug delivery A potential way of anti-inflammatory therapy. Pharmaceutica Acta Helvetiae. 1998;73:19-26.

4. Sakhalkar HS, Dalal MK, Salem AK et al. Leukocyte-inspired biodegradable particles that selectively and avidly adhere to inflamed endothelium in vitro and in vivo. Proceedings of the National Academy of Sciences. 2003;100:15895-15900.

5. Muzykantov VR, Christofidou-Solomidou M, Balyasnikova I et al. Streptavidin facilitates internalization and pulmonary targeting of an anti-endothelial cell antibody (platelet-endothelial cell adhesion molecule 1): a strategy for vascular immunotargeting of drugs. Proceedings of the National Academy of Sciences. 1999;96(5):2379-2384.

6. Moghimi SM, Porter CJH, Muir IS, Davis SS, ILLUM L. Non-phagocytic uptake of intravenously injected microspheres in rat spleen: influence of particle size and hydrophilic coating. Biochemical and biophysical research communications(Print). 1991;177:861-866.

7. Anderson SA, Rader RK, Westlin WF et al. Magnetic resonance contrast enhancement of neovasculature with $\alpha_v\beta_3$-targeted nanoparticles. Magnetic Resonance in Medicine. 2000;44:433-439.

8. Kiani MF, Yuan H, Chen X, Smith L, Gaber MW, Goetz DJ. Targeting microparticles to select tissue via radiation-induced upregulation of endothelial cell adhesion molecules. Pharmaceutical Research. 2002;19:1317-1322.

9. Abra RM, Hunt CA. Liposome disposition in vivo. III. Dose and vesicle-size effects. Biochimica et biophysica acta. 1981;666:493.

10. Decuzzi P, Lee S, Bhushan B, Ferrari M. A theoretical model for the margination of particles within blood vessels. Annals of biomedical engineering. 2005;33:179-190.

11. Patil VRS, Campbell CJ, Yun YH, Slack SM, Goetz DJ. Particle diameter influences adhesion under flow. Biophysical Journal. 2001;80:1733-1743.

12. Gentile F, Curcio A, Indolfi C, Ferrari M, Decuzzi P. The margination propensity of spherical particles for vascular targeting in the microcirculation. J Nanobiotechnology. 2008;6:9.

13. Goldsmith HL, Marlow JC. Flow behavior of erythrocytes. J Colloid Interface Sci. 1979;71:466-478.

14. Munn LL, Melder RJ, Jain RK. Role of erythrocytes in leukocyte-endothelial interactions: mathematical model and experimental validation. Biophys J. 1996;71:466-478.

15. Deosarkar SP, Malgor R, Fu J, Kohn LD, Hanes J, Goetz DJ. Polymeric particles conjugated with a ligand to VCAM-1 exhibit selective, avid, and focal adhesion to sites of atherosclerosis. Biotechnology and Bioengineering. 2008;101

16. Kaufmann BA, Sanders JM, Davis C et al. Molecular imaging of inflammation in atherosclerosis with targeted ultrasound detection of vascular cell adhesion molecule-1. Circulation. 2007;116:276.

17. Migliorini C, Qian YH, Chen H, Brown EB, Jain RK, Munn LL. Red blood cells augment leukocyte rolling in a virtual blood vessel. Biophysical journal. 2002;83:1834-1841.

18. Aarts PA, van den Broek SA, Prins GW, Kuiken GD, Sixma JJ, Heethaar RM. Blood platelets are concentrated near the wall and red blood cells, in the center in flowing blood. Arteriosclerosis. 1988;8:819-824.

19. Eckstein EC, Tilles AW, Millero FJr. Conditions for the occurrence of large near-wall excesses of small particles during blood flow. Microvasc Res. 1988;36:31-39.

20. Nagaoka T, Yoshida A. Noninvasive evaluation of wall shear stress on retinal microcirculation in humans. Invest Ophthalmol Vis Sci. 2006;47:1113-1119.

21. Koutsiaris AG, Tachmitzi SV, Batis N et al. Volume flow and wall shear stress quantification in the human conjunctival capillaries and post-capillary venules in vivo. Biorheology. 2007;44:375-386.

22. Decuzzi P, Ferrari M. The adhesive strength of non-spherical particles mediated by specific interactions. Biomaterials. 2006;27:5307-5314.

23. Lawrence MB, Kansas GS, Kunkel EJ, Ley K. Threshold levels of fluid shear promote leukocyte adhesion through selectins (CD62L,P,E). J Cell Biol. 1997;136:717-727.

24. Greenberg AW, Brunk DK, Hammer DA. Cell-free rolling mediated by L-selectin and sialyl Lewis(x) reveals the shear threshold effect. Biophys J. 2000;79:2391-2402.

25. Bevilacqua MD, Ph. D, MP, Nelson PD, RM, Mannori MD, Ph. D, G, Cecconi MD, O. Endothelial-leukocyte adhesion molecules in human disease. Annual review of medicine. 1994;45:361-378.

26. Eniola AO, Hammer DA. Characterization of biodegradable drug delivery vehicles with the adhesive properties of leukocytes II: effect of degradation on targeting activity. Biomaterials. 2005;26:661-670.

27. Muro S, Garnacho C, Champion JA et al. Control of endothelial targeting and intracellular delivery of therapeutic enzymes by modulating the size and shape of ICAM-1-targeted carriers. Mol Ther. 2008;16:1450-1458.

28. Sakhalkar HS, Hanes J, Fu J et al. Enhanced adhesion of ligand-conjugated biodegradable particles to colitic venules. FASEB J. 2005;19:792-794.

29. Eniola-Adefeso O, Huang RB, Smith CW. Kinetics of LFA-1 mediated adhesion of human neutrophils to ICAM-1--role of E-selectin signaling post-activation. Ann Biomed Eng. 2009;37:737-748.

30. Green CE, Schaff UY, Sarantos MR, Lum AF, Staunton DE, Simon SI. Dynamic shifts in LFA-1 affinity regulate neutrophil rolling, arrest, and transmigration on inflamed endothelium. Blood. 2006;107:2101-2111.

31. Chen S, Alon R, Fuhlbrigge RC, Springer TA. Rolling and transient tethering of leukocytes on antibodies reveal specializations of selectins. Proc Natl Acad Sci U S A. 1997;94:3172-3177.

32. Ham AS, Goetz DJ, Klibanov AL, Lawrence MB. Microparticle adhesive dynamics and rolling mediated by selectin-specific antibodies under flow. Biotechnol Bioeng. 2007;96:596-607.

33. Chang KC, Hammer DA. The forward rate of binding of surface-tethered reactants: effect of relative motion between two surfaces. Biophys J. 1999;76:1280-1292.

34. Slack SM, Turitto VT. Fluid dynamic and hemorheologic considerations. Cardiovasc Pathol. 1993;2:11S-21S.

35. Abbitt KB, Nash GB. Rheological properties of the blood influencing selectin-mediated adhesion of flowing leukocytes. American Journal of Physiology- Heart and Circulatory Physiology. 2003;285:229-240.

36. Pearson MJ, Lipowsky HH. Influence of erythrocyte aggregation on leukocyte margination in postcapillary venules of rat mesentery. Am J Physiol Heart Circ Physiol. 2000;279:H1460-71.

37. Melder RJ, Munn LL, Yamada S, Ohkubo C, Jain RK. Selectin- and integrin-mediated T-lymphocyte rolling and arrest on TNF-alpha-activated endothelium: augmentation by erythrocytes. Biophys J. 1995;69:2131-2138.

38. Evans E, Leung A, Heinrich V, Zhu C. Mechanical switching and coupling between two dissociation pathways in a P-selectin adhesion bond. Proc Natl Acad Sci U S A. 2004;101:11281-11286.

39. Caputo KE, Lee D, King MR, Hammer DA. Adhesive dynamics simulations of the shear threshold effect for leukocytes. Biophys J. 2007;92:787-797.

40. Bevilacqua MP. Endothelial-leukocyte adhesion molecules. Annu Rev Immunol. 1993;11:767-804.

41. Sharan M, Popel AS. A two-phase model for flow of blood in narrow tubes with increased effective viscosity near the wall. Biorheology. 2001;38:415-428.

42. Abbitt KB, Nash GB. Characteristics of leucocyte adhesion directly observed in flowing whole blood in vitro. Br J Haematol. 2001;112:55-63.

43. Pappu V, Bagchi P. Hydrodynamic interaction between erythrocytes and leukocytes affects rheology of blood in microvessels. Biorheology. 2007;44:191-215.

44. Kim S, Kong RL, Popel AS, Intaglietta M, Johnson PC. Temporal and spatial variations of cell-free layer width in arterioles. Am J Physiol Heart Circ Physiol. 2007;293:H1526-35.

CHAPTER 4

TARGETING THERAPEUTICS TO THE VASCULAR WALL IN ATHEROSCLEROSIS – CARRIER SIZE MATTERS

ABSTRACT

Vascular-targeted imaging and drug delivery systems are promising for the treatment of atherosclerosis due to the vast involvement of endothelium in the initiation and growth of plaque. Herein, I investigated the role of particle size in dictating the ability of vascular-targeted spherical particles to interact with the vascular wall from pulsatile and recirculating human blood flow relevant in atherosclerosis. *In vitro* parallel plate flow chambers (PPFC) with straight or vertical step channel were used to examine the localization and binding efficiency of inflammation-targeted polymeric spheres sized from 0.2 to 5 μm to inflamed endothelium from disturbed reconstituted and whole blood flow. The efficiency of particle binding in disturbed reconstituted blood flow increases as spherical diameter increases from 500 nm to 5 μm. No significant difference was observed between adhesion of 200 nm and 500 nm spheres. Binding efficiency for all particle size was enhanced in disturbed whole blood flow except adhesion of 5 μm in pulsatile whole blood. The presented data shows that the binding efficiency of vascular-

targeted drug carriers in blood flow is a function of particle size, wall shear rate, flow type, blood composition and ligand characteristics. Overall, the presented results suggest that micron-sized spherical particles (2 μm), not *nano*spheres, are optimal for vascular-targeted drug delivery applications in medium to large vessel relevant in atherosclerosis.

4.1 Introduction

Atherosclerosis is the major cause of coronary artery disease – the leading cause of mortality in the US [1]. Current treatments for atherosclerosis include oral statins aimed at reducing high cholesterol (LDL) levels and surgical interventions such as balloon angioplasty and stent placement. However, acute coronary events can still occur in patients who have undergone aggressive statin therapy [2], and surgical intervention does not address the underlying cause of the disease and thus cannot prevent reoccurrence of stenosis. Consequently, targeted imaging and drug delivery systems have gained interest as a means to improve current therapies [3]. Imaging modalities for atherosclerosis are typically focused on noninvasive detection of the disease state, which can allow for better understanding of disease pathology and thus offer opportunities for more effective treatments. Similarly, targeted drug delivery can offer a high drug efficacy at target site while minimizing side effects often associated with systemic delivery. Overall, previous works exploring imaging and drug targeting in atherosclerosis have focused on targeting vascular wall (VW) expressed molecules associated with plaque rupture, such as fibrin [4, 5], and inflammation (e.g. selectins, ICAM-1 and VCAM-1) [6-8]. Regardless of the adhesion moiety targeted, the overall efficacy of vascular-targeted therapies depends on the ability of carriers to marginate (localize and adhere) to the VW in sufficient density similar to the margination of white blood cells [9] prescribed by hemorheology and hemodynamics [10].

Limited works in the literature have focused on the ability of targeted *nano*spheres, commonly proposed carriers, to interact with the VW in disturbed flow – an important consideration for the design of effective vascular-targeted therapy for

atherosclerosis which preferentially affects arteries in areas with high disturbance in blood flow (e.g. where low average wall shear, pulsatility and blood recirculation co-exist) [11]. Existing studies of vascular-targeted carriers have investigated binding dynamics only in laminar buffer flow [12] and most have focused on microspheres only [13, 14]. Published *in vivo* works of nanospheres targeting the VW have mostly focused on capillary beds/post-capillary venules where the role of hemorheology is likely minimal [15]. Works describing nanospheres binding to the wall in large vessels [6, 16] have either been with spheres injected directly to the wall and/or have not evaluated binding as a function of particle size. I recently reported that the binding efficiency of vascular-targeted spheres in laminar blood flow directly correlated with their size [17, 18]; however, this trend may not necessarily extend to particle dynamics in disturbed blood flow relevant in atherosclerosis. Here, I present data for the binding dynamics of inflammation-targeted polystyrene (PS) spheres of nanometer to micrometer size to the endothelium in disturbed blood flow via *in vitro* assays with human blood.

4.2 Results

The experimental set up used in this chapter is described in detail in Chapter 2.

4.2.1 Adhesion of spheres in pulsatile flow

Sialyl-Le^A, aICAM, and aVCAM-coated spheres suspended in reconstituted blood specifically bind to activated endothelial cell (aEC) monolayers from pulsatile flow. Fig. 4.1A shows that the level of sLe^A-sphere adhesion increased with increasing spherical diameter from 0.5 to 5 μm for pulsatile profiles I and II. No significant difference was observed between adhesion of 200 nm and 500 nm spheres. Overall, sLe^A-nanosphere

adhesion was ~ 4-11 and ~ 4-13 fold lower than that of microsphere adhesion in pulsatile profile I and II, respectively. Normalization of binding by the total number of particles introduced into the PPFC indicated that there was no significant difference in particle binding between the two pulsatile profiles (data not shown). Both types of pulsatile flow improved particle adhesion for all sizes compared to binding in laminar flow at the same peak shear rates and at a fixed total number of particles as shown in Fig. 4.1B (i.e. 15 mins of pulsatile profile I flow compared to 5 mins of laminar flow at 1000 s^{-1}, and 5 mins of profile II flow compared to 2 mins of laminar flow at 1200 s^{-1} – fixed blood volume). Only firm adhesion (no rolling) was observed for all sLe^A-coated spheres at the site density used.

Antibody coated spheres did not adhere in profile I flow with peak WSR at 1000 s^{-1} (not shown). At 500 s^{-1} of peak WSR, aICAM-spheres displayed similar adhesion trend to the ones observed with sLe^A-spheres (Fig. 4.1C), i.e. aICAM-nanospheres displayed 5-10 fold lower adhesion than microspheres. Also, adhesion in pulsatile flow was enhanced ~2 fold for 0.5-2 μm aICAM-spheres and 50 fold for the 5 μm spheres compared to adhesion in laminar flow at 500 s^{-1} (data not shown). The binding of aVCAM-coated spheres was minimal at 500 s^{-1} of peak WSR. At 200 s^{-1}, 500 nm aVCAM-spheres had a 3.4 fold lower binding density at the wall than aVCAM microspheres. There was no significant difference in binding densities between 2 and 5 μm aVCAM-spheres (Fig. 4.1D).
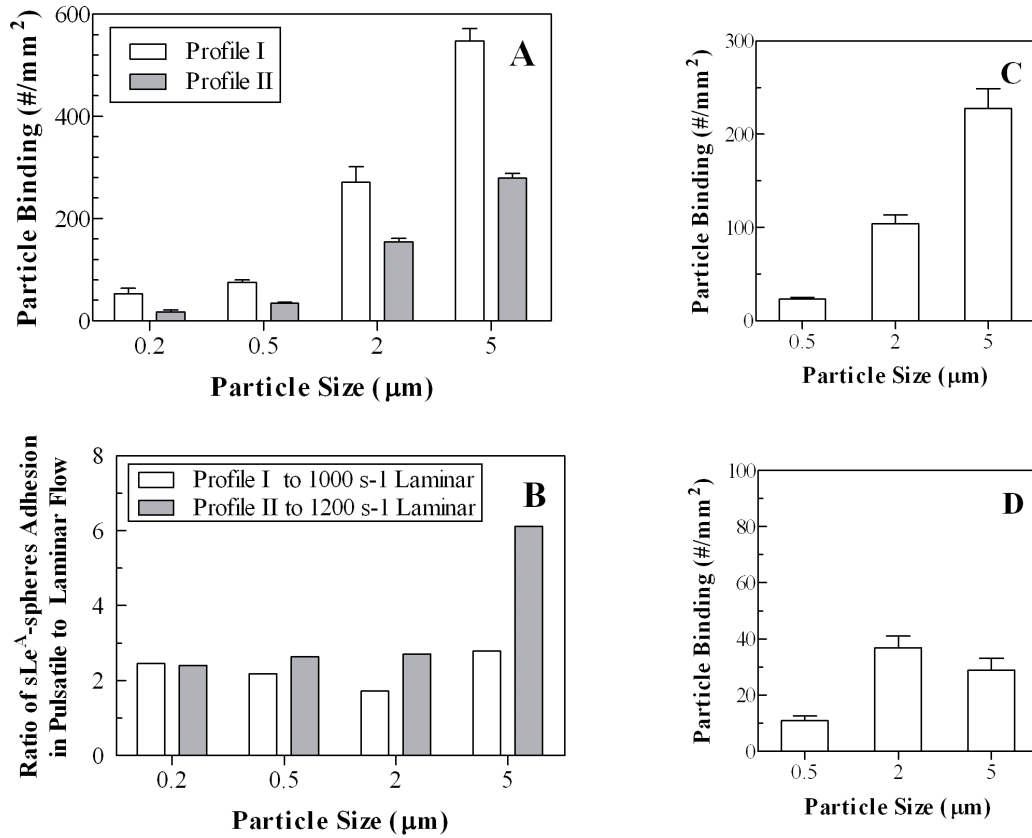
Figure 4.1 (A) sLe^A-spheres binding in pulsatile reconstituted blood flow (open bar = profile I at peak WSR = 1000 s^{-1} and shaded bar = profile II). (B) Ratio of sLe^A-spheres adhesion in pulsatile flow to adhesion in laminar flow at peak shear rates (1000 s^{-1} for profile I and 1200 s^{-1} for profile II). (C) anti-ICAM-1 and (D) anti-VCAM-1 coated spheres binding in pulsatile reconstituted blood flow (profile I) with peak WSR at 500 s^{-1} and 200 s^{-1}, respectively.

4.2.2 Adhesion of spheres in recirculating flow

Particle binding in recirculating reconstituted blood was observed in the VSFC. At 200 s^{-1}, the adhesion of 2 and 5 μm spheres increased with distance from the step up to just beyond the reattachment point (observed at 170 μm from step – see Chapter 2) and then decreased along the channel length to far downstream (Fig. 4.2A). No obvious peak in adhesion was observed for nanospheres. The ratio of peak adhesion for microspheres to their adhesion levels at far downstream appears to directly correlate with size. Specifically, the "peak to far downstream" adhesion ratio was 2.4 and 3.6 for 2 and 5 μm spheres, respectively.   There was no significant difference in the "peak to far downstream" ratios between 200 and 500 nm spheres (1.5 and 1.2 respectively) but these ratios were significantly lower than observed with microspheres.   Furthermore, the adhesion of all sLe^A spheres at the far downstream region (laminar flow regime [19]) was significantly higher compared with the adhesion of the same particles in laminar flow in channels with no step at the same height and WSR (see Fig. 6A in [18]).   Overall, nanosphere adhesion at 200 s^{-1} was 6-20 fold <u>lower</u> than that of microspheres at peak adhesion and 3-6 fold lower at far downstream. A similar trend was observed for particle adhesion in VSFC at 500 s^{-1} as shown in Fig. 4.2B. Microsphere adhesion peaked between 400 and 500 μm (reattachment point at 400 μm from step), and the adhesion of nanospheres was ~15-25 fold <u>lower</u> than that of microspheres at peak adhesion.   Only firm adhesion was observed for all sLe^A-spheres in the VSFC.
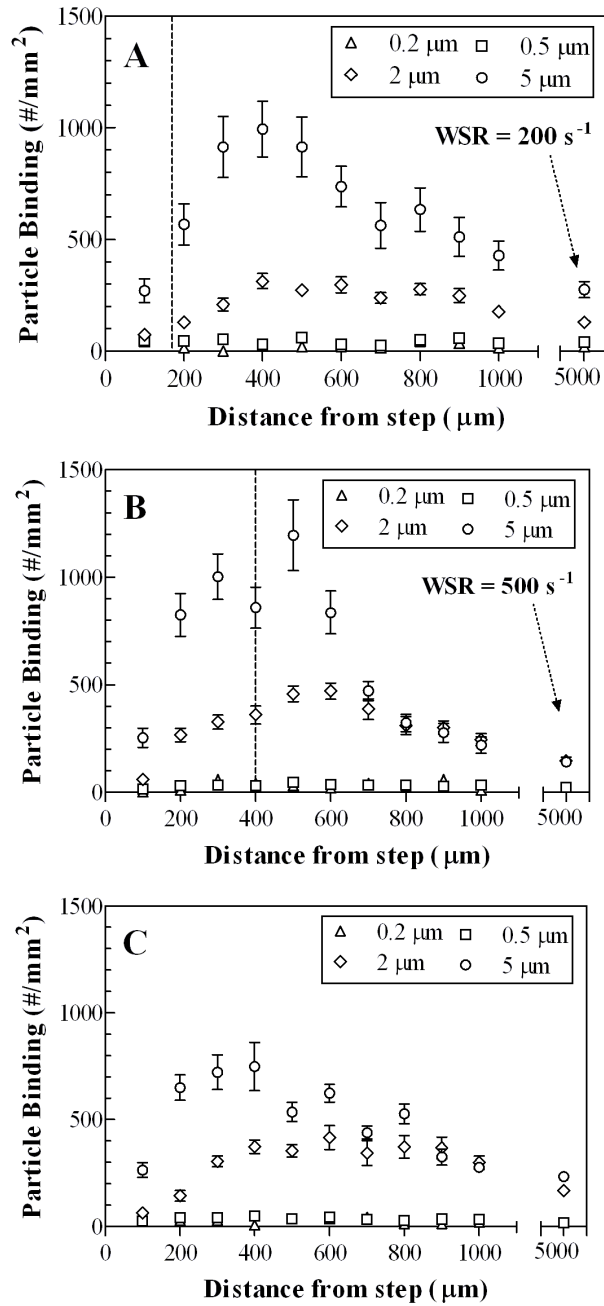
Figure 4.2 sLe[A]-coated spheres binding in the VSFC with reconstituted blood flow. Far downstream conditions is (A) 200 s^{-1} of laminar shear, (B) 500 s^{-1} of laminar shear, and (C) pulsatile profile II (average WSR = 480 s^{-1}). Dash line represents observed reattachment point.

4.2.3 Adhesion of spheres in combined pulsatile and recirculating flow

Microspheres did not show any obvious peak in their adhesion in pulsatile reconstituted blood flow in the VSFC (Fig. 4.2C) likely due to the fluctuation of the reattachment point with changes in WSR of the pulsing flow. Nanosphere adhesion was ~7-21 fold lower at peak adhesion relative to microsphere adhesion with pulsatile flow in the step channel. When compared to adhesion under laminar flow in the same VSFC and average WSR of ~500 s^{-1} (Fig. 4.2B), pulsatility did not enhance microsphere adhesion in the recirculation region (Fig. 4.2C). Far downstream adhesion in the VSFC was significantly different between pulsatile (Fig. 4.2C) and laminar flow (Fig. 4.2B) only for 5 μm spheres.

4.2.4 Adhesion of spheres in whole blood flow

As in reconstituted blood experiments, sLe^A microspheres displayed higher binding than nanospheres in pulsatile (profile I) whole blood flow (~45% Hct; Fig. 4.3A). However, 2 μm spheres showed significantly higher adhesion than 5 μm spheres. Overall, the adhesion of 0.2, 0.5 and 2 μm sLe^A spheres in pulsatile whole blood flow was significantly higher (~2–4 fold) than levels observed in reconstituted blood at 30% Hct (Fig. 4.1A). No difference in adhesion was observed for 5 μm sLe^A spheres between whole and reconstituted pulsatile blood flow. The amount of white blood cells (WBCs) bound to ECs along with spheres was statistically the same (~2500 site/μm^2) for all particle sizes (data not shown).
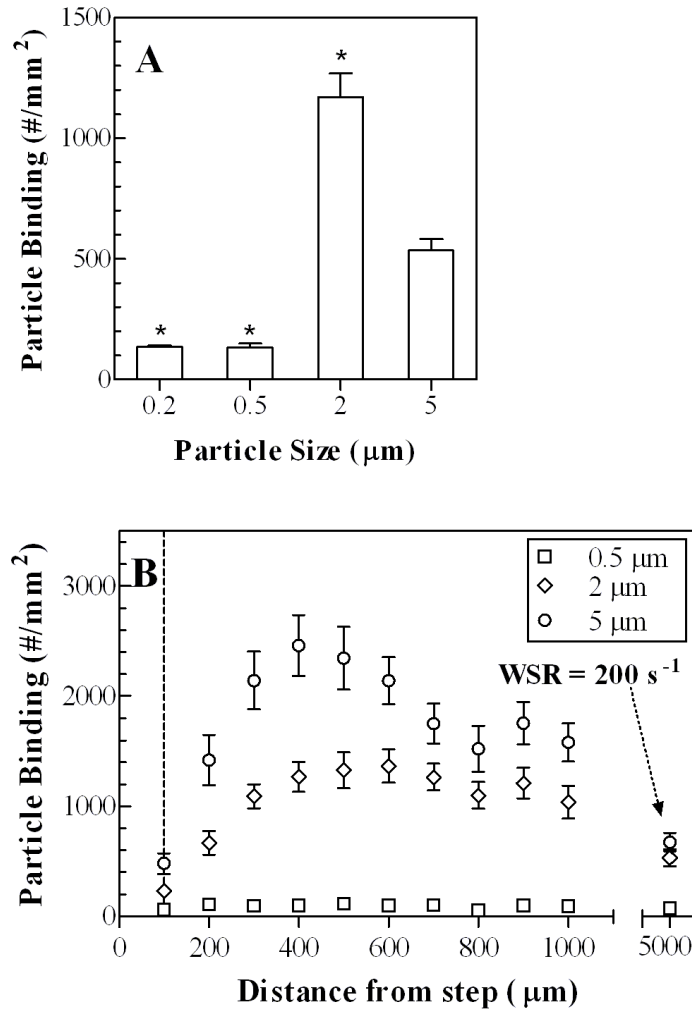
Figure 4.3 sLe^A-coated spheres binding in whole blood. (A) Pulsatile (profile I) flow in the straight channel PPFC and (B) steady flow at 200 s^{-1} (main chamber) in the VSFC. * = Significant increase in particle binding relative to adhesion in pulsatile (profile I) reconstituted blood flow for particles of the same sizes. Dash line represents observed reattachment point.

Microspheres still displayed significantly higher adhesion than nanospheres for whole blood experiments in the VSFC at 200 s^{-1} (Fig. 4.3B). However, unlike pulsatile whole blood flow, 5 μm sLe^A-spheresdisplayed ~2 fold higher adhesion than 2 μm spheres in the recirculation/reattachment region. The difference in adhesion between 2 and 5 μm spheres was not significant at far downstream. Furthermore, all sphere sizes showed higher levels of adhesion when compared to adhesion levels in similar experiments using reconstituted blood (Fig. 4.2A). The gain in whole blood adhesion density for VSFC experiments was the highest for 2 μm spheres (~4 fold compared to 2-3 fold for 0.5 and 5 μm spheres) in all three regions. The adhesion of WBCs was again the same for all particle sizes in all regions of the VSFC (data not shown).

4.3 Discussion

Targeting particles to the vascular wall for drug delivery and/or imaging is of great interest in the treatment of atherosclerosis. Here, I investigated the role of particle size in dictating the ability of polymeric spheres to localize and adhere to inflamed endothelium in physiological flow conditions relevant to atherosclerosis. E-selectin, ICAM-1 and VCAM-1 are known to be overexpressed by endothelial cells (ECs) in atherosclerosis [20]. Others also showed that *in vivo* selectivity to ECs over plaque in mice was greatest when VCAM-1 and selectin were targeted [21, 22]. Thus, I evaluated the binding of 200 nm to 5 μm sLe^A-, anti-ICAM-1 (aICAM), or anti-VCAM-1 (aVCAM) coated polystyrene spheres to activated ECs (aECs) from human reconstituted or whole blood flow *in vitro* with channels of various. Overall, my results showed that

the binding efficiency of vascular-targeted spheres in blood flow is a function of particle size, wall shear rate, flow type, blood composition and ligand characteristics.

Specifically, the adhesion of sLe^A-spheres in pulsatile reconstituted blood flow pulsing about a zero shear (profiles I) or between low and high shear (profile II) increased with particle diameter (from 0.5 to 5 μm; Fig. 4.1A). This suggests that particle margination efficiency increased with increasing spherical diameter since experiments were conducted at a fixed particle flow concentration. The 2-3 fold enhancement of particle adhesion with pulsatile flow in the straight channel PPFC (Fig. 4.1B) directly correlates with the increase in the residence time of particles in the PPFC with pulsatile flow relative to laminar flow, suggesting that increased residence time is likely the major factor contributing to adhesion increase under pulsatile flow. The 6-fold increase in the adhesion of 5 μm spheres in profile II flow relative to their adhesion under laminar flow at the peak WSR of 1200 s^{-1} is likely due to the adhesion limitations faced at this WSR with the sLe^A site density used. I previously showed that at 1200 s^{-1} of laminar shear and ~800 sLe^A sites/μm^2, 5 μm sphere adhesion occurs in a "reaction-limited" regime (RLR) where particles are able to localize to the wall but do not effectively adhere due to high disruptive forces acting on them [18]. Thus, these spheres enjoyed a longer residence time and lower disruptive forces (on average) at the wall in pulsatile profile II relative to laminar flow of the same maximum WSR. The extensive increase in the adhesion of 5 μm aICAM-1 spheres in profile I relative to laminar flow can be similarly explained. Overall, aICAM and aVCAM-spheres displayed lower adhesion (all sizes) than observed for sLe^A-spheres even with the higher antibody site densities on these particles and the lower peak WSRs studied. This is likely due to the

low capture efficiency (i.e. the rate of bond formation) exhibited by the antibody-ICAM-1/VCAM-1 interactions in flow compared to high on-rates that exist for sLe^A-selectin interactions [23].

For adhesion in the VSFC, particle adhesion increased as particle size increased from 0.5 to 5 μm (Fig. 4.2A and Fig. 4.2B). No difference in adhesion was observed between 0.2 and 0.5 μm spheres. Peak microsphere adhesion occurs at the reattachment area due to low parallel shear forces and a maximum normal velocity on the wall [19], consistent with previous reports of platelets (~ 2 μm) and leukocytes (~ 7-15 μm) adhesion in similar VSFC [19, 24]. There also appears to be a significant recirculation-induced redistribution of particles to the wall in VSFC based on the higher particle adhesion far downstream from the step compared to previous observation with straight channel laminar flow (no recirculation) under the same shear conditions [18]. Microspheres also appear to enjoy a higher redistribution to the wall than nanospheres as evidenced in their higher "peak-to-far downstream" adhesion ratios. Overall, pulsatile flow in the VSFC did not enhance adhesion when compared with adhesion in laminar flow at the same average shear in the VSFC (Fig. 4.2B and Fig. 4.2C); it is likely that pulsatile flow disrupts particle distribution associated with the recirculation flow.

The presence of competing leukocytes in whole blood did not prevent spheres from binding – even at their disproportionately higher concentration (~7.5x10^6 neutrophils/mL of blood). The 2 and 4 fold higher adhesion of nano- and 2 μm spheres in pulsatile whole blood (Fig. 4.3A) relative to reconstituted blood (Fig. 4.1A) is likely due to the difference in hematocrit level between the two, ~45% and 30% Hct respectively. Others have previously reported that the width of the cell-free layer (CFL)

that exists near the wall in blood flow decreases with increasing hematocrit due to RBCs occupying more volume inside the channel [25]. A smaller CFL in whole blood flow results in a more direct contact between RBCs and particles, increasing their concentration proximal to the wall, thus promoting higher adhesion. A similar hematocrit effect has been reported for platelet adhesion [26]. No hematocrit effect was seen for adhesion of 5 μm spheres, which is consistent with previous observations for leukocyte (7 − 12 μm in size) adhesion in blood with hematocrit changes in the range studied here [10, 27]. Here, it is likely that the CFL is on the order of the 5 μm size and thus direct contact between RBCs and spheres is disruptive to binding. Interestingly, 5 μm spheres show a significantly higher adhesion density (~2 fold) at higher whole blood hematocrit in the VSFC (Fig. 4.2A and Fig. 4.3B). This may suggest that the rotational motion induced by the sudden expansion at the step creates a different particle distribution pattern in whole blood than present in flows (laminar or pulsing) in straight channels as previously suggested by others [24].

It is also likely that RBC aggregation contribute to the adhesion trend in reconstituted blood relative to whole blood since the ~1.3 wt% dextran used here is in the range of dextran plasma concentrations previously shown to induce RBC aggregration particularly at low shear [28]. However, no significance difference in sLe^A sphere (0.5 and 2 μm) binding densities was observed in preliminary head-to-head comparison between pulsatile profile I assays utilizing blood reconstituted (30% hct) with dextran-free plasma and ones with dextran in plasma as shown in Fig. 4.1 (data not shown). This is not to say that dextran-induced RBC aggregation is absent in my assays. Instead, it is likely that aggregation effects are minimal since targeted particles are exposed to

aggregating conditions, i.e. low shear, for a minimal amount of time (e.g. only ~3 sec in a 21 sec cycle in pulsatile profile I). The presence of physical and/or reactive interactions between targeted spheres and leukocytes present in whole blood but essentially absent in reconstituted blood may also play a role in particle binding, e.g. secondary recruitment of spheres by WBCs already bound to ECs as previously reported for particles and neutrophils [29]. The absence of such an enhancement in the whole blood binding of 5 μm spheres (i.e. no increase in particle binding) may be due to steric hindrance associated with the relative size of these spheres and leukocytes though data obtained for recirculating flow assays suggests otherwise. Overall, detailed experiments are needed to fully elucidate the role of particle-WBC synergy in the adhesion of particles of various sizes in different types of flow.

Overall, my results showed that nanospheres in pulsatile and recirculating blood flow displayed minimal adhesive interaction at the wall relative to microspheres in *in vitro* experiments with human blood. This finding suggests that nanospheres have a much lower margination efficiency in disturbed human blood flow and thus may not be optimum for use as drug carrier or imaging probe in the treatment of atherosclerosis. Instead, spheres with 2 μm diameter appear to be optimum for achieving high margination to the vessels wall in disturbed bulk blood flow.

References

1. Lloyd-Jones D, Adams RJ, Brown TM, et al. Heart disease and stroke statistics-2010 update: a report from the American Heart Association. Circulation 2010;121:e46-e215.

2. Manolopoulos VG, Tavridou A, Adameova A, et al. Drugs Targeting Atherosclerosis: Current and Emerging Approaches. Curr Pharm Des 2009;15:3091-3.

3. Moghimi SM, Hunter AC, Murray JC. Nanomedicine: current status and future prospects. FASEB J 2005;19:311-30.

4. Peters D, Kastantin M, Kotamraju VR, et al. Targeting atherosclerosis by using modular, multifunctional micelles. Proc Natl Acad Sci U S A 2009;106:9815-9.

5. Sirol M, Fuster V, Badimon JJ, et al. Chronic thrombus detection with in vivo magnetic resonance imaging and a fibrin-targeted contrast agent. Circulation 2005;112:1594-600.

6. Deosarkar SP, Malgor R, Fu J, Kohn LD, Hanes J, Goetz DJ. Polymeric particles conjugated with a ligand to VCAM-1 exhibit selective, avid, and focal adhesion to sites of atherosclerosis. Biotechnol Bioeng 2008;101:400-7.

7. Eniola-Adefeso O, Hammer DA. In vitro characterization of leukocyte mimetic for targeting therapeutics to the endothelium using two receptors. Biomaterials 2005;26:7136-44.

8. Weller GER, Villanueva FS, Tom EM, Wagner WR. Targeted ultrasound contrast agents: in vitro assessment of endothelial dysfunction and multi-targeting to ICAM-1 and sialyl Lewisx. Biotechnol Bioeng 2005;92:780-8.

9. Springer TA. Traffic signals for lymphocyte recirculation and leukocyte emigration: the multistep paradigm. Cell 1994;76:301-14.

10. Munn LL, Melder RJ, Jain RK. Role of erythrocytes in leukocyte-endothelial interactions: mathematical model and experimental validation. Biophys J 1996;71:466-78.

11. Ku DN, Giddens DP, Zarins CK, Glagov S. Pulsatile flow and atherosclerosis in the human carotid bifurcation. Positive correlation between plaque location and low oscillating shear stress. Arteriosclerosis 1985;5:293-302.

12. Decuzzi P, Lee S, Bhushan B, Ferrari M. A theoretical model for the margination of particles within blood vessels. Ann Biomed Eng 2005;33:179-90.

13. Eckstein EC, Tilles AW, Millero FJr. Conditions for the occurrence of large near-wall excesses of small particles during blood flow. Microvasc Res 1988;36:31-9.

14. Patil VRS, Campbell CJ, Yun YH, Slack SM, Goetz DJ. Particle diameter influences adhesion under flow. Biophys J 2001;80:1733-43.

15. Lu W, Sun Q, Wan J, She Z, Jiang XG. Cationic albumin-conjugated pegylated nanoparticles allow gene delivery into brain tumors via intravenous administration. Cancer Res 2006;66:11878-87.

16. Chan JM, Zhang L, Tong R, et al. Spatiotemporal controlled delivery of nanoparticles to injured vasculature. Proc Natl Acad Sci U S A 2010;107:2213-8.

17. Huang RB, Mocherla S, Heslinga MJ, Charoenphol P, Eniola-Adefeso O. Dynamic and cellular interactions of nanoparticles in vascular-targeted drug delivery (review). Mol Membr Biol 2010;27:312-27.

18. Charoenphol P, Huang RB, Eniola-Adefeso O. Potential role of size and hemodynamics in the efficacy of vascular-targeted spherical drug carriers. Biomaterials 2010;31:1392-402.

19. Skilbeck C, Westwood SM, Walker PG, David T, Nash GB. Dependence of adhesive behavior of neutrophils on local fluid dynamics in a region with recirculating flow. Biorheology 2001;38:213-27.

20. O'Brien KD, McDonald TO, Chait A, Allen MD, Alpers CE. Neovascular expression of E-selectin, intercellular adhesion molecule-1, and vascular cell adhesion molecule-1 in human atherosclerosis and their relation to intimal leukocyte content. Circulation 1996;93:672-82.

21. Ferrante EA, Pickard JE, Rychak J, Klibanov A, Ley K. Dual targeting improves microbubble contrast agent adhesion to VCAM-1 and P-selectin under flow. J Controlled Release 2009;140:100-7.

22. McAteer MA, Schneider JE, Ali ZA, et al. Magnetic resonance imaging of endothelial adhesion molecules in mouse atherosclerosis using dual-targeted microparticles of iron oxide. Arteriosclerosis, thrombosis, and vascular biology 2008;28:77-83.

23. Lawrence MB, Springer TA. Leukocytes roll on a selectin at physiologic flow rates: distinction from and prerequisite for adhesion through integrins. Cell 1991;65:859-73.

24. Skilbeck CA, Walker PG, David T, Nash GB. Disturbed flow promotes deposition of leucocytes from flowing whole blood in a model of a damaged vessel wall. Br J Haematol 2004;126:418-27.

25. Sharan M, Popel AS. A two-phase model for flow of blood in narrow tubes with increased effective viscosity near the wall. Biorheology 2001;38:415-28.

26. Jordan A, David T, Homer-Vanniasinkam S, Graham A, Walker P. The effects of margination and red cell augmented platelet diffusivity on platelet adhesion in complex flow. Biorheology 2004;41:641-53.

27. Abbitt KB, Nash GB. Rheological properties of the blood influencing selectin-mediated adhesion of flowing leukocytes. Am J Physiol Heart Circ Physiol 2003;285:H229-40.

28. Bishop JJ, Popel AS, Intagliettaa M, Johnsona PC. Rheological effects of red blood cell aggregation in the venous network: a review of recent studies. Biorheology 2001;38:263-74.

29. Walcheck B, Moore KL, McEver RP, Kishimoto TK. Neutrophil-neutrophil interactions under hydrodynamic shear stress involve L-selectin and PSGL-1. A mechanism that amplifies initial leukocyte accumulation of P-selectin in vitro. J Clin Invest 1996;98:1081.

CHAPTER 5

PARTICLE-CELL DYNAMICS IN BLOOD FLOW-
IMPLICATIONS FOR VASCULAR-TARGETED DRUG
DELIVERY

ABSTRACT

The outcome of targeted drug delivery is generally determined from the efficiency of vascular-targeted carriers (VTCs) in localizing and adhering (margination) at the specific targeted sites. Red blood cells (RBCs) and hemodynamics have been shown to dictate VTC behavior in reconstituted blood flow (blood devoid leukocytes and platelets), as discussed in the previous chapters. However, other blood cell components in whole blood may also affect the VTC margination, yet very limited work has been elucidated. Thus, this study aims to investigate the role of leukocytes (WBCs) and platelets on the margination of VTC to the vascular wall under physiological blood flows. Specifically, inflammation-targeted spherical VTCs, 0.2, 0.5, 2, 5 and 10 μm in diameter, were observed for their adhesion on activated endothelial cells via a parallel flow chamber (PPFC) in laminar, pulsatile and recirculating blood flow. In general, the binding density of spheres in whole blood flow is a function of particle size and is primarily dictated by RBCs and WBCs. Specifically, adhesion of nanospheres was minimal compared to

microspheres in all flow types studied. Red blood cell can either promote or hinder particle adhesion depending on the ratio of cell free layer (CFL) width to particle size. Leukocyte tends to prevent microsphere adhesion via (1) competition for the available binding space on endothelial wall and (2) physical interaction (rolling motion) with the previously bound particles that eventually knock them off from the wall. On the other hand, resting platelets have no effect on particle binding due likely to their low adhesion at the wall in this study. Overall, in this work, I elucidate the physical and molecular dynamics of spherical particles with blood cells in physiological blood flow; my results can serve as a road map for designing efficient VTCs for imaging and targeted drug delivery applicable in many human diseases.

5.1 Introduction

The notion of targeted delivery of therapeutics/imaging agents, the process of delivering drugs/imaging agents encapsulated within (or attached to) a carrier to a targeted site, is now a norm in medicine, representing a mainstay in the diagnosis and treatment of many chronic and serious human ailments. In many cases, the vascular wall endothelium (a monolayer of endothelial cells lining the lumen of blood vessels) is the target of such engineered delivery system since it participates in several physiological and pathological processes, including angiogenesis and inflammation [1-3], and represents a direct contact with the bloodstream that is the most common route for carrier entry into the body. The local delivery of anti-angiogenic and pro-angiogenic therapies to the vascular wall in cancer and ischemic cardiovascular diseases, respectively, are classic examples of vascular-targeted drug delivery [4]. Similarly, drug/imaging carriers are often designed to target inflammation afflicted vascular wall in several serious conditions including coronary artery disease stemming from atherosclerosis [5, 6].

Overall, appropriately designed vascular-targeted carriers (VTCs) must possess the capacity to (1) easily navigate the bloodstream while maintaining hemostasis, (2) avoid rapid immune clearance, (3) localize from the bloodstream to the vessel wall in target vessel/organ and (4) bind at the vascular wall via targeting chemistry (target specificity). The first two attributes have been well teased out. For instance, a nanometer size range and surface pegylation significantly improve the *in vivo* circulation of particulate carriers [7], and several publications in the literature have focused on investigating the possible toxicology effect of carriers (particularly nanocarriers) on blood cells such as hemolysis, thrombogenicity and complement activation [8, 9]. The last two of the highlighted

attributes constitute carrier margination (localization and adhesion) but have typically been studied in the context of target specificity only (adhesion) due to the assumption that all particulate carriers can localize to the vascular wall from blood flow. This assumption likely stems from earlier studies showing red blood cells (RBC), the most abundant cell components of blood, promote the adhesion of white blood cells (WBCs) [10, 11], platelet [12, 13] and microparticles [14] by preferentially align at the center of blood flow while pushing other cells or particles to a RBC-free plasma layer (CFL) near the vascular wall. However, we previously demonstrated via *in vitro* parallel plate flow chamber (PPFC) assays with human blood and *in vivo* in a mouse model of atherosclerosis that particle binding from flow to inflamed endothelial cells was enhanced in the presence of human RBCs only for microspheres with diameter greater than 1 μm [15, 16]. Nanospheres at the same particle-surface targeting ligand density as microspheres showed low binding in blood flow due to their high entrapment in the RBC core during blood flow that result in their low localization to the endothelial wall. However, our previous *in vitro* assays were with reconstituted human blood (RBCs in plasma with no platelets or WBCs). Thus, it is not clear whether the observed patterns in reconstituted blood or *in vivo* in mice would translate to adhesion patterns in human whole blood since WBCs and platelets also localized to the CFL area and thus can interact with VTCs to alter their binding.

Indeed, very limited studies have focused on the effects of blood cells, particularly interactions of leukocytes and platelets, on particles/VTCs dynamics in blood flow and their subsequent adhesion at the vascular wall. Existing works investigating the interplay between platelets and leukocytes have shown that activated platelets and leukocytes themselves can enhance leukocyte recruitment to the vascular wall by their molecular

interactions [17, 18]. Though VTCs are often engineered to mimic leukocytes, the interaction of platelets and leukocytes with these carriers and their effect on carrier adhesion to the vascular wall may not necessarily be similar to the ones reported for leukocyte adhesion due to differences in their sizes (particularly at the nano-range) and viscoelastic properties. Thus, it is imperative that the synergy between WBCs/platelets and VTCs that eventual effect carrier margination to the vascular wall, either by physical or molecular interaction, be elucidated in order to inform the design of high performing VTCs.

In this work, we elucidate drug carrier-blood cell synergy and how this potentially affects VTCs margination to the vascular wall. We specifically focus on the effects of RBCs, WBCs and platelets on the binding of Sialyl Lewis A- or aICAM- coated polystyrene (PS) spheres of different sizes to inflamed human umbilical vein endothelial cells (HUVECs) via PPFC assays, representing the targeting of endothelial-expressed selectins and ICAM-1 molecules, respectively. In this work, we predominantly focus on Sialyl Lewis^A (sLe^A), a member of a class of carbohydrates molecules that have been previously proposed for use to target carriers in several diseases [19-22], due to its favorable binding kinetic in flow and since it would represent the highest possibility for interactions with leukocyte and platelets that also express considerable levels of selectin molecules. We report here that RBCs and WBCs specifically alter the adhesion of spherical particles depending on their size and type of blood flow, i.e. laminar, pulsatile and recirculating human blood flow, while platelets exhibited no effects on particle adhesion for all conditions studied.

5.2   Results

The experimental set up used in this chapter is described in detail in Chapter 2.

5.2.1   Effect of RBCs on particle adhesion in reconstituted blood flow

The volume composition (hematocrit) of RBCs is known to vary from high values in medium and large vessels to low values in the capillaries. To elucidate the role of hematocrit levels (%Hct) on particle binding to endothelial cells (ECs) from blood flow, the margination of particle were conducted in reconstituted blood, i.e. blood devoid of platelets and WBCs, having different hematocrits. Fig. 5.1 shows the binding density of sLe^A-coated particles on activated ECs after a given period of laminar (at 500 s^{-1} of WSR), pulsatile (with backward and forward flow with peak WSR at 1000 s^{-1}) and recirculating (200 s^{-1} of WSR at far downstream region) reconstituted blood flow for 30 and 45% Hct values. The binding density of particles in laminar blood flow with 30 %Hct significantly increased with increase in particle size from 500 nm to 5 μm (Fig. 5.1A). There was no significant difference in the adhesion density observed for 200 nm particles relative to 500 nm ones. Also, particle adhesion density significantly decreased (~2.6 fold) with the increase in particle size from 5 to 10 μm. An increase in blood hematocrit to 45% resulted in only a slight alteration in particle binding trend where adhesion density only significantly increased with particle size increases from 0.2 to 2 μm. The increase in particle size from 2 to 5 μm did not yield a significant increase in particle binding, and a decrease in binding density was observed with the increase in size from 5 to 10 μm similar to observation with the 30 %Hct laminar flow.

Figure 5.1 Adhesion of sLe^A-particle in (A) laminar (WSR = 500s^{-1}, 5 mins), (B) pulsatile (profile I, peaked WSR = 1000 s^{-1}, 15 mins) and (C) recirculating (WSR = 200 s^{-1}, 5 min) reconstituted blood (RB) flow at 30% (open) and 45% Hct (close).
Dash line and solid line represent observed reattachment point at 30% and 45% Hct in the VSFC, respectively.

Overall, an increase in hematocrit from 30 to 45% resulted in no significant effect on the laminar blood flow binding of 0.2 and 10 μm particles while significantly enhancing the binding of 0.5 and 2 μm spheres by 205 and 23%, respectively. The laminar flow binding of 5 μm particles was slightly (18%) hindered (p value = 0.004) with the same magnitude of increase in reconstituted blood hematocrit.

The binding trend observed for particles in pulsatile reconstituted blood flow at 30 %Hct was similar to observation for laminar flow at 45% Hct. As shown in Fig. 5.1B, the adhesion of spheres significantly increased with increase in particle size from 0.2 to 2 μm. There was no significant change in binding with the increase in particle size from 2 to 5 μm. However, an increase in reconstituted blood hematocrit to 45% for pulsatile flow resulted in a significant decrease in the binding of 5 μm spheres relative to the 2 μm ones. Spheres of 10 μm diameter did not exhibit any adhesion in pulsatile flow at the two %Hct tested. Overall, only the 2 μm spheres saw a net gain in their adhesion density with increase in hematocrit from 30 to 45% in pulsatile flow; the adhesion of other spheres tested did not change with increase in hematocrit for this flow type.

For reconstituted blood flow in the VSFC, minimal particle binding to ECs was observed in the region near the step (0 – 50 μm downstream of step) as shown in Fig. 5.1C. The binding density for all particle sizes, however, increased with increase in distance from the step up to the region just beyond the flow reattachment point – beyond which flow moves forward and towards a laminar profile (~200 μm from step for both 30 and 45% Hct). There was also no difference in the adhesion of all particles between the two RBC compositions studied in the recirculation zone (i.e. upstream of reattachment point). Beyond the flow reattachment point, particle binding either plateaued or decreased

with increase in distance away from the step depending on the size of the particles and the composition of RBCs. Specifically, 2 and 5 μm spheres saw increases in their binding density beyond flow reattachment with the increase in hematocrit from 30 to 45% (237% and 72%, respectively) due to the significant drop in their binding from peak value with the 30% Hct blood flow while particle binding in the 45% Hct blood remained constant. No effect of RBC composition was observed for nanospheres and 10 μm spheres in the area immediate of the flow reattachment. In the far downstream region of the VSFC (> 5000 μm from the step) where flow was again fully developed, particle adhesion trend relative to particle size was unchanged from observation in the recirculation zone – there was no significant difference ($p<0.01$; student's t test) in the magnitude of adhesion observed for all particles interacting between the two RBC compositions studied.

5.2.2   Effect of white blood cell (WBCs) on particle adhesion in whole blood flow

To probe the contribution of WBCs (leukocytes) to particle adhesion patterns in blood flow, the margination of spheres of different sizes were observed in leukocyte-depleted blood (LDB) (RBC and platelets in plasma) relative to whole blood. Since dextran is necessary for a high-yield WBC removal from whole blood, dextran was added to whole blood in the same concentration (~ 0.6% w/v) as with LDB to allow direct comparison. Fig. 5.2 shows the binding density of particles in laminar, pulsatile and recirculating LDB relative to whole blood. In general, the adhesion trend relative to particle size was not significantly altered in LDB relative to whole blood for all flow type studied. The adhesion of smaller sized spheres was also not significantly altered with the removal of leukocytes from whole blood for all flow types.
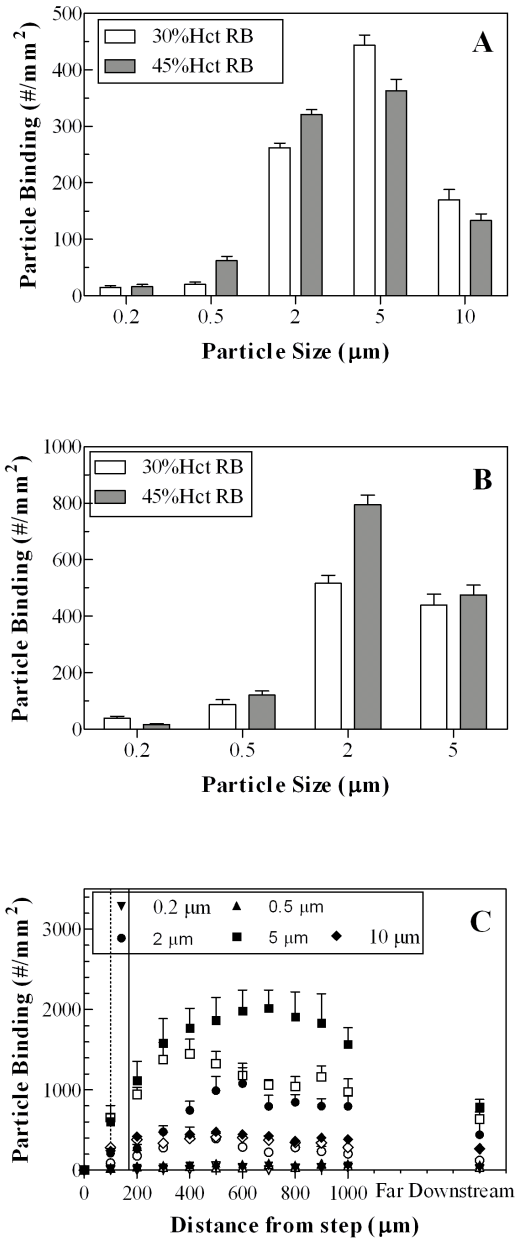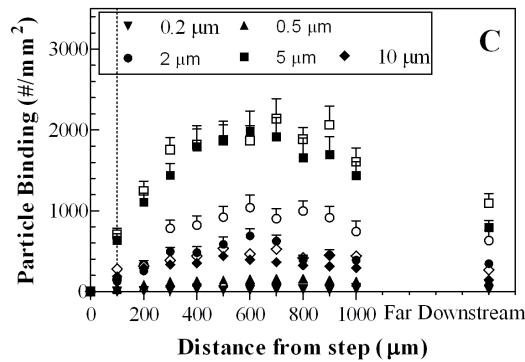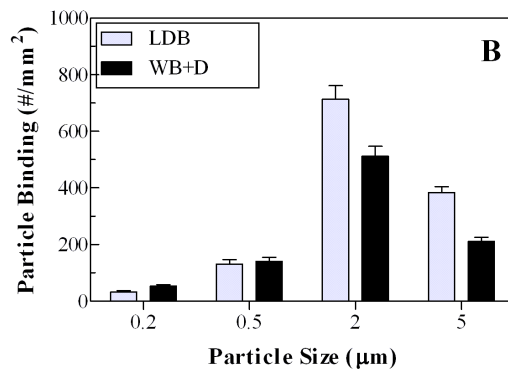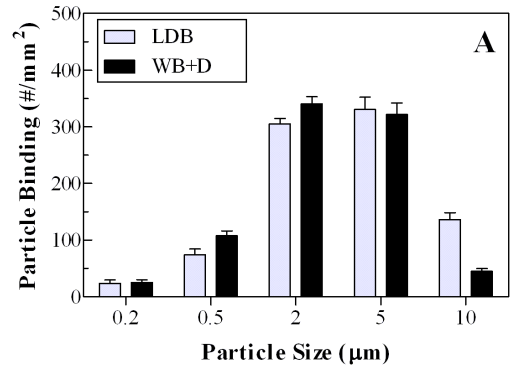
Figure 5.2 Adhesion of sLe^A-particle in (A) laminar (WSR = 500s^{-1}, 5 mins), (B) pulsatile (profile I, peaked WSR = 1000 s^{-1}, 15 mins) and (C) recirculating (WSR = 200 s^{-1}, 5 min) leukocyte-depleted blood (LDB, open) and whole blood (WB+D, close) flow.

Dash line represents observed reattachment point in the VSFC. Both blood flow conditions have the same % Hct and have equal amount of dextran.

However, the presence of WBCs in blood negatively impact binding of 10 μm spheres in laminar flow since the binding density for these particles was significantly higher in laminar flow with LDB relative to whole blood as shown in Fig. 5.2A   Both the 2 and 5 μm spheres similarly exhibited higher adhesion in pulsatile LDB relative to whole blood (~70% for both sizes) as shown in Fig. 5.2B. For experiments in the VSFC (Fig. 5.2C), only 2 μm-sized spheres were observed to show significantly higher (78%; p = 0.003) in recirculating LDB flow relative to the whole blood in regions just beyond flow reattachment. At far downstream of recirculation in the VSFC, the effect of WBC removal mirrored observation in laminar flow in the straight channel where only 10 μm spheres exhibited differential adhesion between the two types of blood. The adhesion of 2 and 5 μm spheres at far downstream of recirculation was not significant between LDB and whole blood (p value = 0.02 and 0.05, respectively).

5.2.3   Rate of microsphere attachment in WBC depleted blood (LDB)

Fig. 5.3 shows the rate of microsphere and leukocyte attachment to EC monolayer from pulsatile LDB and whole blood flow for 15 min. As shown, the adhesion of 2 μm spheres in LDB and whole blood increased over time and were not significant from each other for all time points up to 13 mins (Fig. 5.3A). At longer times, the adhesion of 2 μm spheres in whole blood appear to plateau while the ones in LDB continued to exhibit a linear increase with time.   The rate of adhesion for 5 μm spheres in LDB was similar to the adhesion rate in whole blood only at flow times less than 6 mins (Fig. 5.3B).
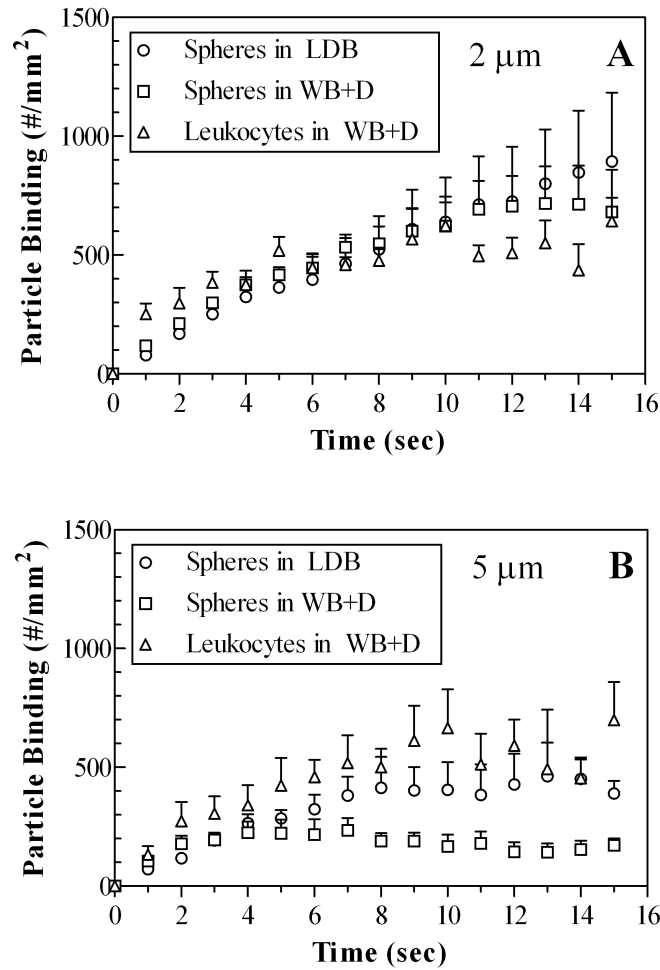
Figure 5.3 Rate of particle and white blood cell (leukocyte) attachment in pulsatile flow (profile I, peak WSR 1000 s-[1], 15 mins): (A) 2 μm and WBC, and (B) 5 μm and WBC binding in leukocyte-depleted blood (LDB) and whole blood (WB). Dash line represents observed reattachment point in the VSFC. Both blood flow conditions have the same % Hct and have equal amount of dextran.

The adhesion of 5 μm in LDB eventually reached a plateau at 8 min of flow; however, their adhesion in whole blood appear to decrease with increase in flow time (slope ≈ -10.23) to a minimum at between 12 and 14 min of flow. Overall, the rate of WBC adhesion in whole blood increased with time up to a maximum of ~ 650 sites/μm^2 at 10 min irrespective of whether 2 or 5 μm sLe^A spheres are present in flow.

5.2.4 Dynamics of WBCs interference with microsphere adhesion in blood flow

To probe whether the reduced microsphere adhesion seen in whole blood relative to LDB is due to molecular interaction associated with the sLe^A ligand on microspheres effecting microsphere-WBC aggregations via molecules-expressed on leukocytes (e.g. L-selectin), some adhesion assays were conducted with 5 μm spheres coated with a monoclonal antibody against ICAM-1 (expressed abundantly on ECs but not by WBCs) at a high enough density to support their adhesion to ECs from blood flow pulsing between -500 and 500 s^{-1} of WSR (Fig. 5.4). The slower reaction kinetics between the antibody and ICAM-1 limits evaluation of the adhesion of anti-ICAM-1 (aICAM-1) microspheres in pulsatile flow with peak WSR at 1000 s^{-1}; i.e. only minimal binding is observed. Similar to sLe^A- microspheres, the adhesion of both the 2 and 5 μm aICAM-microspheres in whole blood was lower compared to their adhesion in LDB (Fig. 5.4C), which may suggest that the interference of WBCs with microspheres binding in whole blood is not due to molecular interaction/aggregation between the two, either in flow or at the endothelial surface. No negative change in adhesion density with time was observed for aICAM microspheres in contrast to sLe^A spheres (Fig. 5.4A and 5.4B).
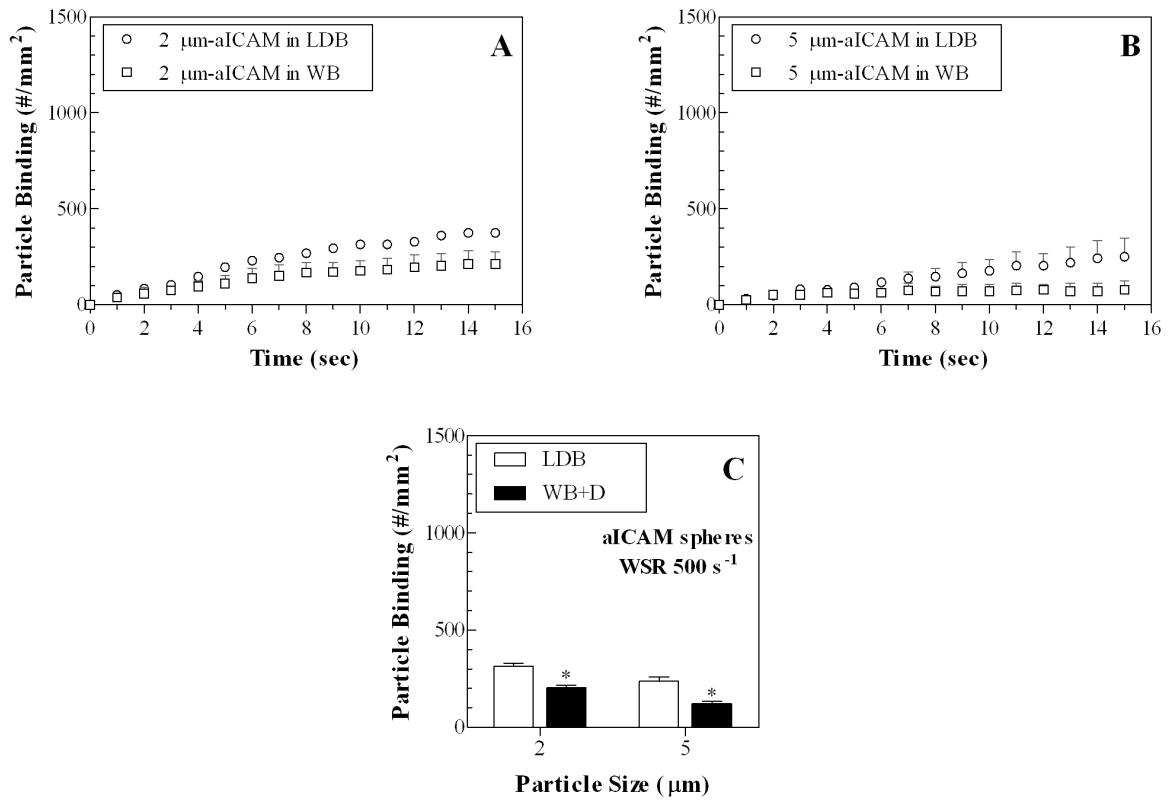
Figure 5.4 Adhesion of aICAM-particle in pulsatile leukocyte-depleted blood (LDB) and whole blood (WB) flow (profile I, peak WSR 500 s^{-1}, 15 mins). Rate of (A) 2 μm and (B) 5 μm aICAM particle attachment and (C) particle binding at 15 mins in LDB and WB.

Both blood flow conditions have the same % Hct and have equal amount of dextran. * p<0.01 compared to particle binding in LDB.

In the absence of molecular interactions, physical competition for adhesion to the inflamed ECs between WBC and microspheres may possibly hinder microsphere adhesion in whole blood. To determine whether this, i.e. the physical removal of WBCs from blood creating a void in the cell-free layer at the wall, results in the higher binding of microspheres in LDB relative to whole blood, assays were conducted with 5 μm spheres in pulsatile LDB flow having non-functional PLGA microspheres (no adhesion ligand) added in at the same concentration (4 x 10^6/mL) and size distribution (average size = 8 μm) as the depleted WBCs (Fig. 5.5). The attachment rate and adhesion densities of 5 μm-sLe^A spheres under pulsatile flow in LDB with non-targeted PLGA spheres were not significantly different from their adhesion in LDB alone (p value = 0.18) but were significantly higher than values obtained for adhesion in whole blood. This suggests that the interference of WBCs with microsphere binding in whole blood likely occurs at the point of binding (i.e. competition) at the EC wall rather than in flow. The negative slope observed for the rate of attachment for 5 μm spheres in whole blood may also suggest an active displacement of microspheres by WBCs in whole blood flow in addition to competition for binding (Fig. 5.3B). To probe this further, video records of adhesion for 5 μm spheres in pulsatile whole blood flow assays were analyzed for particle-microspheres interaction at the wall. Indeed, several collisions between WBCs and these particles were observed and resulted in the detachment of previously bound spheres. This collision-induced particle detachment likely results from higher drag force acting on particles at the instance of collision to overcome the previously sufficient adhesive force at the wall.
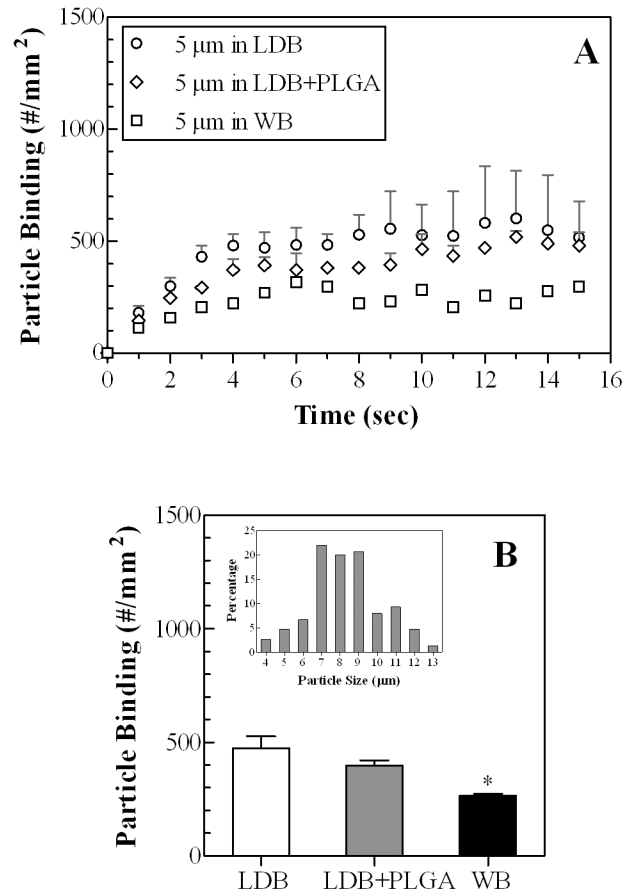
Figure 5.5 Adhesion of sLe^A-particle (1000 site/μm^2) in pulsatile leukocyte-depleted blood alone and with non-functional PLGA microspheres (LDB, LDB+PLGA) and whole blood (WB) flow (profile I, WSR = 1,000 s^{-1}, 15 mins). (A) Rate of 5 μm sLe^A-particle attachment and (B) Particle binding at 15 mins. Insert B = PLGA particle size distribution.

All blood flow conditions have the same % Hct and have equal amount of dextran. * p<0.01 compared to particle binding in LDB.

To confirm this hypothesis, 2 and 5 μm spheres with twice higher density of sLe^A, 2000 sites/μm^2, were observed in whole blood pulsatile flow with peak WSR 1000 s^{-1} (Fig. 5.6). There was no significant difference in the attachment rate and adhesion of microspheres between pulsatile flow with LDB and whole blood for 2 μm spheres at this higher density of sLe^A. For 5 μm spheres, the higher ligand density resulted in a significant reduction in the difference in adhesion density between LDB and whole blood, from 70% down to 27% difference (Fig. 5.6C). A second set of experiments with the adhesion of 2 and 5 μm observed in pulsatile flow at a lower peak WSR of 500 s^{-1} (Fig. 5.7) similarly showed no significant difference in the attachment rate and adhesion of these spheres between LDB and whole blood.

5.2.5   Effect of platelets and dextran on particle adhesion in whole blood flow

Fig. 5.8 shows the adhesion of sLe^A spheres in laminar, pulsatile and recirculating platelet-depleted blood (PDB) relative to whole blood. Across all blood flow patterns tested, the binding density of sLe^A-spheres of all sizes in platelet-depleted blood was not significantly different from the binding density obtained for the same particles in whole blood. This would suggest that any interactions between platelets and VTCs that exist in whole blood minimally affect the margination of these carriers to the vascular wall. An interesting observation, however, from the whole blood experiments shown in Fig. 5.8 is that the presence of dextran in the whole blood flow as shown in Fig. 5.2 negatively affects the binding of 2 μm spheres in all types of blood flows while having no effect on all other spherical sizes.
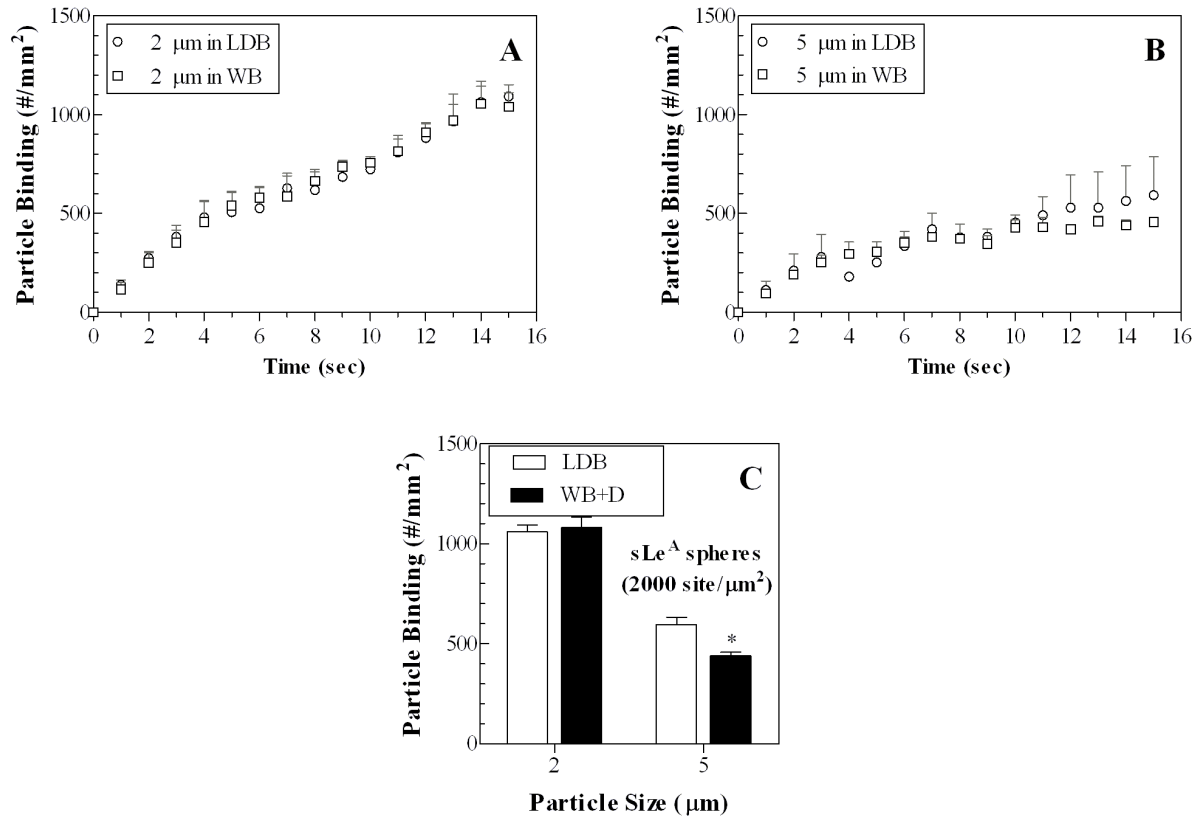
Figure 5.6 Adhesion of sLe^A-particle (2000 site/μm^2) in pulsatile leukocyte-depleted blood (LDB) and whole blood (WB) flow (profile I, peak WSR 1000 s^{-1}, 15 mins). Rate of (A) 2 μm and (B) 5 μm sLe^A-particle attachment and (C) particle binding at 15 mins in LDB and WB.

Both blood flow conditions have the same % Hct and have equal amount of dextran. * p<0.01 compared to particle binding in LDB.
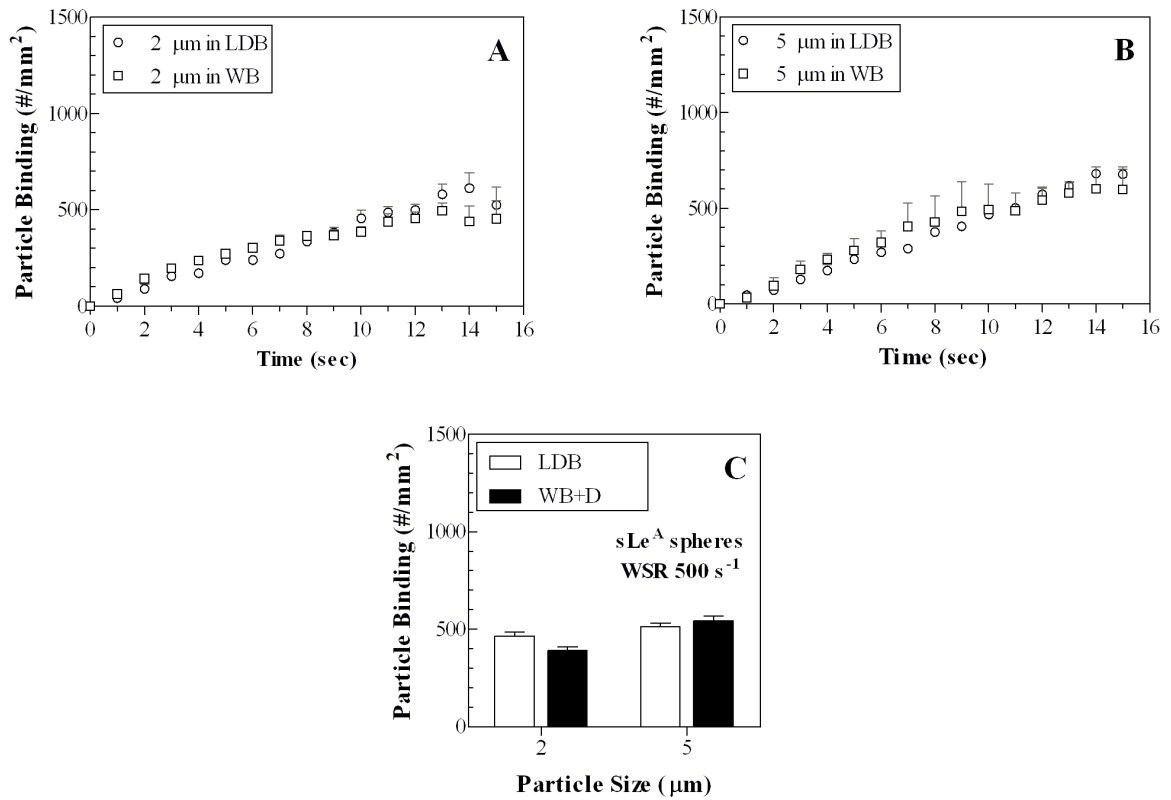
Figure 5.7 Adhesion of sLe^A-particle (1000 site/μm^2) in pulsatile leukocyte-depleted blood (LDB) and whole blood (WB) flow (profile I, peak WSR 500 s^{-1}, 15 mins). Rate of (A) 2 μm and (B) 5 μm sLe^A-particle attachment and (C) particle binding at 15 mins in LDB and WB.

Both blood flow conditions have the same % Hct and have equal amount of dextran. * p<0.01 compared to particle binding in LDB.
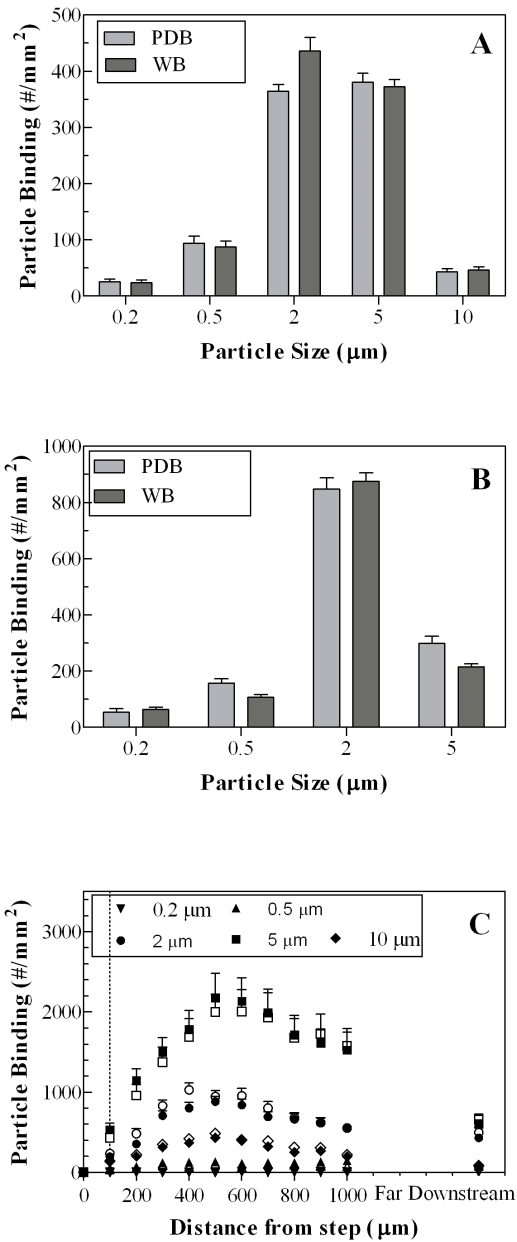
Figure 5.8 Adhesion of sLe^A-particle in (A) laminar (WSR = 500s^{-1}, 5 mins) (B) pulsatile (profile I, peaked WSR = 1000 s^{-1}, 15 mins) and (C) recirculating (WSR = 200 s^{-1}, 5 min) platelet-depleted blood (PDB, open) and whole blood (WB, close) flow.

Dash line represents observed reattachment point in the VSFC. Both blood flow conditions have the same % Hct.

The effect of dextran on 2 μm spheres is the most pronounced in the pulsatile blood flow profile with as much as 42% reduction in binding density in the presence of dextran.

5.3 Discussion

Targeting of particulate carriers to the vascular wall for imaging and delivery of drugs remains attractive for the diagnosis and treatment of several diseases. In general, targeting of imaging carrier can provide enhanced resolution and sensitivity through concentration of imaging agents at the diseased site. Similarly, vascular-targeted drug carriers can provide safer (localized delivery) and more efficient (reduced drug cargo) intervention through localization and release of encapsulated therapeutics at the target sites. While the concept of targeted drug delivery system dates back several decades now, only a handful of these technologies have made it to clinical use. In fact, many novel therapeutics/delivery systems that show great promise in preclinical research at the bench and in animal models have failed in the clinics [23, 24]. This gap between preclinical research and clinical outcomes may be, in part, due to, carrier design strategies heavily focused on target epitope while neglecting key parameters such as the dynamic forces associated with blood flow, hemorheology and blood cell-carriers interactions that all may significantly impact the capacity for vascular-targeted carriers (VTCs) to interact with the vascular wall. Overall, VTCs with optimized targeting moiety but lacking the capacity to marginate (localize and adhere) to the blood vessel wall would likely deliver their cargo systemically rather at the intended site. A detail understanding of interactions between VTCs and blood cells in different types of blood flow patterns that exist in the human circulation would help inform the design of VTCs for optimal functionality in

humans. Herein, we evaluated the role of RBCs, leukocytes and platelets on the binding of inflammation-targeted polystyrene spherical particles sized from 200 nm to 10 μm diameter to inflamed endothelial cell (EC) monolayers via parallel plate flow assays with physiological blood flow conditions. We show that the role of blood cells in dictating the adhesion of spherical particles to the wall from blood flow is coupled to the particle size and/or targeting ligands, blood shear rate and flow types.

In general, the margination of nanospheres to EC monolayers was minimal relative to the margination of small microspheres in all types of flow patterns and blood compositions. This observation is in agreement with our previous observation in reconstituted blood (RBC only in plasma) flow and is due to the propensity for RBCs to preferentially migrate and align in the center of flow while driving microspheres to the CFL adjacent to the vascular wall allowing for their frequent contact with endothelium whereas nanospheres are entrapped within the RBC core [15, 16, 25]. Previously presented control experiments with nanospheres endowed with 2.5 times higher sLe[A] ligand density than microspheres tested at the same shear rate showing no significant increase in their adhesion density confirmed that transport to the wall rather than reaction at the wall was indeed limiting nanosphere adhesion [16]. The 2 μm spherical diameter appears to be the most optimum size for margination in laminar and pulsatile whole blood flow, particularly at high wall shear rates (during the peak WSR of pulsatile flow), likely due to the high slip velocity (i.e. the velocity of particles before forming a bond at the wall [26]) and disruptive force experienced by 5 and 10 μm spheres during flow and at the reaction site respectively, i.e. adhesion is reaction rather than transport limited.

In recirculating blood flow, particle binding, particularly for microspheres, increased with distance away from the step, peaking slightly beyond the reattachment point and decreasing toward far downstream where flow is laminar (Fig. 5.1C). In the vortex region, there are two directional velocities, the axial velocity parallel to the wall (V_x) and the normal velocity (V_z) with directions acting away and toward to the wall at the step and reattachment point, respectively [27]. Particles are therefore brought towards the wall with the flow streamline at the reattachment point. This is in part responsible for the observation of peak adhesion beyond the reattachment point. The accumulation of particles at the wall proximity in this region appear to disproportionally favor small to medium-sized microspheres over nanospheres as suggested by the 4 and 13 folds difference in the adhesion density between 2 and 5 μm relative to the 0.5 μm spheres, respectively, compared to only 3 and 6 folds difference between these microspheres and 0.5 μm spheres at the far downstream region (Fig. 5.2C). This particle distribution trend in the recirculation flow is likely due to the higher rotational motion inducing higher frequency and magnitude of collision between microparticles and RBCs. However, the low WSR of 200 s^{-1}, i.e. low blood flow rate, in the recirculation channel also likely contribute to the resurgence of the 5 μm spheres as the optimal size for binding in the VSFC though a similar trend was not seen with laminar blood flow at 200 s^{-1} in a straight channel of similar height to the VSFC (data not shown). Accordingly, microspheres are favored for binding relative to nanospheres in all flow types. It is curious that the recirculating flow, which presumably interferes with the well-packed RBC cores, also overwhelming enhance the adhesion of microspheres over nanospheres.

The role of RBC volume fraction on carrier margination is apparent in Fig. 5.1. The slight change in particle binding pattern observed in laminar reconstituted blood flows with 45% Hct relative to 30% Hct is likely due to the shrinking of the plasma CFL with increase in blood hematocrit. Several studies have indicated the importance of CFL on the adhesion of blood cells and particle to the vascular wall [10]. The width of this CFL has been reported to vary in the range between 2.5 – 7 μm depending on several factors including the hematocrit level, blood vessel size and WSR [28-30]. An increase in blood hematocrit enlarges the RBC core thereby reducing the CFL width [30]. Thus, at a higher hematocrit, particles would localize into a thinner CFL resulting more frequent collision between particles and with RBCs. The increase in collision induces the lateral migration of particles towards the endothelium, which eventually leads to their binding at the wall, as seen with the increase of the binding observed for the 0.5 and 2 μm spheres with higher hematocrit. However, increase in particle collision in the CFL can also prevent the particle binding, particularly for larger microspheres. Specifically, a large number of particles at the wall would increase competition for the binding space and/or provide redundant collision that leads to the detachment of previously bound particles from the wall, as observed with the decrease in the binding of 5 μm spheres at higher RBC volume fraction. This also likely explains the disproportionately higher effect of increased hematocrit on the binding density of 0.5 μm (~ 205%) relative to 2 μm (23 %) spheres, in that the nanospheres likely experience minimal negative collision due to low initial concentration at the wall and their size. The lack of a hematocrit effect on the adhesion of 0.2 μm spheres across all flow types may be due to a combination of their extremely poor localization and their significantly smaller size compared to the CFL

width. The observed effects of RBC on particle binding here also agree well with previous publications evaluating the effect of blood hematocrit on the adhesion of blood cells in laminar flow. Specifically, the binding of platelet (~ 2 μm) increases as blood hematocrit changes from 0 to 50 % whereas leukocyte (~ 8 -12 μm) adhesion increases with blood hematocrit only changes from 0 to 30%. Further increase in hematocrit from 30 to 60% Hct had no effect on leukocyte adhesion [10, 12]. The lack of a negative effect of hematocrit on WBC adhesion at higher value as was found for the 5 μm spheres in laminar flow in this work is likely due to the deformable nature of the former that may help minimize the negative force imparted by collision.

It is not surprising that the increase in blood hematocrit only enhanced the margination of 2 μm spheres in pulsatile flow while having no effect on other particle sizes. The pulsing of blood flow in a backward to forward direction around zero shear likely resulted in transient CFL width, where the CFL become larger as WSR decreases [28, 29]. Thus, the increase in CFL width during periods of low WSR may cancel the gain observed for the 0.5 μm spheres in laminar flow. Meanwhile, a larger CFL width would lower the collision frequency of large particles (5 μm), which may counterbalance the smaller CFL effect gained from increasing % Hct. Thus, increasing blood hematocrits had no effect on the binding of 0.5 and 5 μm in pulsatile flow. The increase in %Hct in recirculating blood flow only promoted the binding of 2 and 5 μm spheres in regions beyond the reattachment point. The lack of a hematocrit effect on the binding of 10 μm spheres, however, is probably due to excessive collision between large particles in the small CFL preventing them from binding. Though, it is possible that these particles formed aggregates and/or are large enough for a significant portion of them to remain

trapped in the recirculation zone.   Indeed, the overall adhesion of 10 μm spheres in recirculating reconstituted blood flow with the two hematocrits tested was low compared to other microspheres.

The comparison of particle binding observed in leukocyte-depleted blood (LDB) and whole blood flow in Fig. 5.2 showed that the presence of WBCs in blood tended to negatively impact microsphere binding whereas no WBC effects were observed for the binding of nanospheres in all flow types. The presence of WBCs in blood negatively impacted the binding of 10 μm spheres in laminar flow of the straight channels at 500 s^{-1} of WSR and that of 2 and 5 μm in pulsatile flow with peak WSR at 1000 s^{-1}. Observation in these two types of flows would suggest that the impact of WBCs on carrier binding is coupled to the shear force impacted by flow, since smaller microspheres saw no effect at 500 s^{-1} of laminar wall shear whereas their adhesion were affected in flow with peak WSR at 1000 s^{-1}. The combination of low shear and unique cell/particle distribution/collision pattern in the vortex and flow reattachment regions of the VSFC again contributed to the lack of a WBC effect on the adhesion of particles of all sizes since the WBC-effect trend at the far downstream region of the VSFC mirrored ones observed in straight channels with laminar flow. Indeed, others have reported a different dynamic of WBCs binding in the VSFCs similar to the one used in this study relative to straight channels of similar heights and WSR [11].

The rate of attachment data presented in Fig. 5.3 suggests that the impact of WBCs on microspheres adhesion is linked to a surface "saturation effect". The adhesion of 2 and 5 μm spheres in pulsatile whole blood flow plateaued about 13 and 5 mins in the 15 min duration of pulsatile, respectively, while their binding in pulsatile LDB exhibited

no plateau or enjoyed a longer period of linear increase. In whole blood the rate of WBC

binding was similar observed to reach a plateau about 10 mins in flow. This particle and

WBC rate of attachment pattern suggest minimal competition between microspheres and

leukocytes during early flow times when the EC substrate provides ample binding space.

As the monolayer surface continued to be populated, however, particles and WBCs begin

to compete to occupy the few available binding spaces on endothelial cells. With the

smaller ratio of WBC to particle diameter for the 5 μm spheres, it makes sense that the

surface saturation effect was observed at earlier time points for these spheres. However,

the negative adhesion observed for 5 μm spheres as leukocyte binding increased

suggested that leukocytes competed off previously bound spheres. This was confirmed by

observation of WBC collision with previously bound 5 um spheres that resulted in their

detachment from video record of experiments (see Supplemental Video for the paper).

Control experiments with anti-ICAM-1 coated beads suggested that molecular

interactions between microspheres and WBCs did not contribute to the decreased in

microsphere adhesion in whole blood (Fig. 5.4C) since their adhesion is also significantly

lower in whole blood relative to LDB though no appreciable amount of ICAM-1 is

expressed by leukocyte to justify the possibility of molecular interaction mediated by

anti-ICAM-1. The lack of a negative rate of attachment observed for aICAM-1 spheres is

due to the stronger adhesion force, i.e. low off-rate, exhibited by the aICAM-ICAM-1

interaction resulting in no removal of bound microspheres upon WBC collision (Fig.

5.4A and 5.4B). Overall, the observation of a similar level of binding of WBCs in

pulsatile whole blood in the presence of 2 and 5 μm spheres would suggest that spheres

may have no impact on the adhesion of leukocytes. This observation is important for

imaging and drug delivery applications since it indicates that the introduction of vascular-targeted carrier in the blood circulatory system even with interactive ligands such as sLe[A] would not enhance or prevent the margination of WBC to endothelial cells during inflammation *in vivo*.

The experiments with non-adhesive spheres, at the same level as normal leukocyte concentration, replacing WBCs in whole blood suggested that the collision and competition of spheres and leukocytes in flow minimally contribute to the reduction of particle binding in whole blood (Fig. 5.5), i.e. the negative impact of WBCs on microsphere binding primarily occurred at the endothelial wall by WBCs knocking off previously bound spheres and/or possessing favorable adhesion kinetics to successfully compete out larger spheres for adhesion. This hypothesis was further confirmed by observing the binding of spheres with twice higher sLe[A] ligands than originally used for pulsatile flow experiments with peak WSR 1000 s^{-1} as presented in Fig. 5.3 where the attachment rates (Fig. 5.6A) and the adhesion levels of 2 μm spheres in LDB and whole blood were not significantly different (Fig. 5.6C) from each other. The residual reduction in the adhesion of 5 μm spheres in whole blood relative to LDB, i.e. ~ 27% decrease for 2000 site/μm^2 versus 70% decrease for 1000 site/μm^2 sLe[A]-spheres suggested that higher adhesive force on 5 μm may be needed to withstand the detachment in whole blood under high WSR. Moreover, the binding of sLe[A] spheres (with 1000 sLe[A] site/μm^2) observed in pulsatile flow with lower peak WSR (500 s^{-1}) as well as in laminar flow (Fig. 5.2A) similarly resulted in no significant differences between microsphere adhesion rate (Fig. 5.7A and 5.7B) and binding density in LDB and whole blood at this lower average disruptive force (Fig. 5.7C). These results suggest that leukocyte would have a minimal

impact on the binding of spheres that have adequate adhesive forces to withstand the drag force impacted by collision with WBCs. Since the drag force on the bound particle can increase with particle size, thus, this can explain why we observed the negative effect of leukocyte on 10 μm binding at lower shear rate in laminar flow in both straight channel (WSR 500 s^{-1}) and far downstream of the step channel (WSR 200 s^{-1}) (Fig. 5.2).

The presence of dextran in WB for the LDB flow experiments had no significant effect on particle binding for most sizes in all flow types as seen with the similar particle binding density in whole blood with (Fig. 5.2) and without dextran (Fig. 5.8) with the exception of the 2 μm spherical size. The binding density of 2 μm in whole blood with dextran was lower relative to whole blood alone in all flow types evaluated (22%, 42% and 35% in laminar, pulsatile and recirculating flow, respectively). Because the average size of CFL is about 2.5-7 μm in width, thus the small change in CFL width is likely to greatly effect the binding of spheres in this size range, as previously shown that 2 μm was the most susceptible size affected by the change in CFL. Dextran is a large carbohydrate molecule that can induce RBC aggregation under low shear rate, while having little effect on RBC deformation under shear rate greater than 100 s^{-1} [31, 32]. Since the pulsatile profile utilized in this study were pulsed around the zero shear, the addition of dextran to whole blood then allowed the increase of RBC aggregation during low shear resulting in the increase in cell free layer (CFL) width. This wider CFL then negatively affected the binding of 2 μm in pulsatile whole blood flow with dextran. Though dextran had a minimal effect on RBC aggregation under high shear flow in laminar (WSR 500 s^{-1}) and recirculating flow (WSR 200 s^{-1}), the addition of dextran can increase the viscosity of

whole blood which then can negatively effect the particle binding, particularly the susceptible sphere size.

Platelets were found to have no significant effect on the binding of all sphere sizes in all flow types (Fig. 5.8). Though, platelet is able to localize into the CFL as with leukocyte and particle; however, due to its small size and disc shape that tends to minimize the interaction with other cells and particles, the collision between platelet and particles in the CFL may be minimal and thus having no effect on particle behavior. Moreover, the majority of platelet in whole blood is unactivated (in resting state), i.e. no P-selectin expression; thus, platelet may have minimal molecular interaction with particle and leukocyte [33]. In addition, in this study, platelets had a minimal binding on endothelium since endothelial cells were activated via IL1-β for 4 hrs, which E-selectin and ICAM-1 are mostly upregulated; these molecules are not responsible for platelet adhesion [33].

In summary, this study elucidated the implication of blood cells and particle dynamics on the efficacy of particle binding in physiological blood flow. Our results suggested that RBC plays an important role on dictating particle binding by creating the cell free layer (CFL) at the wall proximity. Leukocyte tends to compete with microspheres for binding by occupying the binding space on the inflamed EC monolayer and negatively impact particle binding, especially microspheres, via their collision motion that can increase the drag force on bound particles. Platelets have a minimal effect on particle binding likely due to its resting condition in whole blood and minimal adhesion on endothelium.

References

1. Dvorak HF, Brown LF, Detmar M, Dvorak AM. Vascular permeability factor/vascular endothelial growth factor, microvascular hyperpermeability, and angiogenesis. The American journal of pathology. 1995;146:1029.

2. Kinlay S, Libby P, Ganz P. Endothelial function and coronary artery disease. Current opinion in lipidology. 2001;12:383.

3. Mantovani A, Bussolino F, Dejana E. Cytokine regulation of endothelial cell function. The FASEB journal. 1992;6:2591-2599.

4. Carmeliet P, Jain RK. Angiogenesis in cancer and other diseases. NATURE-LONDON-. 2000;249-257.

5. Panyam J, Labhasetwar V. Biodegradable nanoparticles for drug and gene delivery to cells and tissue. Advanced drug delivery reviews. 2003;55:329-347.

6. Ruehm SG, Corot C, Vogt P, Kolb S, Debatin JF. Magnetic resonance imaging of atherosclerotic plaque with ultrasmall superparamagnetic particles of iron oxide in hyperlipidemic rabbits. Circulation. 2001;103:415-422.

7. Alexis F, Pridgen E, Molnar LK, Farokhzad OC. Factors affecting the clearance and biodistribution of polymeric nanoparticles. Molecular pharmaceutics. 2008;5:505-515.

8. Dobrovolskaia MA, Aggarwal P, Hall JB, McNeil SE. Preclinical studies to understand nanoparticle interaction with the immune system and its potential effects on nanoparticle biodistribution. Molecular pharmaceutics. 2008;5:487-495.

9. Dobrovolskaia MA, McNeil SE. Immunological properties of engineered nanomaterials. Nature nanotechnology. 2007;2:469-478.

10. Munn LL, Melder RJ, Jain RK. Role of erythrocytes in leukocyte-endothelial interactions: mathematical model and experimental validation. Biophysical journal. 1996;71:466-478.

11. Skilbeck CA, Walker PG, David T, Nash GB. Disturbed flow promotes deposition of leucocytes from flowing whole blood in a model of a damaged vessel wall. British journal of haematology. 2004;126:418-427.

12. Jordan A, David T, Homer-Vanniasinkam S, Graham A, Walker P. The effects of margination and red cell augmented platelet diffusivity on platelet adhesion in complex flow. Biorheology. 2004;41:641-654.

13. Turitto VT, Baumgartner HR. Platelet interaction with subendothelium in a perfusion system: physical role of red blood cells. Microvascular research. 1975;9:335-344.

14. Kiani MF, Yuan H, Chen X, Smith L, Gaber MW, Goetz DJ. Targeting microparticles to select tissue via radiation-induced upregulation of endothelial cell adhesion molecules. Pharmaceutical research. 2002;19:1317-1322.

15. Charoenphol P, Mocherla S, Bouis D, Namdee K, Pinsky DJ, Eniola-Adefeso O. Targeting Therapeutics to the Vascular Wall in Atherosclerosis-Carrier Size Matters. Atherosclerosis. 2011;217:364-370.

16. Charoenphol P, Huang RB, Eniola-Adefeso O. Potential role of size and hemodynamics in the efficacy of vascular-targeted spherical drug carriers. Biomaterials. 2010;31:1392-1402.

17. Cerletti C, de Gaetano G, Lorenzet R. Platelet–Leukocyte Interactions: Multiple Links Between Inflammation, Blood Coagulation and Vascular Risk. Mediterranean journal of hematology and infectious diseases. 2010;2

18. Hundelshausen PV, Koenen RR, Weber C. Platelet-Mediated Enhancement of Leukocyte Adhesion. Microcirculation. 2009;16:84-96.

19. Ali M, Hicks AER, Hellewell PG, Thoma G, Norman KE. Polymers bearing sLex-mimetics are superior inhibitors of E-selectin-dependent leukocyte rolling in vivo. The FASEB journal. 2004;18:152-154.

20. Boutry S, Laurent S, Elst LV, Muller RN. Specific E-selectin targeting with a superparamagnetic MRI contrast agent. Contrast media & molecular imaging. 2006;1:15-22.

21. Van Langendonckt A, Donnez J, Defrère S, Dunselman GAJ, Groothuis PG. Antiangiogenic and vascular-disrupting agents in endometriosis: pitfalls and promises. Molecular human reproduction. 2008;14:259-268.

22. Zhang W, Stanimirovic D. Current and future therapeutic strategies to target inflammation in stroke. Current Drug Targets-Inflammation &# 38; Allergy. 2002;1:151-166.

23. Allen TM, Cullis PR. Drug delivery systems: entering the mainstream. Science. 2004;303:1818.

24. Simons M, Bonow RO, Chronos NA et al. Clinical trials in coronary angiogenesis: issues, problems, consensus: an expert panel summary. Circulation. 2000;102:e73-e86.

25. Huang RB, Mocherla S, Heslinga MJ, Charoenphol P, Eniola-Adefeso O. Dynamic and cellular interactions of nanoparticles in vascular-targeted drug delivery (review). Molecular membrane biology. 2010;27:190-205.

26. Chang KC, Hammer DA. The forward rate of binding of surface-tethered reactants: effect of relative motion between two surfaces. Biophysical journal. 1999;76:1280-1292.

27. Skilbeck C, Westwood SM, Walker PG, David T, Nash GB. Dependence of adhesive behavior of neutrophils on local fluid dynamics in a region with recirculating flow. Biorheology. 2001;213-227.

28. Fedosov DA, Caswell B, Popel AS, Karniadakis GEM. Blood Flow and Cell‑Free Layer in Microvessels. Microcirculation. 2010;17:615-628.

29. Kim S, Kong RL, Popel AS, Intaglietta M, Johnson PC. Temporal and spatial variations of cell-free layer width in arterioles. American Journal of Physiology-Heart and Circulatory Physiology. 2007;293:H1526-H1535.

30. Sharan M, Popel AS. A two-phase model for flow of blood in narrow tubes with increased effective viscosity near the wall. Biorheology. 2001;38:415-428.

31. Bishop JJ, Popel AS, Intaglietta M, Johnson PC. Rheological effects of red blood cell aggregation in the venous network: a review of recent studies. Biorheology. 2001;38:263.

32. Reinke W, Gaehtgens P, Johnson PC. Blood viscosity in small tubes: effect of shear rate, aggregation, and sedimentation. American Journal of Physiology-Heart and Circulatory Physiology. 1987;253:H540-H547.

33. Frenette PS, Johnson RC, Hynes RO, Wagner DD. Platelets roll on stimulated endothelium in vivo: an interaction mediated by endothelial P-selectin. Proceedings of the National Academy of Sciences. 1995;92:7450.

CHAPTER 6

EFFECT OF RED BLOOD CELL SIZE ON THE BINDING EFFICACY OF SPHERICAL VASCULAR-TARGETED DRUG CARRIER

ABSTRACT

Several animal models have been extensively used in experimental researches including in the fields of imaging and vascular-targeted drug delivery. Despite the comparable physiological environment of animal models and human relative to an *in vitro* assay, there are still many variations that can significantly impact experimental results relative to human system such as differences in hemorheology, hemodynamics and the structure of vasculature. Here, this study aims to investigate the role of hemorheology of various animal models and human on dictating the binding efficiency of spherical vascular-targeted drug carriers (VTDCs) at the wall in physiological blood flow. Specifically, the adhesion of sLe^A-coated particles, 0.2, 0.5, 2 and 5 μm, to inflamed endothelial cells monolayers were conducted via a parallel plate flow chamber assay (PPFC). Particle binding was observed in washed blood (red blood cells (RBCs) suspended in saline) and whole blood in laminar, pulsatile and recirculating flow. Our results suggest that RBCs dictate the particle binding in blood flow by aligning at the

flow center and forming the cell free layer (CFL) at the wall vicinity. The CFL width may vary with RBC size and rheology, at fixed hematocrit (RBC volume fraction in blood), and this variation can affect the binding density/trend of particles since the proper ratio of particle size to CFL width is necessary for the optimal particle binding. Additionally, plasma compositions also appear to affect the trend of particle adhesion in different animal species. Overall, this work sheds light on the potential deviation of results investigated *in vivo* by utilizing animal models from what might be the expected outcome in human.

6.1 Introduction

To date, vascular-targeted drug delivery has gained tremendous interest for use as alternative treatment for several diseases. To this end, several works have focused on characterizing the capacity for vascular-targeted drug carriers (VTDCs) to adhere vividly at the targeted sites either via various static *in vitro* assays [1], flow chamber assays ranging in complexity from buffer to blood flows [2, 3], and various animal models of human diseases [4, 5]. *In vivo* assays are preferentially used due to challenges associated with recreating the complexity of human body with *in vitro* assays and since the over-interpretation of results may lead to failure of VTDCs in human. Animals prominently used in drug delivery research include rodents, rabbits, pigs, dogs and monkeys [6-9]. However, many of these animal species have different blood flow environments and hemorheology from human, e.g. differences in shear rates, plasma protein compositions that affect blood viscosity and red blood cell (RBC) aggregation, and more importantly blood cell properties (i.e. size, shape and deformability), that may limit the extrapolation of the generated data to human physiology [10]. These would be of particular importance for drug delivery application to diseases typically associated with or affecting medium and large blood vessels, e.g. atherosclerosis, where VTDCs must navigate in bulk blood flow where the hemorheology effect on VTDC localization and adhesion would be prominent.

Indeed, we recently reported that human RBCs have a significant influence on the binding efficiency of spherical particles to the inflamed endothelial cells (ECs) under physiological bulk blood flow via *in vitro* flow assays [2, 11]. We show that small

microspheres exhibit a high capacity to marginate (localize and adhere) to inflamed human ECs at the wall from steady and disturbed human blood flow, while nanospheres and large microspheres exhibit limited margination due to interactions with RBCs and high shear, respectively. The observed size effect on the margination of spheres could be explained by the well-documented preferential migration of RBCs away from the wall and alignment at the center of the flow while creating a RBC-free layer (CFL) at the wall proximity. This movement of RBCs causes microspheres (as well as leukocytes and platelets) in blood flow to concentrate in the CFL via exclusion, enhancing their collision and contact with the vascular wall. Additionally, the RBC core imparts a normal acting force that, depending on the CFL height to sphere size ratio, helps stabilize adhesion of these particles [12]. A significant fraction of nanospheres in bulk blood flow, however, is entrapped within the RBC core resulting in their low margination – i.e. they exhibit a low capacity to localize to the CFL. The low margination exhibited by larger microspheres (> 5 μm) is due to high disruptive forces acting to prevent adhesion and the negative impact of RBC collision at the wall that destabilizes adhesion.

The CFL width has been reported to vary from 2.5 - 7 μm in humans and some small animals depending on the hydrodynamic shear rate of flow, vessel size, the volume fraction of RBC or percent hematocrit (% Hct), and the aggregability and deformability of the RBCs [13-17]. Therefore, the subtle differences in the physical properties of RBCs among various animal models that possibly result in their differential lateral migration and hence the formation of CFL of various extents may eventually lead to variations in particle behavior and margination in different animal models. For example, the volume, and aggregability of RBCs in mouse blood, a common animal species used for vascular-

targeting research, are significantly smaller/lower than in humans [10, 18]. Similar variations in RBCs/blood characteristics between human and other common laboratory animals prominent in drug delivery research have been reported, including for pigs, rabbits, dogs and monkeys. Yet, to date, very limited works have investigated the impact of variations between animal models and human hemorheology on the hemodynamics of cells and particles as it relates to their margination to the vascular wall. The few works that exist have primarily focused on platelet adhesion in high shear laminar flow – Grabowski *et al.* found differences in platelet adhesion in whole blood flow of different mammalian species via controlled *in vitro* assays [19], and Aarts *et al.* observed via flow assays with RBCs of various animals that the adhesion of human platelet increased with increasing RBC sizes [20]. It is not clear whether this observed effect of RBC size on platelet adhesion would hold for the margination of VTDCs of different sizes, particularly in the nano-size range.

This study aims to elucidate the role of RBC dimension coupled with other blood components on dictating the binding efficiency of spherical particles sized from 200 nm to 5 μm in blood flow. Specifically, the adhesion of inflammation-targeted polystyrene spheres to inflamed endothelial cells from flow of washed blood (RBCs suspended in saline at fixed 40 % Hct) from different animals and from human and mouse whole blood flow were observed via a parallel plate flow chamber (PPFC) under physiological flow. Overall, our results show that the capacity of VTDCs to marginate to the vascular wall is significantly influenced by blood components, flow types and most importantly, RBC size.

6.2 Results

The experimental set up used in this chapter is described in detail in Chapter 2.

6.2.1 Effect of RBC size on particle adhesion in washed blood flow

To study the effect of red blood cell (RBC) size (diameter and volume) on the localization and adhesion of vascular-targeted drug carriers to the vessel wall, the binding of sLe^A -coated spherical particles, 0.2, 0.5, 2 and 5 μm diameter, to inflamed endothelial cells in laminar, pulsatile and recirculating human, pig, cow, mouse and goat washed blood (RBC in buffer at 40% Hct) flow were observed in a PPFC. The diameters and volumes of the different animal RBCs used are summarized in Table 6.1 and the RBC morphology observed under a light microscope is shown in Fig. 6.1.

Species	Diameter (μm)	Volume (μm^3)	Ratio of Volume to Diameter (μm^2)
Human	8	90	11.25
Pig	7.0	58	8.3
Cow	5.8	58	10
Mouse	6.8	48	7.1
Goat	4	18	4.5

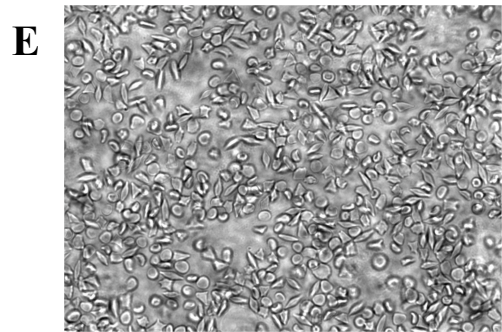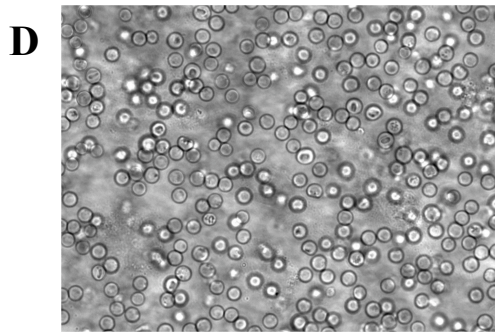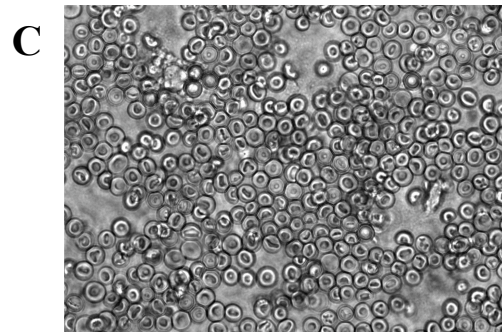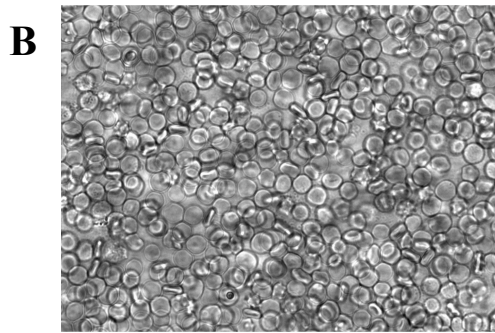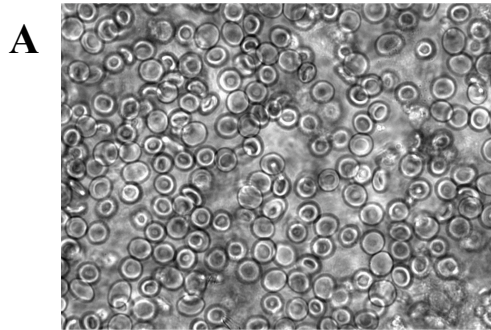**Table 6.1** Red blood cell size of human and different animal species.

Figure 6.1 Morphology of (A) human, (B) pig, (C) cow, (D) mouse and (E) goat red blood cells suspended in saline under light microscope at 20x magnification.

Fig. 6.2 shows the particle binding densities observed in laminar washed blood flow at wall shear rates (WSRs) of 200 and 500 s^{-1}. At 200 s^{-1} of laminar human washed blood flow, particle adhesion density increased as their diameter increased from 0.2 to 5 µm while the binding densities of 0.5, 2 and 5 µm spheres in pig, cow and mouse washed blood flow, were not significantly different from each other. The 0.2 µm sized spheres displayed minimal binding in laminar washed blood flow for all species (Fig. 6.2A). At 500 s^{-1}, the adhesion densities of microspheres (2 and 5 µm) in human washed blood was significantly increased relative to their adhesion at 200 s^{-1} with 5 µm spheres displaying the highest adhesion (Fig. 6.2B). The binding of nanospheres was not affected by this magnitude of change in WSR, resulting in greater differences between the binding density of microspheres and nanospheres in human washed blood at the higher WSR (500 s^{-1}). In contrast, the increase in WSR to 500 s^{-1} enhanced the binding density of particles of all sizes in pig, cow and mouse washed blood, though the increase in the adhesion of 0.5 µm spheres binding was not significant in all animal species (Fig. 6.2B). Overall, at WSR 500 s^{-1}, microsphere binding was significantly higher relative to nanospheres and no significant differences were observed between the binding of the two microspheres (between 2 and 5 µm) in pig, cow and mouse washed blood flow (Fig. 6.2B). Furthermore, there was no significant difference between the adhesion density in mouse and goat laminar washed blood at WSR 500 s^{-1} for nanospheres and 2 µm spheres while 5 µm spheres exhibited lower adhesion in goat blood (Fig. 6.2B).
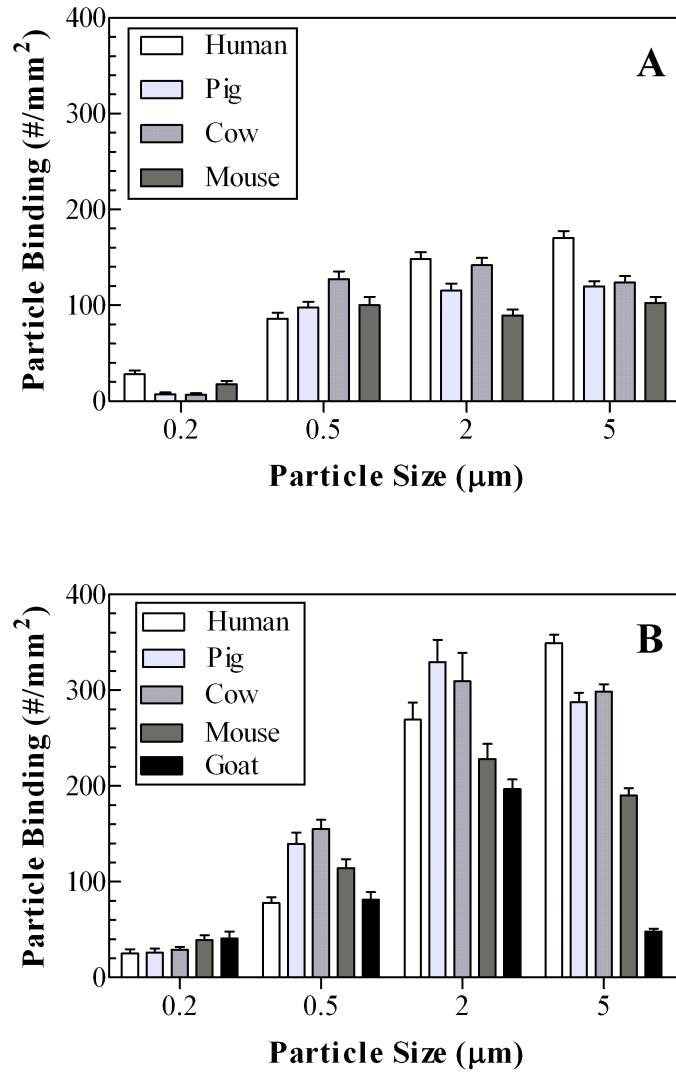
Figure 6.2 Adhesion of sLe^A-particles in human, pig, cow, mouse and goat laminar washed blood flow at WSR (A) 200 s^{-1} and (B) 500 s^{-1}.

In an attempt to speculate on the correlation between particle adhesion and RBC size, the binding density of spheres in laminar washed blood flow at WSR 500 s^{-1} were replotted as a function of RBC diameter, RBC volume and the ratio of RBC volume to diameter. As shown in Fig. 6.3A, the adhesion trend of particles particularly microspheres did not show an explicit correlation with RBC diameter since a large difference in the binding density of both 2 and 5 μm spheres were observed between pig and mouse washed blood flow despite these two species having comparable RBC diameters. However, particle adhesion appear to be a function of RBC volume as shown in Fig. 6.3B. Specifically, the binding of 0.2 μm spheres slightly decreased with increasing RBC volume whereas the binding of 5 μm spheres linearly increased (slope = 4.2) as RBC volume increased. The adhesion of 0.5 and 2 μm spheres increased with increasing RBC volume reaching an optimal binding at RBC volume of 58 μm^3 (i.e. cow and pig washed blood) and decreased as RBC volume further increased. To tease out the couple effect of RBC diameter and volume, the particle binding density was replotted against the ratio of RBC volume to diameter (Fig. 6.3C). Overall, the correlation of particle binding to this ratio was similar to the one observed with RBC volume.

The binding trend observed for particles in pulsatile washed blood flow (profile II, pulsed only in the forward direction between low (120 s^{-1}) and high WSR (1200 s^{-1})), was similar to observation in laminar flow at WSR 500 s^{-1}. As shown in Fig. 6.4A, the adhesion of microspheres was significantly higher than nanospheres in human, pig and mouse washed blood. In each species, the binding density increased as particle size increased from 0.2 to 2 μm while no significant difference was observed between the binding density of 2 and 5 μm spheres.
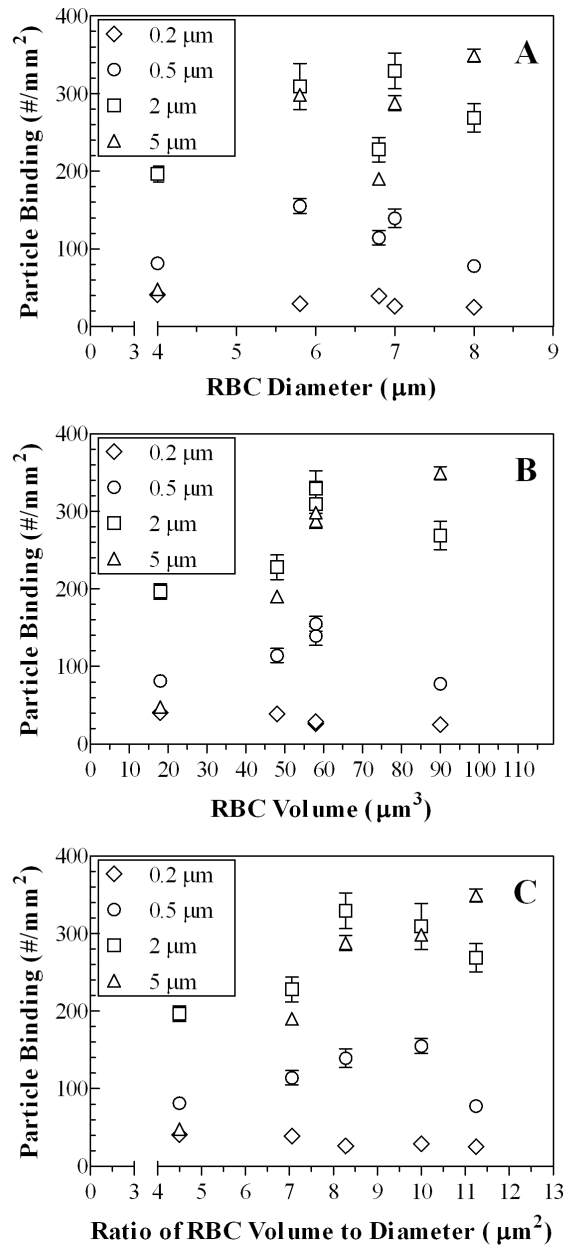
Figure 6.3 Adhesion of sLe^A-particles in human, pig, cow, mouse and goat laminar washed blood flow at WSR 500 s^{-1} as a function of (A) RBC diameter, (B) RBC volume and (C) the ratio of RBC volume to diameter.
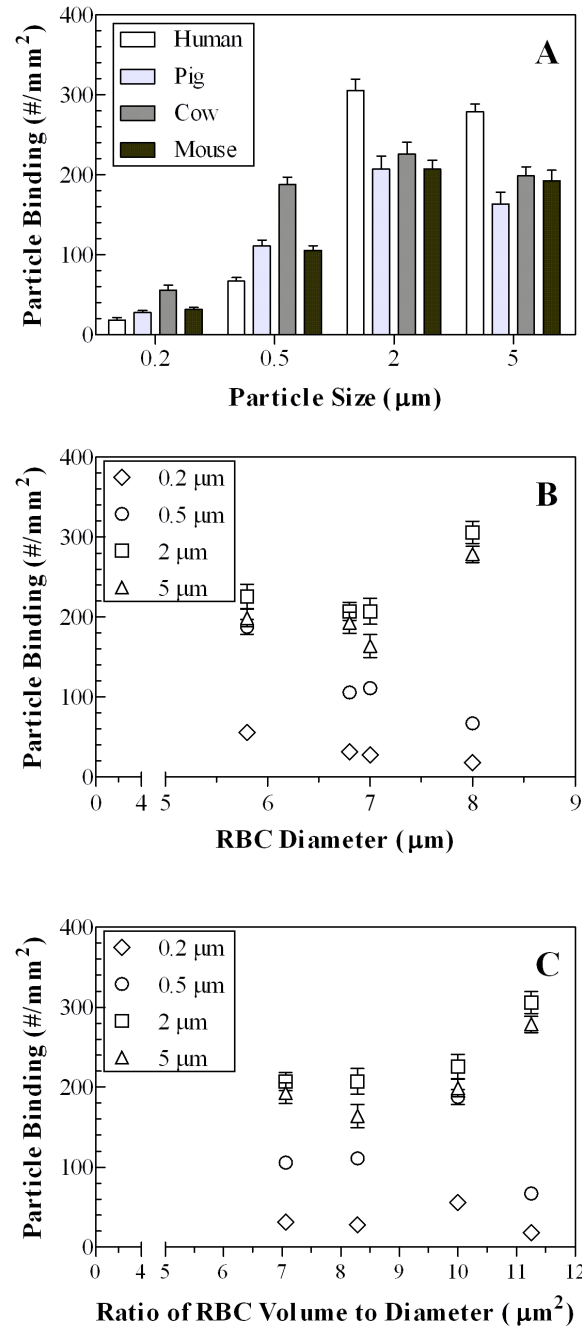
Figure 6.4 (A) Adhesion of sLe^A-particles in human, pig, cow, mouse and goat pulsatile washed blood flow (pulsatile profile II, pulsed between WSR 120 s^{-1} and 1200 s^{-1}). Total time = 5 mins. Particle binding was plotted as a function of (B) RBC diameter and (C) the ratio of RBC volume to diameter.

In contrast, in cow pulsatile washed blood, the particle adhesion was similar to their binding trends in laminar flow at WSR 200 s^{-1}. Specifically, there was no significant difference in the binding density of 0.5, 2 and 5 μm spheres, while the adhesion of 0.2 μm particle was minimal relative to other sizes. Overall, the binding density of microspheres (2 and 5 μm) in human pulsatile blood flow is significantly higher relative to other animal bloods while nanospheres (200 and 500 nm) showed the optimal binding in cow pulsatile washed blood (Fig. 6.4A). The particle binding in pulsatile washed blood flow appeared to be a function of RBC diameter, which we did not observe in laminar washed blood flow (Fig 6.4B). Specifically, the binding density of nanospheres linearly decreased as RBC diameter increased with slope -17.2 and -54.2 for 0.2 and 0.5 μm spheres, respectively, suggesting that the capacity for 0.5 μm spheres to bind in pulsatile flow is more susceptible to the change of RBC diameter relative to 0.2 μm particles. Again, there is no obvious correlation between the microsphere binding density in pulsatile flow and RBC diameter, though their binding decreased as RBC diameter increased reaching a minimum point at 7 μm of RBC diameter (i.e. pig washed blood). Beyond this point, the microsphere binding increased with increase in RBC diameter. Fig. 6.4C shows the particle binding plotted with the ratio of RBC volume and diameter. The nanosphere binding increased as the ratio increased peaking with the ratio of 10 that correlates to cow washed blood and significantly dropped as the ratio increased while the binding of microspheres slightly fluctuated as the ratio of RBC volume to diameter increased from 7 to 10 prior to rise as the ratio increased to 11.25 (i.e. human washed blood). The binding densities of microspheres were correlated with the ratio of RBC volume to diameter with the 2nd order polynomial curve.

For recirculating washed blood flow in the VSFC, particle binding was plotted with distance from the vertical step toward far downstream where laminar flow (WSR = 200 s^{-1}) was re-established. In general, the binding density of spheres in human washed blood was a function of particle size, where 5 μm exhibited the optimal adhesion as shown in Fig. 6.5A. The binding density of microspheres (2 and 5 μm) increased with the distance away from the step reaching their peak binding at distances slightly beyond the reattachment point (~ 170 μm from the step). Beyond this point, the binding density of 2 μm spheres plateaued while the adhesion of 5 μm spheres decreased toward far downstream. There was no significant difference measured for the binding of 2 and 5 μm particles at far downstream. Nanosphere binding in human washed blood in the VSFC, however, did not show any obvious peak and was not significantly different from each other in both recirculating and far downstream area (Fig. 6.5A). In pig washed blood, the binding density of spheres similarly increased as their diameter increased from 0.5 to 5 μm in the recirculating area. At far downstream, no significant difference was observed between the binding density of nanospheres and 2 μm particles while 5 μm spheres exhibited the optimal binding (Fig. 6.5B). Overall, the adhesion of 5 μm spheres in pig recirculating washed blood flow decreased while the binding of other sphere sizes was unchanged relative to their binding densities in human blood. Particle binding in mouse recirculating washed blood was similar to the one observed in human and pig washed blood where the binding density of spheres increased as particle size increased from 0.5 to 5 μm, though the adhesion of 2 and 5 μm was only significantly different from each other at the peak binding near the reattachment point (Fig. 6.5D).
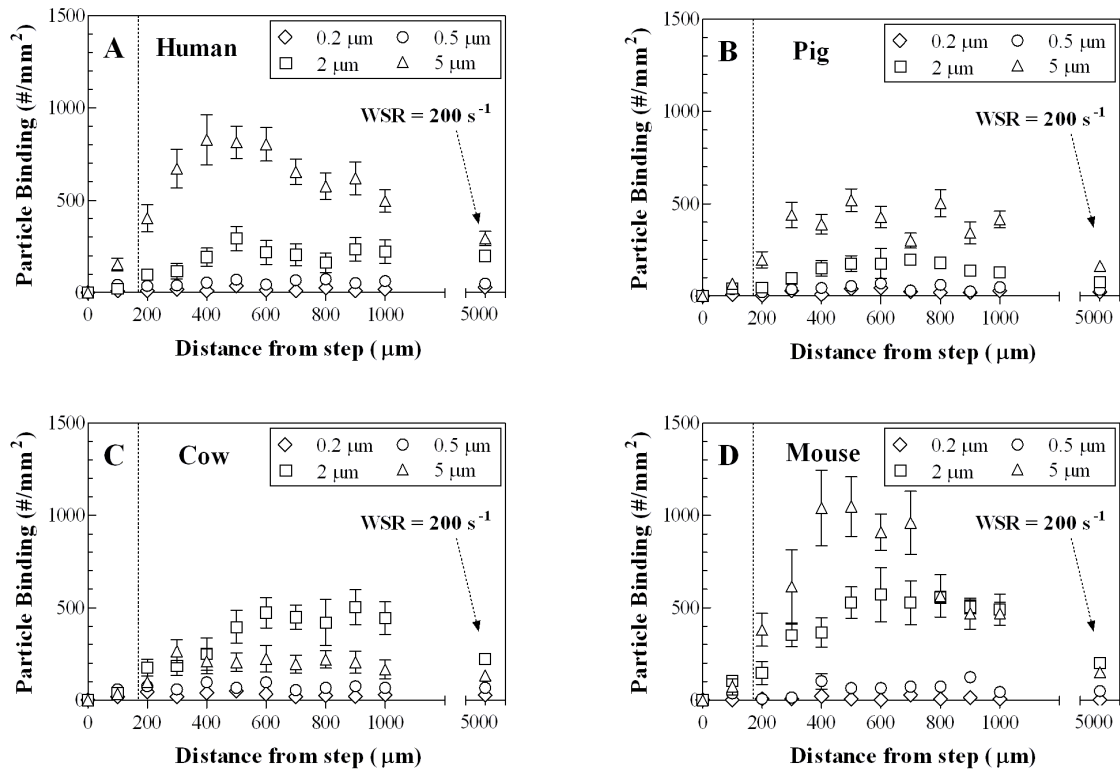
Figure 6.5 Adhesion of sLe^A particle in recirculating washed blood flow with (A) human, (B) pig, (C) cow and (D) mouse red blood cells at WSR 200 s^{-1} of far downstream.

Dash line represents observed reattachment point.

There was no significant difference between nanosphere binding in all region of the VSFC in mouse washed blood. In addition, the adhesion density of microspheres in mouse recirculating washed blood was surprisingly slightly higher than the ones in human recirculating washed blood flow which was in contrast to the lower microsphere binding observed in mouse laminar and pulsatile washed blood flow. In cow washed blood, the 5 μm particle binding in the VSFC decreased such that their binding density was lower than the binding level of 2 μm particles unlike observation with other species blood. Nevertheless, the binding density of microspheres in cow washed bloods was still higher than nanospheres in the VSFC, similar to the particle binding trend observed in other species (Fig. 6.5C).

Fig. 6.6 shows the particle binding density replotted from Fig. 6.5 as a function of particle size. Overall, the binding of nanospheres in recirculating washed blood did not depend on RBC size, i.e. the species. The adhesion of 2 μm spheres in cow and mouse washed blood was significantly different from the ones in human and pig washed blood only at 600-700 μm from the step (Fig. 6.6C). Spheres with 5 μm diameter exhibited significantly higher binding in human and mouse washed blood than in cow and pig washed bloods only at their peak adhesion (Fig. 6.6D). The binding densities of 0.5, 2 and 5 μm spheres at the peak adhesion (~ 500 μm from the step) showed trends with the ratio of RBC volume to RBC diameter where the particle binding decreased as the ratio increased reaching minimal bindings and the binding densities increased again as the ratio increased beyond the minimum point. No obvious correlation between the binding of 0.2 μm spheres and RBC morphology has been observed in recirculating washed blood flow (data not shown).

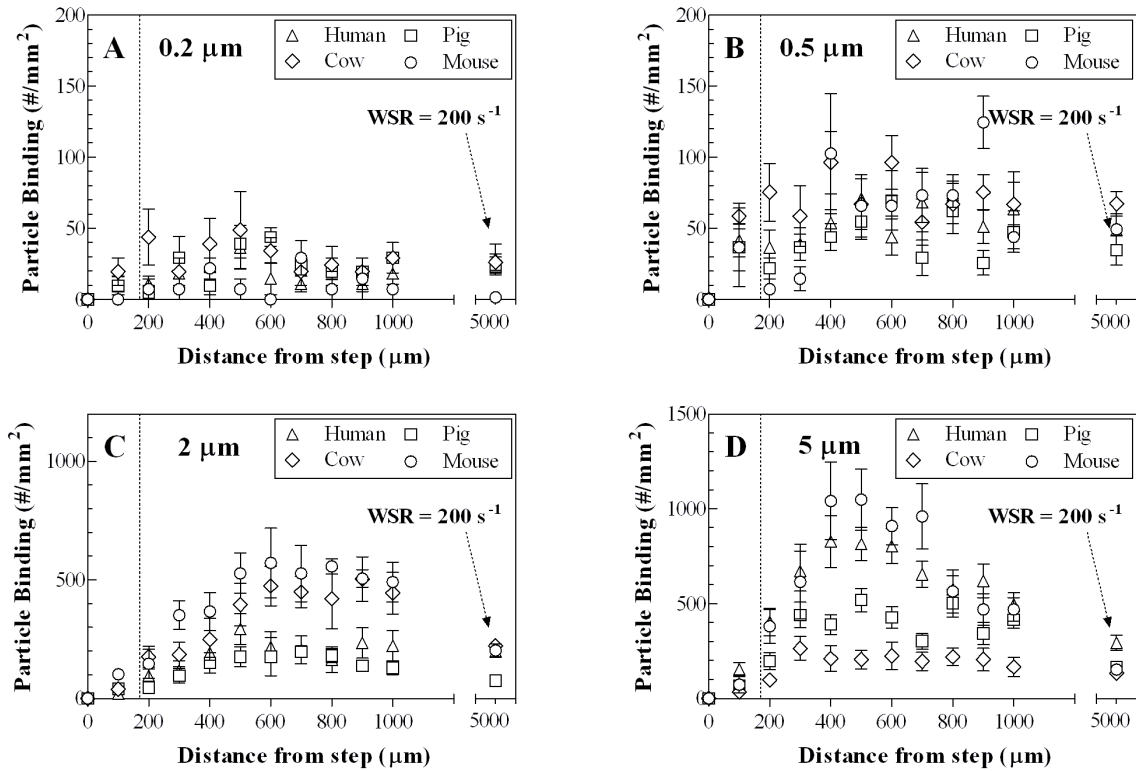**Figure 6.6** Adhesion of sLe^A particle (A) 0.2 μm, (B) 0.5 μm (C) 2 μm and (D) 5 μm in recirculating washed blood flow of human and animal red blood cells with WSR 200 s^{-1} at far downstream.

Dash line represents observed reattachment point.

6.2.2 Particle binding in human and mouse whole blood flow

To probe for the contribution of other blood cells and plasma constituents, spheres of different sizes were observed for their binding in human and mouse whole blood flow. Though human and mouse whole blood were collected in different anticoagulants i.e. ACD and heparin, respectively, no significant difference was observed on particle adhesion in human whole blood containing ACD or heparin, which suggested that anticoagulant may have minimal effect on particle binding in this study. Additionally, I showed that the introduction of mouse whole blood over human endothelial cells did not affect the human cell functionality as confirmed by observation of the similar binding density of spheres from human whole blood on the fresh human cell monolayers and the one that was pre-exposed with mouse whole blood flow for 5 min (data not shown). Fig. 6.7 shows the binding density of spheres in laminar whole blood flow at WSR 200 s^{-1} to 1000 s^{-1}. Overall, particle adhesion in human whole blood was similar to observation in human washed blood where microspheres (2 and 5 μm) binding was significantly higher than nanospheres at all shear rates studied; however, 2 μm spheres exhibited the peak adhesion in whole blood, which was likely due to the slight higher % Hct in human whole blood and as discussed in Chapter 5. Conversely, in mouse whole blood, the 0.5 and 2 μm spheres displayed the optimal binding depending on the magnitude of the WSR whereas 5 μm spheres had minimal binding at all shear rates, which is contradictory with the binding trends observed in washed blood. When comparing the binding density between these two species, the 0.5 μm spheres showed higher adhesion in laminar mouse whole blood flow relative to human whole blood by ~ 2.5-3 folds.
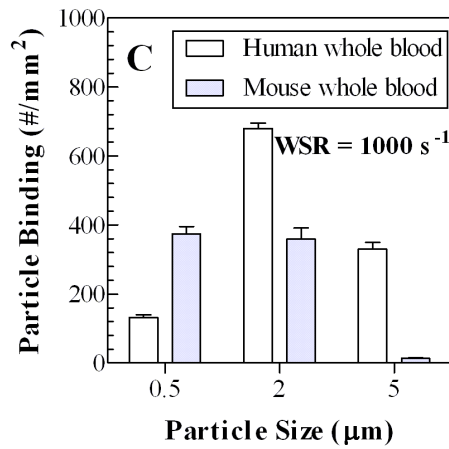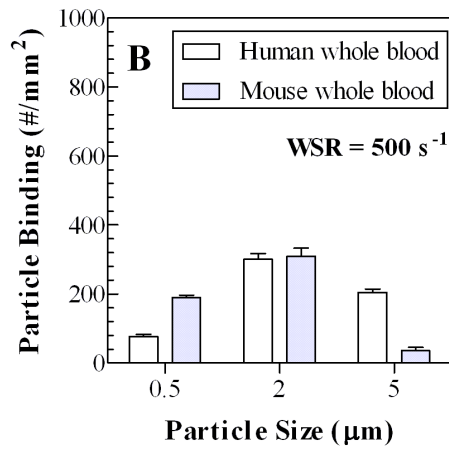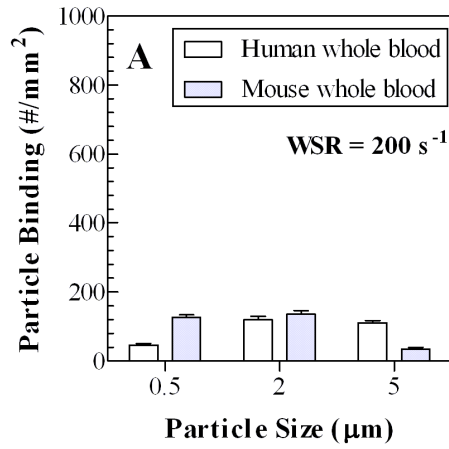
Figure 6.7 Adhesion of sLe^A-particles in human and mouse laminar whole blood flow at WSR (A) 200, (B) 500 and (C) 1000 s^{-1}.

There were no significant differences in the binding of 2 μm particles besides at WSR 1000 s^{-1} where the adhesion in human whole blood was ~ 2 folds higher. Interestingly, the differences in 5 μm binding density between these two species increased as WSR increased. Specifically, the binding in human whole blood was ~ 3-24 folds higher than the one in mouse whole blood as the shear rate increased from 200 to 1000 s^{-1}.

Fig. 6.8 shows particle binding in pulsatile whole blood flow (profile I) pulsed in the backward and forward direction with a peak WSR at 1000 s^{-1}. The particle binding trends of sLe^{A}-spheres in pulsatile whole blood flow was similar to the one observed in laminar whole blood flow, where 2 and 5 μm particles displayed the higher binding than nanospheres in human whole blood and 0.5 and 2 μm spheres exhibited higher adhesion in mouse whole blood than 5 μm spheres, which again was contradictory to the pattern of particle binding in mouse pulsatile washed blood. To study whether the significant difference of the binding trends observed in mouse whole blood versus washed blood was due to contributions from mouse plasma components, spheres of different sizes were observed for their binding in plasma-removed blood in pulsatile flow. As shown in Fig. 6.8, the binding density of microspheres (2 and 5 μm) in human plasma-removed blood was lower relative to whole blood while 0.5 μm spheres displayed the same level of adhesion in the presence or absence of plasma. The removal of plasma from mouse blood decreased the binding density of nanospheres (0.5 μm) whereas mouse plasma had no effect on microsphere binding.

Fig. 6.9 shows the binding of sLe^{A}- spheres from human and mouse whole blood in the VSFC.
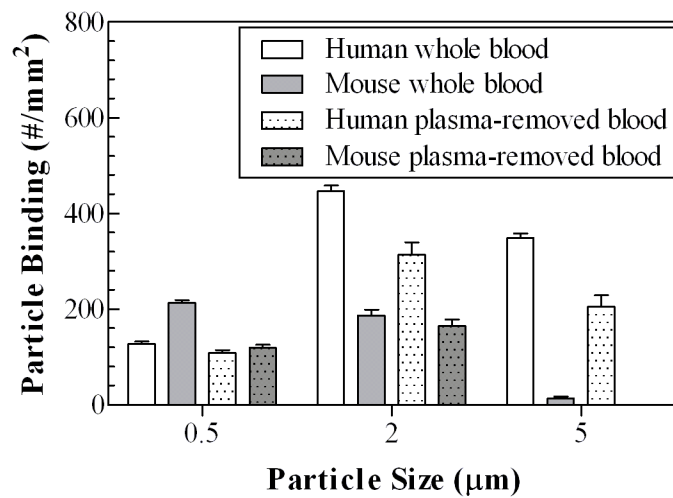
Figure 6.8 Adhesion of sLe^A- particles in pulsatile human and mouse (A) whole blood flow and (B) plasma removed blood at WSR 1000 s^{-1} for 5 min.
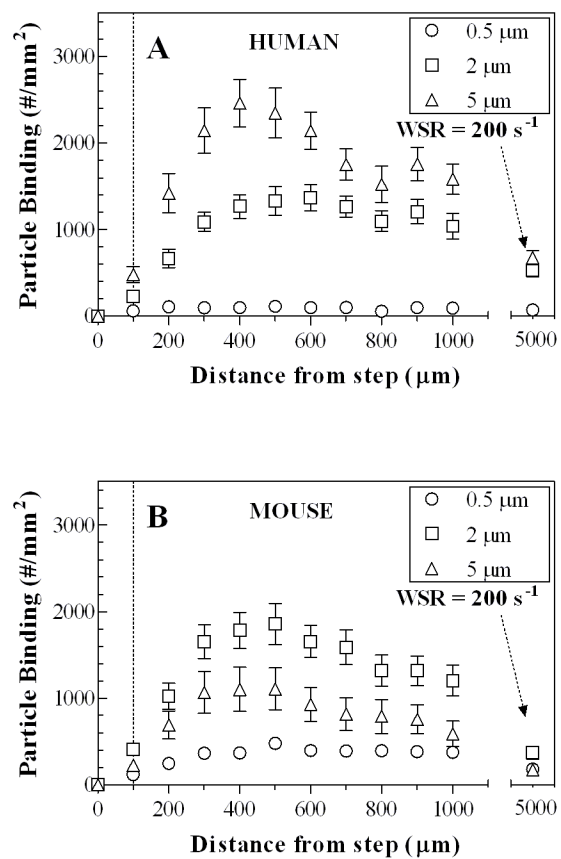
Figure 6.9 Adhesion of sLe^A –particles (1000 sLe^A site/μm^2) in recirculating (A) human
and (B) mouse whole blood flow at WSR 200 s^{-1}.
Dash line represents observed reattachment point.

The sLe^A-particle binding pattern in human whole blood was similar to the one seen in human washed blood where microspheres displayed significantly higher binding relative to nanospheres, though the binding densities for all particle sizes significantly increased in human whole blood relative to human washed blood (Fig. 6.9A). In mouse recirculating whole blood, the adhesion of 0.5 and 2 μm sLe^A-spheres were significantly enhanced relative to their binding in mouse recirculating washed blood while the binding of 5 μm spheres was unchanged. Overall, 2 μm sLe^A-spheres displayed the optimal adhesion in mouse recirculating whole blood (Fig. 6.9B) while 5 μm sLe^A spheres remain optimal in mouse washed blood.

6.3   Discussion

Due to many advantages gained from utilizing imaging modalities and vascular-targeted drug delivery in the early diagnosis and treatment of diseases, several research work have been focused on the design and engineering of the optimal vascular-targeted carriers for use to localize contrast and/or therapeutic agents to a target site in several human diseases, including in cancer and cardiovascular diseases. To ensure the *in vivo* functionality of designed delivery system, most researchers utilize animal models of human diseases, and this primarily represents the core of preclinical research prior to advancement to clinical testing. Mouse, rat, rabbit, pig, dog and monkey models are extensively used for testing in the preclinical research relating to vascular-targeting [6-9], despite the significant differences in blood rheology, hemodynamics and the vasculature structure of these animals relative to human [10, 18, 22, 23]. Though, the potential

correlation and the suggested scaling factor of a particular animal to human, respective to their differences in macroscopic scale, i.e. shear stress, are available [22, 23], limited works have studied the potential implications of the variations in microscopic scale, including different size of blood cells and plasma constituents, on the efficiency of vascular-targeted drug delivery relative to human physiology. Due to the significant influence of RBCs and other blood cells on particle margination in blood flow as thoroughly described in the previous chapters, it is likely that the distinct hemorheology that exists in animal models relative to humans, particularly the difference of red blood cell (RBC) size, can result in the differential pattern of targeted carrier localization and adhesion (margination) of particles of various sizes to the vascular wall. Herein, the adhesion of sLe^A- coated particles, 0.2, 0.5, 2 and 5 μm in diameter, to the inflamed endothelial cells in flow of human, pig, cow, mouse and goat washed blood (40% Hct RBCs suspended in saline) and whole blood was observed *in vitro* via a parallel plate flow chamber (PPFC) assays with physiological shear conditions. Overall, the presented results showed that the binding efficiency of sLe^A-particles varies with the dimension of RBCs corresponding to different animal models and flow types. I also suggested that the ratio of particle to red blood cell size has significant influences on the margination of vascular-targeted carriers in blood flow.

For instances, at WSR 500 s^{-1} of laminar flow, the binding density of 0.5 μm spheres in pig and cow washed blood were significantly higher relative to other species whereas 5 μm spheres exhibited the optimal binding in human washed blood. The discrepancies in the particle binding density are likely due to different sizes of their RBCs; however, it is not clear how differences in RBC dimension can alter particle

localization and adhesion to the wall. Since these adhesion experiments were observed at fixed RBC volume fraction (at 40% Hct); therefore, a larger number of RBCs with smaller volume as it is for pig and cow RBCs, relative to human, would be required to yield the same hematocrit in the same blood volume. However, under the same flow conditions, the large number of small RBCs is likely to be packed similarly to the low number of large RBCs, as shown in their equivalent RBC packing height during the step of %Hct measurement via centrifugation (see Chapter 2). This equivalent RBC packing suggests that these RBCs may similarly align under shear flow resulting in equivalent cell free layer (CFL) widths at the vascular wall proximity, which eventually leads to the comparable binding density of spheres at a given particle size. However, my experimental data showed conflicting results where different particle binding densities for a given particle size were observed in various species suggesting that CFL width might be varied among animal models. It is possible that the higher number of small RBCs as in mouse and goat blood may cause frequent collisions and intensified hydrodynamic interactions among RBCs that tend to expand the RBC core, i.e. CFL width decreases [24]. Additionally, RBC deformability is known to strongly affect the alignment of RBCs under shear flow, i.e. deformable RBCs tend to migrate to the center of flow while rigid RBCs, less susceptible to the shear flow, are likely to stay adjacent to the wall [17]. Since small-sized RBCs are likely to be less susceptible to deformation under shear force, i.e. lower "apparent" deformability, due to their small surface area, relative to large-size RBCs; therefore, small RBCs are likely to exhibit low migration to the center of flow resulting in the smaller CFL width. This agrees well with my first hypothesis. Accordingly, the binding of nanospheres (0.5 μm) in the smaller CFL (in pig and cow

blood) likely increased due to the increase in particle-wall collisions and the impact of normal force from RBC core that enhanced and stabilized their adhesion, as observed in laminar flow at WSR 500 s^{-1} [12]. However, a shrinking of plasma CFL would lead to a higher packing of larger spheres (5 μm) and excessive collision among particles that can hinder the particle binding as observed in low binding of 5 μm spheres in pig and cow laminar washed blood. The lower binding densities of 2 and 5 μm spheres in mouse and goat (having the smaller RBC volume relative to pig and cow) laminar washed blood (WSR 500 s^{-1}) further verified these explanations.

Overall, the adhesion density displayed by spheres of a given size in laminar washed blood flow at WSR of 500 s^{-1} appears to be a strong function of RBC volume for the spheres with diameter greater than 0.2 μm as shown in Fig. 6.3B. The disconnection in the adhesion density obtained for spheres between pig and mouse washed blood with approximately the same diameter would suggest that the RBC diameter plays a minimal role in carrier adhesion though the clearer adhesion trend seen in the plot of particle adhesion density versus RBC volume to diameter ratio in Fig. 6.3C would suggest some minimal dependence on RBC diameter. The strong dependence of particle binding on RBC volume may again be related to the characteristics of the CFL generated. Specifically, the low capacity of 0.5 and 2 μm sphere binding observed in mouse and goat washed blood that have smaller RBC volumes may be due to non-existence or narrow CFL formed at fixed hematocrits such that the presence of RBCs at the wall proximity disturb and negatively affect the adhesion of particles at the wall. As the RBC volume increases to the certain ranges where these RBCs form the wider CFL width allowing particles to localize to the wall, the accumulation of particles in the CFL

enhances collision among particles and/or with RBCs leading to the increase in particle binding as seen in pig and cow washed blood. Beyond the optimal RBC volume, the binding of particles decreases again due to the larger CFL width where the normal force imparted by RBC and the collision among particles have a minimal effect on promoting particle adhesion to the wall. On the other hand, 5 μm spherical diameter is in line with the maximum CFL height range that commonly existing in human physiological conditions (2.5-7 μm) [13, 14], thus, the further decrease in CFL width as the RBC volume gets smaller would tend to negatively effect the binding of large microspheres. The lack of a RBC volume effect (i.e. the effect of CFL width) on the adhesion of 0.2 μm spheres is likely due to their extremely poor localization to the wall and their small size relative to the CFL width [2, 11].

The particle binding in human, pig and mouse pulsatile washed blood flow was similar to observation in laminar flow at WSR 500 s^{-1} where the adhesion of microspheres was favored over that of nanospheres. No significant difference was observed between the binding density of the two microspheres evaluated (2 and 5 μm) in pulsatile washed blood flow (Fig. 6.4), The slight decrease in the binding density of 5 μm spheres relative to 2 μm spheres in human washed blood is likely due to the high slip velocity (i.e. the velocity of particle before forming a single bond at the wall) that 5 μm spheres experience at high shear during the peak WSR of pulsatile flow [2]. The higher binding of 0.5 μm particles in pig and mouse washed bloods relative to human could again be explained by the smaller CFL width of the former. Since the CFL width becomes smaller as WSR increases, at fixed hematocrit and channel height [21], the combination of small RBC size and the increase in WSR in pulsatile flow can further

shrink the CFL width resulting in the lower binding of large microspheres (2 and 5 μm) observed in pig and mouse blood. Overall, there was no significant difference between the particle binding density in pig and mouse pulsatile washed blood flow likely due to their similar RBC diameter. Though the volume of pig and cow RBCs are similar, the difference in nanosphere binding density seen in pulsatile flow suggested that RBC diameter significantly contribute to particle binding in pulsatile flow as observed by the increase in nanosphere binding with decreasing RBC diameter (Fig. 6.4B). The rotation of RBCs in pulsing flow, that would be RBC diameter dependent, may disturb the packing of RBC and hence the formation of the CFL.

In general, the binding of nanoparticles in recirculating washed blood flow (WSR = 200 $^{-1}$) was minimal for all species and no significant differences among various species were observed, likely due to the extremely poor localization of nanospheres to the wall in this flow type, as suggested in the previous chapters (Fig. 6.6A and 6.6B). Spheres with 2 and 5 μm diameters exhibited the optimal binding in mouse/cow and human recirculating washed blood flow, respectively, particularly at the peak adhesion probably due to large accumulation of microspheres brought along with the vortex streamline at the reattachment point. In addition, the optimal RBC size forms the proper CFL width beyond the reattachment point also enhance the microsphere binding (Fig. 6.6C and 6.6D). No explicit correlation between the particle binding and RBC morphology was observed in recirculating flow for spheres with 0.2, 0.5 and 2 μm diameters, probably due to the flow complexity that redistributes the RBCs and particles in the vortex and far downstream as suggested in Chapter 4, though the 2nd order polynomial curve fitted well between the binding density of 5 μm spheres and the ratio of RBC volume to diameter.

In general, the pattern of sLe^A-particle binding in all flow types of human whole blood was similar to observation in human washed blood where microspheres exhibited the higher binding than nanospheres. However, the sLe^A-particle binding trends in mouse whole blood were significantly different from mouse washed blood, particularly the minimal binding of 5 μm spheres observed in mouse laminar whole blood flow. The slightly higher binding of 5 μm over 0.5 μm-sLe^A spheres near the reattachment point of recirculating mouse whole blood flow may be due to the large gain of 5 μm localization to the wall in this flow type (Fig. 6.9B). Overall, the discrepancies of particle binding in laminar mouse washed and whole blood flow suggested that plasma induced aggregation properties might have a strong impact on the particle behavior in blood flow since all other blood cells were present in the washed blood experiments for mice (see Chapter 2). To probe the effect of plasma on particle behavior, the adhesion of spherical particles was observed in plasma-removed blood in pulsatile flow (Fig. 6.8). Overall, removing plasma from human whole blood resulted in the reduction of microspheres (2 and 5 μm) adhesion likely due to the absence of cell free layer (CFL) at low WSR of pulsatile flow, as large protein molecules in plasma are necessary for bridging human RBCs to form aggregates at the flow center [25]. Conversely, there were no changes in microsphere binding in mouse plasma-removed blood relative to whole blood while the binding density of 0.5 μm particles decreased to the similar binding level as observed in human whole blood when mouse plasma was removed (Fig. 6.8). However, the decrease in nanosphere binding in mouse plasma-removed blood may not be due to the absence of CFL at low WSR as seen in human blood since mouse RBC does not aggregate under low WSR [10]. Additionally, the binding of 5 μm spheres did not gain back as the mouse

plasma was removed possibly due to the excess plasma left during the removal step (see Chapter 2) that may interfere their adhesion. Overall, This result suggested that mouse plasma compositions could play a significant role on particle binding; however, further detailed studies are needed for clarification.

Overall, though this work has not fully elucidated the understanding in different trends of particle binding observed in several animal models commonly used in the preclinical research, our findings addressed many important factors including the effect of RBC size and other blood cells that can affect the binding efficiency of vascular-targeted carriers. This study also raises the awareness of potential deviation of results investigated *in vivo* and the expected outcome in human, which is an important message to many research fields.

References

1. Zhang N, Chittasupho C, Duangrat C, Siahaan TJ, Berkland C. PLGA Nanoparticle− Peptide Conjugate Effectively Targets Intercellular Cell-Adhesion Molecule-1. Bioconjugate chemistry. 2007;19:145-152.

2. Charoenphol P, Huang RB, Eniola-Adefeso O. Potential role of size and hemodynamics in the efficacy of vascular-targeted spherical drug carriers. Biomaterials. 2010;31:1392-1402.

3. Klibanov AL, Rychak JJ, Yang WC et al. Targeted ultrasound contrast agent for molecular imaging of inflammation in high‑shear flow. Contrast media & molecular imaging. 2006;1:259-266.

4. Deosarkar SP, Malgor R, Fu J, Kohn LD, Hanes J, Goetz DJ. Polymeric particles conjugated with a ligand to VCAM‑1 exhibit selective, avid, and focal adhesion to sites of atherosclerosis. Biotechnology and bioengineering. 2008;101:400-407.

5. McAteer MA, Schneider JE, Ali ZA et al. Magnetic resonance imaging of endothelial adhesion molecules in mouse atherosclerosis using dual-targeted microparticles of iron oxide. Arteriosclerosis, thrombosis, and vascular biology. 2008;28:77-83.

6. Hamberg LM, Hunter GJ, Maynard KI et al. Functional CT perfusion imaging in predicting the extent of cerebral infarction from a 3-hour middle cerebral arterial occlusion in a primate stroke model. American journal of neuroradiology. 2002;23:1013-1021.

7. Lazarous DF, Shou M, Scheinowitz M et al. Comparative effects of basic fibroblast growth factor and vascular endothelial growth factor on coronary collateral development and the arterial response to injury. Circulation. 1996;94:1074-1082.

8. Moghadasian MH. Experimental atherosclerosis:: A historical overview. Life sciences. 2002;70:855-865.

9.   Tolentino MJ, Brucker AJ, Fosnot J et al. Intravitreal injection of vascular endothelial growth factor small interfering RNA inhibits growth and leakage in a nonhuman primate, laser-induced model of choroidal neovascularization. Retina. 2004;24:132.

10.   Windberger U, Bartholovitsch A, Plasenzotti R, Korak KJ, Heinze G. Whole blood viscosity, plasma viscosity and erythrocyte aggregation in nine mammalian species: reference values and comparison of data. Experimental physiology. 2003;88:431.

11.   Charoenphol P, Mocherla S, Bouis D, Namdee K, Pinsky DJ, Eniola-Adefeso O. Targeting Therapeutics to the Vascular Wall in Atherosclerosis-Carrier Size Matters. Atherosclerosis. 2011;217:364-370.

12.   Munn LL, Melder RJ, Jain RK. Role of erythrocytes in leukocyte-endothelial interactions: mathematical model and experimental validation. Biophysical journal. 1996;71:466-478.

13.   Bagchi P. Mesoscale simulation of blood flow in small vessels. Biophysical journal. 2007;92:1858-1877.

14.   Sharan M, Popel AS. A two-phase model for flow of blood in narrow tubes with increased effective viscosity near the wall. Biorheology. 2001;38:415-428.

15.   Tateishi N, Suzuki Y, Soutani M, Maeda N. Flow dynamics of erythrocytes in microvessels of isolated rabbit mesentery: cell-free layer and flow resistance. Journal of biomechanics. 1994;27:1119-1125.

16.   Yamaguchi S, Yamakawa T, Niimi H. Cell-free plasma layer in cerebral microvessels. Biorheology. 1992;29:251-260.

17.   Zhang J, Johnson PC, Popel AS. Effects of erythrocyte deformability and aggregation on the cell free layer and apparent viscosity of microscopic blood flows. Microvascular research. 2009;77:265-272.

18. Gregory TR. Nucleotypic effects without nuclei: genome size and erythrocyte size in mammals. Genome. 2000;43:895-901.

19. Grabowski EF, Didisheim P, Lewis JC, Franta JT, Stropp JQ. Platelet adhesion to foreign surfaces under controlled conditions of whole blood flow: human vs rabbit, dog, calf, sheep, pig, macaque, and baboon. ASAIO Journal. 1977;23:141.

20. Aarts PA, Bolhuis PA, Sakariassen KS, Heethaar RM, Sixma JJ. Red blood cell size is important for adherence of blood platelets to artery subendothelium. Blood. 1983;62:214.

21. Eniola AO, Willcox PJ, Hammer DA. Interplay between rolling and firm adhesion elucidated with a cell-free system engineered with two distinct receptor-ligand pairs. Biophysical journal. 2003;85:2720-2731.

22. Greve JM, Les AS, Tang BT et al. Allometric scaling of wall shear stress from mice to humans: quantification using cine phase-contrast MRI and computational fluid dynamics. American Journal of Physiology-Heart and Circulatory Physiology. 2006;291:H1700.

23. Weinberg PD, Ross Ethier C. Twenty-fold difference in hemodynamic wall shear stress between murine and human aortas. Journal of biomechanics. 2007;40:1594-1598.

24. Fedosov DA, Caswell B, Popel AS, Karniadakis GEM. Blood Flow and Cell-Free Layer in Microvessels. Microcirculation. 2010;17:615-628.

25. Armstrong JK, Wenby RB, Meiselman HJ, Fisher TC. The hydrodynamic radii of macromolecules and their effect on red blood cell aggregation. Biophysical journal. 2004;87:4259-4270.

CHAPTER 7

CONCLUSIONS AND FUTURE WORKS

7.1 Conclusions and Significant Contributions

To date, vascular-targeted drug delivery remains attractive interest for localized delivery of therapeutics, encapsulated in a carrier, to the specific diseased targets. This process offers high drug efficacy at the target sites while minimizing drug side effects associated with other healthy tissues. Due to these advantages over the traditional therapies, vascular-targeted drug delivery can be used as an alternative treatment for many serious diseases, including cancer, pulmonary and cardiovascular diseases – the leading cause of death in the world. To design the optimal drug carrier for vascular-targeted drug delivery, there are three important criteria that need to be considered, i.e. targeting, physical and hemodynamics properties. Firstly, the targeting specificity of drug carrier can be achieved by modifying the carrier surface with ligands having a specific binding affinity with the target sites. In this study, it appears that sialyl-lewis A (sLe^A), a carbohydrate ligand for selectins, is suitable for use on vascular-targeted drug carriers (VTDC) in targeting the inflamed tissues. My results showed that sLe^A-coated particle is not only able to selectively target the intended sites but also effectively captured under high shear flow at the similar rate as the leukocyte binding. However, the drawback of

this sLe^A-particle is its weak adhesive force, in which particle, particularly large microspheres, can simply detach once adherence under high shear flow and/or by the addition of drag force associated with leukocyte rolling motion, as discussed in Chapter 3 and 5. Therefore, decorating the surface of VTDC with dual-targeted ligands, i.e. both sLe^A and monoclonal antibody (aICAM or aVCAM), at the optimal ligand ratio may be a better carrier model for future works in effectively targeting the vascular wall with high binding efficiency. Specifically, sLe^A molecules assist in capturing particle to the vascular wall under shear flow, while antibody molecules help particle to withstand the high shear force and remain adherence.

As discussed in Chapter 3 and 4, prior to their selectively binding at the targeted sites, the VTDCs must be able to localize through the bulk blood flow to the wall proximity. The physical properties of drug carrier, hemodynamics, and the structure of vasculature, have been shown to significantly govern the localization of VTDC in blood flow. My results indicate that wall shear rate (WSR) and the size of blood vessel affect the behavior of VTDC in both buffer and blood flow. Specifically, the normalized particle binding density decreases as WSR and channel height increase, due to high particle slip velocity encountered at high WSR or in large channel. Additionally, the presence of RBCs enhances the localization and adhesion of particles for all sizes, especially microspheres, by aligning at the center of flow and creating the cell free layer (CFL) at the wall vicinity. The migration of RBCs away from the vascular wall causes the lateral displacement of particle into the CFL area, which increases their opportunity for interaction and adhesion at the wall. Since the width of CFL varies with a percent of hematocrit, blood vessel size and WSR, the particle binding density also changes with

this variation. Indeed, ideally, the optimal ratio of particle size to CFL width would yield the maximum particle binding efficiency. Moreover, my results demonstrated that flow types could affect particle behavior in blood flow. Specifically, the increase of residence time along with average low shear force (i.e. lower particle slip velocity) in pulsatile flow can promote the binding of particles relative to laminar flow. Recirculating flow also redistributes and localizes particle, particularly microspheres, to the wall near the reattachment point due to the presence of maximal normal velocity interacting toward the vessel wall and minimal axial velocity. Overall, this work provides in depth understanding on drug carrier margination in bulk blood flow and suggests that $2-5$ μm spherical particle, not nanoparticles, are the optimal size for VTDC in targeting the vascular wall of medium-to large sized arteries in physiological blood flow. These findings are beneficial to vascular-targeted drug delivery and imaging techniques since the suggested optimal carrier size can be utilized to effectively deliver medications or assisting in early disease diagnosis, which can possibly decrease the mortality in several serious diseases.

In Chapter 5, the influence of other blood cells, leukocytes (white blood cells) and platelets, on particle binding efficiency was discussed. Overall, leukocytes tend to prevent and/or compete with the binding of particles particularly microspheres. The rolling motion of leukocytes along inflamed endothelium can collide with previously adherent particles resulting in the increase of drag force on particle that may overcome their adhesive force causing the particle removal. Despite this negative effect of leukocytes, microspheres still efficiently target the vascular wall relative to nanospheres in physiological whole blood flow. On the other hand, resting platelets present in whole

153

blood has a minimal role on particle adhesion, likely due to their low binding affinity on the inflamed endothelium and their physical property that tend to minimize collision. Understanding in the role of individual blood cells on prescribing the VTDC binding efficiency is valuable since this knowledge allows the flexibility in VTDC design for various target sites and/or patients having different blood cell population.

Last but not least, this study also shed light on the different particle behavior observed in animals and human blood, likely due to the variations in RBC rheology and other blood cells, as discussed in Chapter 6. For instances, nanoparticles showed significantly improved adhesion in mouse whole blood relative to their minimal binding in human whole blood. This study raises the awareness of inadequacy in utilizing animal models to represent human body.

7.2   Future Works

Though this dissertation has elucidated the role of particle size, hemodynamics, and hemorheology which are significant criteria necessary for designing the optimal vascular-targeted carriers (VTCs) used in imaging and therapeutic delivery, particularly for chronic inflammatory diseases, the investigation in this field could be further developed and extended in the following directions.

(1.)   Further investigate the potential factors responsible for the different particle binding density in human and animal whole blood, previously observed in Chapter 6. Specifically, the effect of plasma constituents, RBC rheology and other blood cells of various animals on particle binding may need to be revisited and carefully examined.

(2.)   Develop and/or improve the *in vitro* flow adhesion assay to resemble the physiological conditions as encountered in human.

    (2.1) Since this work focuses on localized delivery of therapeutic agents to atherosclerosis, which often occurs in medium to large-sized arteries, thus, human arterial endothelial cells (HAEC) co-cultured with smooth muscle cells may be more suitable to use as an adhesion substrate in *in vitro* flow assay. Though, human umbilical vein endothelial cells (HUVECs) employed in this dissertation is widely used as an *in vitro* model of inflamed endothelial cells lining of blood vessels; however, the pattern and level of receptors expression on HAEC and HUVEC during inflammation may be different. In addition, the

smooth muscle cells lining underneath arteries endothelium could also effect the regulation of receptors. Consequently, the variation of receptor expression may impact the binding efficiency of VTCs and their adhesion trend, relative to particle size.

(2.2) Observe the adhesion of VTC at the bifurcation or arterial trees- mimicking flow channel, which are the prone site of atherosclerotic plaque formation. This study would determine the trend of particle binding and possibly suggest the optimal VTC size used for targeting specifically to the plaque area.

(2.3) The flow adhesion assay could further develop to a 3-dimensional flexible tube where particles are allowed to adhere to the surrounded tube wall. Though, my study previously suggested that gravity had a minimal role on particle adhesion in blood flow; however, the particle binding trend in the 3D tube could be different due to various factors including the velocity profile that occurred in different coordinating system. Additionally, the tube flexibility could affect the adhesive affinity of particle to the endothelial cell substrate, which may also alter the particle binding trend.

(3.) Investigate the potential role of biomaterials on particle behavior in blood flow.

Though polystyrene (PS) polymeric particle, VTCs used in this dissertation, is commonly employed for *in vitro* assays, however, poly (lactic-co-glycolic) acid (PLGA) and polycaprolactone (PCL) polymeric particles are preferable for *in vivo* research due to their biodegradability and biocompatibility. This study has elucidated the role of PS particle size on dictating the binding efficiency in blood

flow; future works need to confirm that other commonly used VTCs including PLGA and PCL particles can effectively marginate in physiological blood flow. Due to the different properties of these biomaterials such as density and surface characteristics, the behavior in blood flow and the interaction with blood cells of these particles could be different and thus may effect their binding efficiency.

(4.) Study the fate of vascular-targeted drug carriers (VTDCs) beyond their margination to the vascular wall.

    (4.1) Determine the role of particle physical properties, e.g. size, shape and surface charge, on dictating the transmigration of VTDC underneath the endothelial cells.

    (4.2) Study the mechanism of VTDC degradation and the pathway of drug release and delivery into the targeted cells.

(5.) Design alternative shapes of VTDCs such as rods and discs.

    Though, this study suggests that 2-5 μm spherical particles (not nanospheres) are the optimal carrier size for VTDCs; these carriers may not be practically used since their size ranges are in line with the size of capillaries (the smallest human blood vessels), then having the possibility to clog the blood flow in microcirculation. Therefore, to avoid the possible occlusion, the carriers with other shapes that can localize from the RBC core, effectively adhere at the vascular wall, and easily travel in microcirculation without causing occlusion may be better to use as alternative VTDCs.